THE DEVELOPMENT OF AN ION MOBILITY-ORBITRAP MASS SPECTROMETER FOR THE ANALYSIS OF LARGE PROTEINS AND PROTEIN COMPLEXES

A Dissertation

by

MICHAEL LAWRENCE POLTASH

Submitted to the Office of Graduate and Professional Studies of
Texas A&M University
in partial fulfillment of the requirements for the degree of

DOCTOR OF PHILOSOPHY

Chair of Committee,	David H. Russell
Committee Members,	Simon W. North
	Matthew Sheldon
	Renyi Zhang
Head of Department,	Simon W. North

May 2019

Major Subject: Chemistry

ABSTRACT

Ion mobility-mass spectrometry (IM-MS) is a powerful technique that provides a nested size-and-charge in mass-to-charge analysis in the gas-phase; however, current instrumentation is limited in resolution, both in mobility and mass domains. Recent developments in Orbitrap mass analyzers improve upon the utility of MS by providing improved resolution over current quadrupole and time-of-flight mass analyzers. Orbitraps have catapulted MS into a new field of native MS, the study of solution-phase structures and noncovalent interactions in the gas-phase. Although the power of these new mass analyzers has been realized, coupling of IMS to Orbitraps poses an analytical challenge due to a duty cycle mismatch: Orbitraps detect on a slower timescale than IMS separation, therefore using Orbitraps as a detector for IMS is difficult. Here, a high-resolution periodic focusing drift tube IMS was coupled to an Orbitrap mass analyzer via a novel interface for the biophysical analysis of large proteins and protein complexes. Fourier transform IMS multiplexing was implemented to overcome the duty cycle mismatch between the two platforms and allow for the analyses of native systems. Finally, the instrument was used to study the structure of a variety of protein complexes and their interactions with small molecules, metals, and posttranslational modifications, all of which have dramatic effects on protein structure, stability, and function.

DEDICATION

This dissertation is dedicated to my wonderful family: my beautiful wife, Natalie, my mom, Tina, and my sister, Nicole. These three women have been incredibly supportive of my graduate work and have needlessly listened to me talk chemistry for much too long. I cannot thank them enough, nor can I tell them how much they have independently been my role models for as long as I have known them.

ACKNOWLEDGEMENTS

This project would not have been made possible without the help of a large number of people within the department and also outside of this department. I would first like to thank my advisor, Dave Russell, who not only envisioned this project and gave me the opportunity to work on it, but also continued to provide guidance and assurance along the way. Two Russell Research group alumni, Dr. Junho Jeon and Dr. Kyle Fort, unknowingly allowed me to scavenge and adapt their instruments to use on my own, and for that I am forever grateful. Dr. Junho Jeon designed the electrospray ionization source used on the instrument as it stands today. I would also like to thank Jacob McCabe who has helped teach me countless methods, ideas, and techniques, and helped make this platform what it is today. A special thanks to three Russell group members who have mentored me throughout my time at Texas A&M: Dr. Roberto Gamez, Dr. Kelly Servage, and Dr. John Patrick.

Greg Matthjiez helped with countless hours of electronics advice, repair, and planning. Even after his retirement, Greg was still just a call away and ready to help at any time. Will Seward of the TAMU Chemistry Machine Shop was responsible for the fabrication of every ion optic that was adapted for this instrument. He took our designs and quickly made them a reality with a level of detail that is second to none. Moreover, he taught me much of what I know when it comes to mechanical design, and patiently waited while I was still learning. Dr. Arthur Laganowsky has played an integral role in both the details of the development of this project and also in broadening my perspective

to look at the bigger picture. He has been a second advisor to me and I could not appreciate enough his door being open at any time. Dr. Brian Clowers at Washington State University graciously introduced me to one of the keys to operating my instrument, Fourier transform ion mobility, and singlehandedly saved me months of programming and experimentation with his advisement.

I would also like to thank my committee members, Dr. North, Dr. Sheldon, and Dr. Zhang, for their guidance and support throughout the course of this research.

Thanks also go to my friends and colleagues and the department faculty and staff for making my time at Texas A&M University a great experience.

Most importantly, I would like to thank my wife, my mom, and my sister, who have supported my endeavors throughout graduate school. They have kept me grounded throughout the entire process, and I truly could not have accomplished this without them.

CONTRIBUTORS AND FUNDING SOURCES

Contributors

This work was supported by a dissertation committee consisting of my advisor, Professor David H. Russell, and Professors Simon North and Matthew Sheldon of the Department of Chemistry and Professor Renyi Zhang of the Department of Atmospheric Sciences. The analyses and text depicted in Chapter IV were conducted equally between Mehdi Shirzadeh and me. All other work conducted for the dissertation was completed by Michael Poltash independently.

Funding Sources

This work was made possible in part by the National Institutes of Health (R01GM121751-01A1 and P41GM121751-01A1) and the National Science Foundation (CHE-1707675).

NOMENCLATURE

ATD	Arrival time distribution
CAD	Computer Aided Design
CCS	Collisional cross section
DC	Direct Current
Duty cycle	percentage of time in which an instrument is performing analysis
DT	Drift tube
ESI	Electrospray Ionization
FT	Fourier transform
FTICR	Fourier Transform Ion Cyclotron Resonance mass analyzer
FWHM	Full Width Half Maximum
IMS	Ion Mobility Spectrometry
MS	Mass spectrometry
m/z	mass to charge ratio
P	Pressure
PF	Periodic focusing
T	Temperature
t_d	drift time
TOF	Time of flight mass spectrometer
TW	Travelling Wave
UF	Uniform field

REIS	Reverse Entry Ion Source
RF	Radiofrequency
R_{IM}	Ion mobility resolution
$R_{m/z}$	Mass spectral resolution
RP	Resolving power

TABLE OF CONTENTS

Page

LIST OF FIGURES

Page

CHAPTER I

INTRODUCTION

Introduction

Over the past two decades Ion mobility (IM)-mass spectrometry (MS) has spawned new approaches for analytical separations of small molecules,[1] including challenging separations problems in the areas of lipidomics,[2, 3] metabolomics,[4] and proteomics.[5, 6] Recent improvements in sample preparation, native electrospray ionization (ESI), and IM-MS technologies are expanding the utility of gas-phase measurements for studies of solution-phase structure(s) as well as how noncovalent protein-ligand interactions affect structure-function relationships.[7, 8] IM-MS provides information that is complementary to other biomolecule structural techniques, such as X-ray crystallography, nuclear magnetic resonance, and cryo-electron microscopy. Unlike traditional techniques that report the population-averaged signal, IM-MS can interrogate heterogeneous populations of conformers and probe individual structure(s).[9] Such measurements are especially important for biophysical characterization of noncovalent protein-ligand interactions by determination of equilibrium binding constants and thermodynamics of the individual binding events.[10-12] These new biophysical capabilities mark an important step in understanding the dynamical effects of protein-ligand interactions, such as deciphering the role of protein conformation and molecular interactions with target molecules.

The rapidly growing field of native IM-MS and structural biology has been frustrated by the inadequate analytical figures-of-merit, viz. resolution in both ion mobility

(R_{IM}) and mass ($R_{m/z}$) dimensions, of commercially available IM-MS instruments.[13] Another, often overlooked, limitation of IM-MS studies of large proteins is the requirement of calibrant protein complexes for the determination of rotationally-averaged ion-neutral collision cross sections (CCS) for commercially available IM-MS instruments, such as the Synapt G1/2.[14, 15] Moreover, calibrant libraries remain sparse for large proteins, protein complexes and membrane protein complexes.[15-17] In addition, the poor mass resolution has hindered the application of native IM-MS to probe interactions of intact protein complexes with small molecules, such as drugs.

An often-underappreciated fact is that many commercial MS and IM-MS platforms were developed for the "omics" era where the key analytical figures-of-merit are high throughput, dynamic range, and limits-of-detection.[18] However, in most cases instrumentation developed for "omic" applications are not optimal for native IM-MS studies.[19] This includes the ability to retain solution-phase conformations during the transition from solution to the gas phase that represents a requisite of native IM-MS.[20] Thus, it is imperative that ESI conditions as well as IM-MS instrument operating parameters be optimized for preserving both non-covalent interactions and solution-phase conformations. The use of static spray, nanoflow ESI (nano-ESI) achieved by small bore capillaries (ranging from a few 100 nm to 10 μm) provides significant improvements in native MS by allowing for the analyses of proteins at lower concentrations (high nM to low μM) and mass spectra that contain fewer background ions.[21, 22] Additionally, nano-ESI accelerates droplet evaporation thereby allowing for more efficient desolvation of protein complexes.[23] Taken together, the quality of results from native IM-MS studies

require careful attention to sample preparation, optimized ESI conditions and proper tuning of the IM-MS.

Discussion

Limitations of Ion Mobility and Mass Resolution

As noted above, native IM-MS has challenged the analytical figures-of-merit deemed suitable for traditional "omics" studies. The characteristics for first-generation (Synapt G1) IM-MS and next-generation drift tube (DT)-IM-MS instruments (IM-Exactive Plus EMR Orbitrap) are compared in Figure 1. R_{IM} and $R_{m/z}$ are defined (Figure 1A) in terms of peak width (full width at half maximum, FWHM), but a more important consideration is resolving power (RP_{IM}), i.e., CCS/ΔCCS, where ΔCCS corresponds to the difference in CCS of two closely spaced peaks of two separable conformers. For example, a RP_{IM} of ≥10 is needed to resolve ΔCCS of 1000 $Å^2$ for an ion having a CCS of 10,000 $Å^2$, whereas a RP_{IM} of 100 can resolve ΔCCS as small as 100 $Å^2$. Similar observations can be made for Δ*m/z* by comparison of the mass resolution for the Synapt G1 travelling wave (TW) IMS and the Orbitrap Exactive Plus EMR instruments (Figure 1C). For example, resolving individual lipid bound states of the 127 kDa trimeric ammonia transport channel (AmtB), an integral membrane protein, mixed with three different lipids represents a modern challenge.[24] Signals for different lipid bound states to AmtB are not resolved by the G1 mass analyzer, whereas these same signals are baseline resolved in the mass spectrum acquired using the Orbitrap mass analyzer. The various bound states are masked by poor $R_{m/z}$ of G1 mass analyzer that impedes the ability to interrogate complex lipid binding to membrane protein complexes.[24]

Although the $RP_{m/z}$ of high magnetic field Fourier transform ion cyclotron resonance (FTICR) instruments exceeds that of the Orbitrap, the analysis of intact protein complexes is limited and coupling of DT-IMS to FTICR instruments is challenging owing to the duty-cycle mismatch.[25] In fact, to our knowledge the only attempt to develop DT-IM using FT-ICR utilized a design that is not compatible with native MS studies.[26, 27] Several groups have made considerable progress in this area using trapped ion mobility spectrometers (TIMS), and they have also made considerable progress in determinations of CCS for soluble proteins.[28, 29]

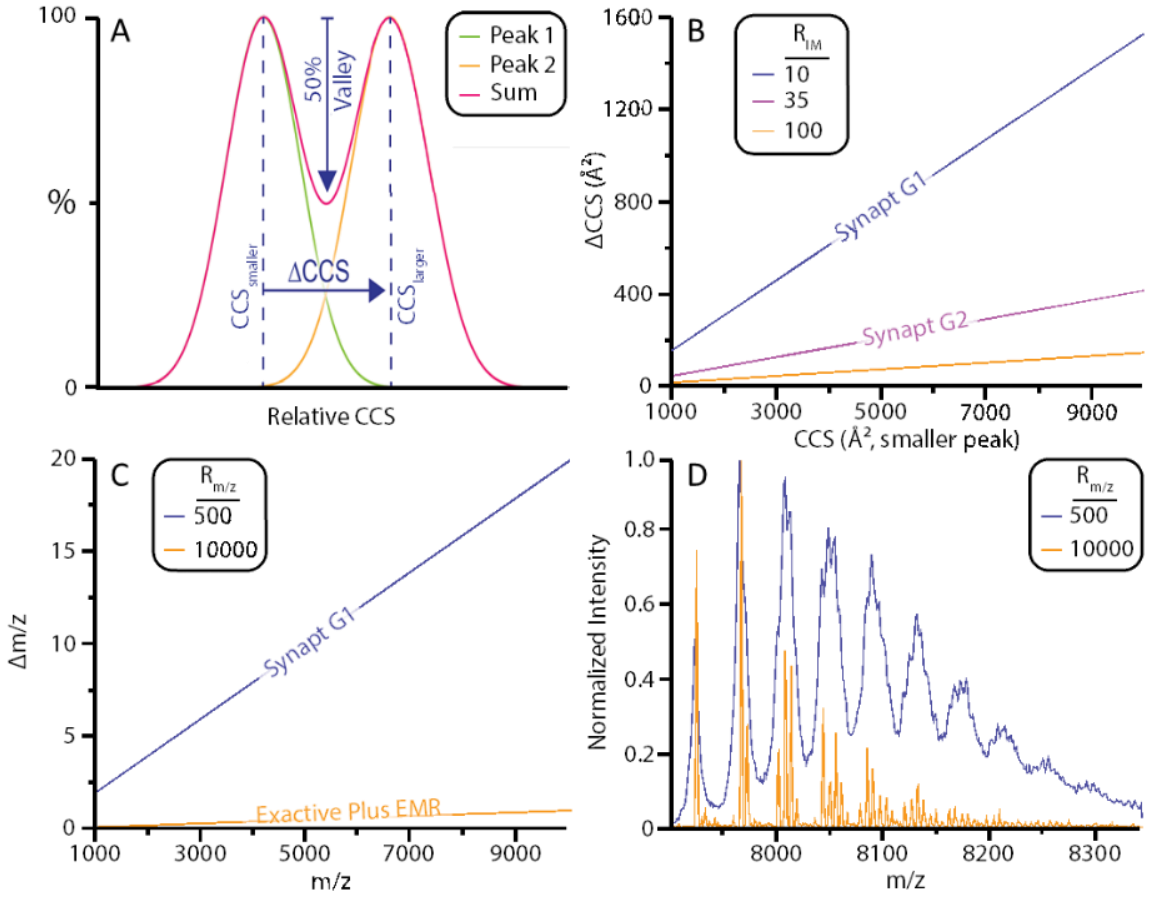

Figure 1. Comparisons of R_{IM} and $R_{m/z}$ for the Synapt G1 and Exactive Plus EMR Orbitrap for the analysis of large biomolecules. (A) Defines R_{IM} in terms of CCS/ΔCCS with a 50% valley between peaks and similarly for $R_{m/z}$ where m/z / $\Delta m/z$. Panels B and C contain plots of resolving power (RP) for both R_{IM} and $R_{m/z}$, respectively. Improved resolution has much more dramatic differences for larger CCS and higher m/z values clearly illustrating the need for increased resolution for large biomolecules. Any point one or above these trend lines indicates combinations that will be resolved. (D) Experimental data of a 127 kDa trimeric membrane protein AmtB mixed with three heterolipids (POPG, POPC, and TMCDL). The ToF $R_{m/z}$ is ~500 at m/z 7,900 as compared to ~10,000 at m/z 7,900 for the Orbitrap.

IMS Analyzers for Large Biomolecules

There are a number of IMS techniques capable of analyzing large biomolecules, viz. DT-IMS, TWIMS, TIMS, differential ion mobility spectrometry (DIMS). Of these techniques DT-IMS currently meets the necessary criteria for native IM-MS studies of protein complexes, especially for membrane proteins and their complexes. The main requisites for native IM-MS are the following:

(i) ESI conditions that are optimized for retaining solution-phase structure during the ion's transition from solution to the gas phase. For the analysis of membrane proteins, they are often encapsulated within detergent micelles and the detergents must be stripped prior to IMS and MS analysis.[30] Native IM-MS studies using a low R_{IM} instrument has demonstrated that after detergent removal the membrane protein retain "native-like" structure with measured CCS in agreement with those calculated from atomic structures.[17] However, higher R_{IM} instrumentation is needed to completely validate no impact on protein structure.

(ii) Determination of accurate CCS for large biomolecules must be determined by first-principles using the Mason-Schamp equation:[31]

$$\Omega = \left(\frac{3ze}{16N_0}\right)\left(\frac{2\pi}{\mu k_b T}\right)^{1/2}\left(\frac{t_d E_z}{L}\right)\left(\frac{760}{P}\right)\left(\frac{T}{273.2}\right) \quad (1)$$

Where Ω is CCS, z is the charge of the ion, e is the elementary charge, N_0 is the number density of the drift gas, μ is the reduced mass of the ion and drift gas, k_b is the Boltzmann constant, T is temperature in Kelvin, t_d is the drift time of the ion, E_z is the applied electric field, P is pressure, and L is the length of the drift tube.

The use of internal calibrations for determining CCS of proteins/protein complexes is limited by the number of accurate protein CCS determined using first-principles,[16] and even fewer for membrane protein complexes.[15, 17] Importantly, the majority of CCS determined using first-principles used an ion mobility device with low R_{IM} (~25).[16]

(iii) IMS must maintain excellent ion transmission of large biomolecules. Native IM-MS often requires low sample concentrations and volumes generating lower signals than smaller biomolecules necessitating more sensitive instrumentation. Traveling Wave and Periodic focusing (PF) described below efficiently transmits large biomolecules for such measurements.

The DT used for this instrument, a PF-DT, was first introduced in 2004,[32] to provide radial confinement of ions thereby minimizing ion losses as they traverse the DT (Figure 2B).[33-35] Recent studies of SIMION trajectories also revealed that ion transmission for the PF-DT increases with increasing ion charge as illustrated in Figure 2C revealing that PF-DT is optimized for studies of large, multiply-charged ions.[36] Importantly, first-principles CCS determination by the Mason-Schamp equation is maintained in PF-DT by incorporating an α-factor to account for the increased path length that arises because the ions trajectories are modulated by the non-linear E-fields. It is important to note, however, that the α–factor approaches unity as the charge on the ion increases.[37]

Ultimately, a high-resolution IM-MS platform engineered for studies of intact protein complexes was constructed by coupling a homebuilt PF-DT-IM to an Orbitrap mass analyzer (see Figure 2A).[38] Briefly, ions generated by a static nano-ESI source pass through a heated capillary where excess solvent can evaporate prior to entering an RF ion

funnel that focuses ions prior to entering the PF-DT-IM analyzer. Ions exiting the mobility PF-DT enter an octupole ion guide en route to the HCD cell of the Orbitrap where they are subsequently transferred to the C-Trap, then injected into the Orbitrap for mass analysis.

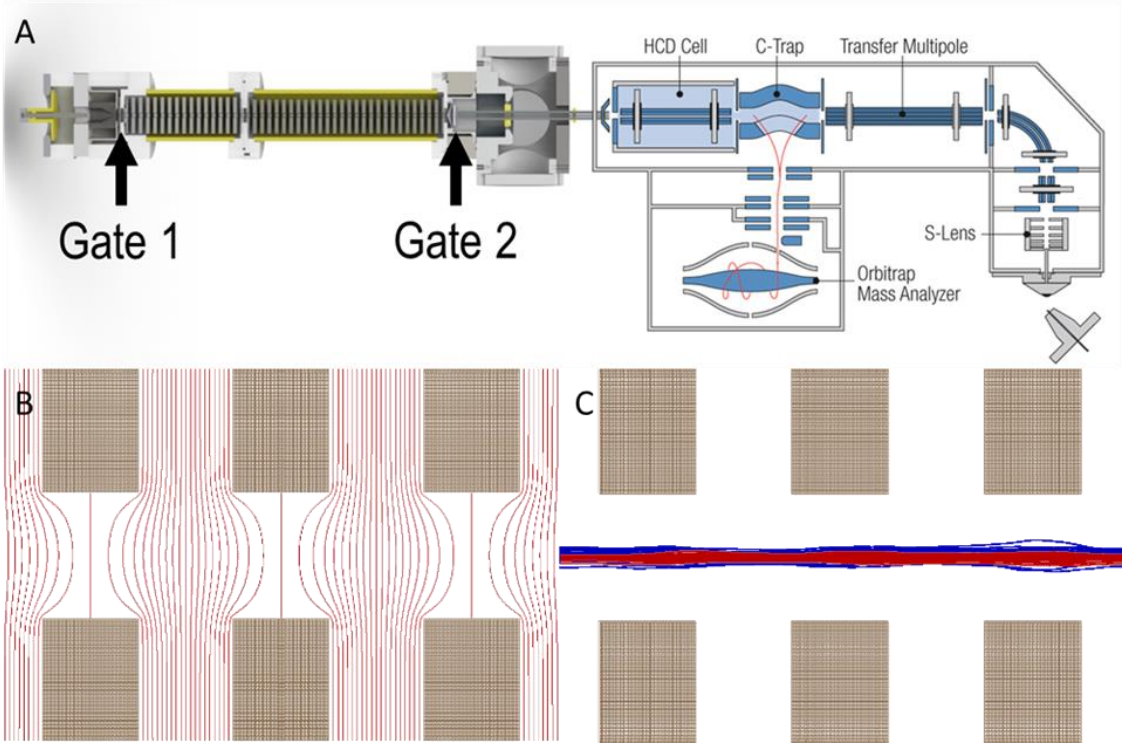

Figure 2. (A) Solidworks rendering of the IM-Orbitrap platform utilizing a nano-ESI source, heated capillary vacuum interface, RF ion funnel, PF DT, octupole ion guide, and an Orbitrap mass analyzer. Dual-gates are required to overcome the inherent duty cycle mismatch between DT IMS separation and Orbitrap mass analysis. (B) The equipotential lines derived from a PF DT electrode design. As ions traverse electrodes, they experience a distant-dependent effective potential giving rise to periodic focusing between each electrode. (C) Ion trajectory simulations of groups of ubiquitin (8.7 kDa, 5^+, blue) and AmtB (126 kDa, 15^+, red) in a PF DT. Note that the larger AmtB protein complex has narrower radial distributions.

Overcoming the Duty-Cycle Mismatch for DT-IMS and Orbitrap MS

Throughout the evolutionary development of IM-MS the "pulse-and-wait" data acquisition scheme has been widely used, especially for IM-TOF MS instruments. "Pulse-and-wait" describes an acquisition method in which a small packet of ions is pulsed into the DTIMS for temporal separation and the ions are detected by using high-speed mass analyzers, i.e. a ToF. As early as the 1970's Karasek recognized limits associated with operating IMS instruments in the "pulse-and-wait" mode. To circumvent this problem, they developed the first dual-gate IMS techniques as a means to monitor analyte specific ion arrival times.[39-41] In fact, the dual gate mode is analogous to selected-ion monitoring MS analysis.[42] Hill et al. later implement a similar approach whereby the dual gate is employed for achieving frequency modulated DT-IM operation, i.e., the potential applied to IM entrance (Gate 1) and exit (Gate 2) aperture plates are synchronously pulsed with a digital waveform.[43, 44] There are two major advantages for frequency modulated DT-IMS: (i) the duty-cycle using frequency modulated dual gate mode is 25% comparted to 1% for "pulse-and-wait" devices, and (ii) Fourier transform of the frequency modulated signal, i.e., ion abundances detected by the Orbitrap as a function of the modulation frequency, yields a frequency domain spectrum that is then converted to ion mobility arrival-time distributions (see Figure 3).

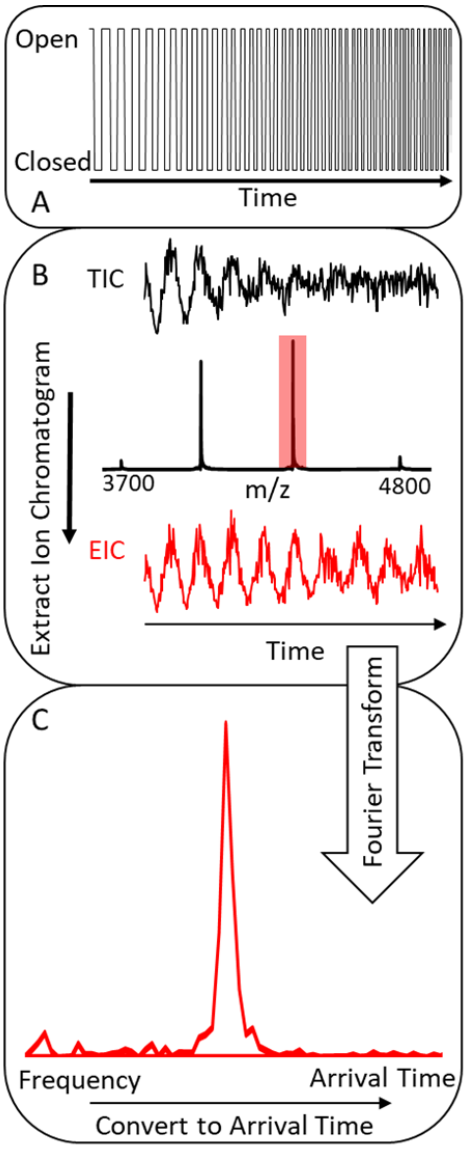

Figure 3. (A) A linear chirp digital wave form (radio frequency) signal applied to Gate 1 and Gate 2 is scanned across a range of frequencies that correspond to the frequencies (ATD-1) of the analyte ions of interest. The open/closed times of this signal are equal, which provides a 50% duty-cycle at each gate, thus the overall duty-cycle is 25%. (B) The resultant total ion chromatograms (TIC) are obtained by continuously acquiring the mass spectrum from which the extracted ion chromatogram (EIC) can be extracted over the *m/z* range scanned. (C) IM profiles can be obtained from a Fourier transform of the EIC where the resultant frequency is converted to arrival time. An exemplative spectrum of streptavidin (~53 kDa) is shown to illustrate FTIMS deconvolution.

Preliminary Studies of Protein Complexes and Ligand Binding

The performance of the native ESI-FT-IM-Orbitrap instrument was initially evaluated using small soluble proteins (ubiquitin, cytochrome C, and lysozyme) as well as several relatively small protein complexes (streptavidin-biotin complex, GlnK-ADP, transthyretin-thyroxine, and transthyretin-Zn(II)).[38] Here, we revisit the latter two examples in order to highlight two very important features of the instrument: (i) acquisition of ion mobility data for both apo and holo-forms of protein complexes, and (ii) the importance of high resolving power for mass analysis for studies of such complexes. Figure 4A illustrates the importance of $R_{m/z}$ to distinguish the tetrameric complex from its nucleotide bound forms. Importantly, Orbitraps possess the $RP_{m/z}$ to resolve not only ADP binding, but also individually bound sodium adducts, a phenomenon that is generally not illuminated by instruments with lower $RP_{m/z}$. Notably, the resolution of these ADP and sodiated species enables more accurate CCS determinations of defined chemical compositions whereas lower $R_{m/z}$ instruments would report on the average (Figure 4B).

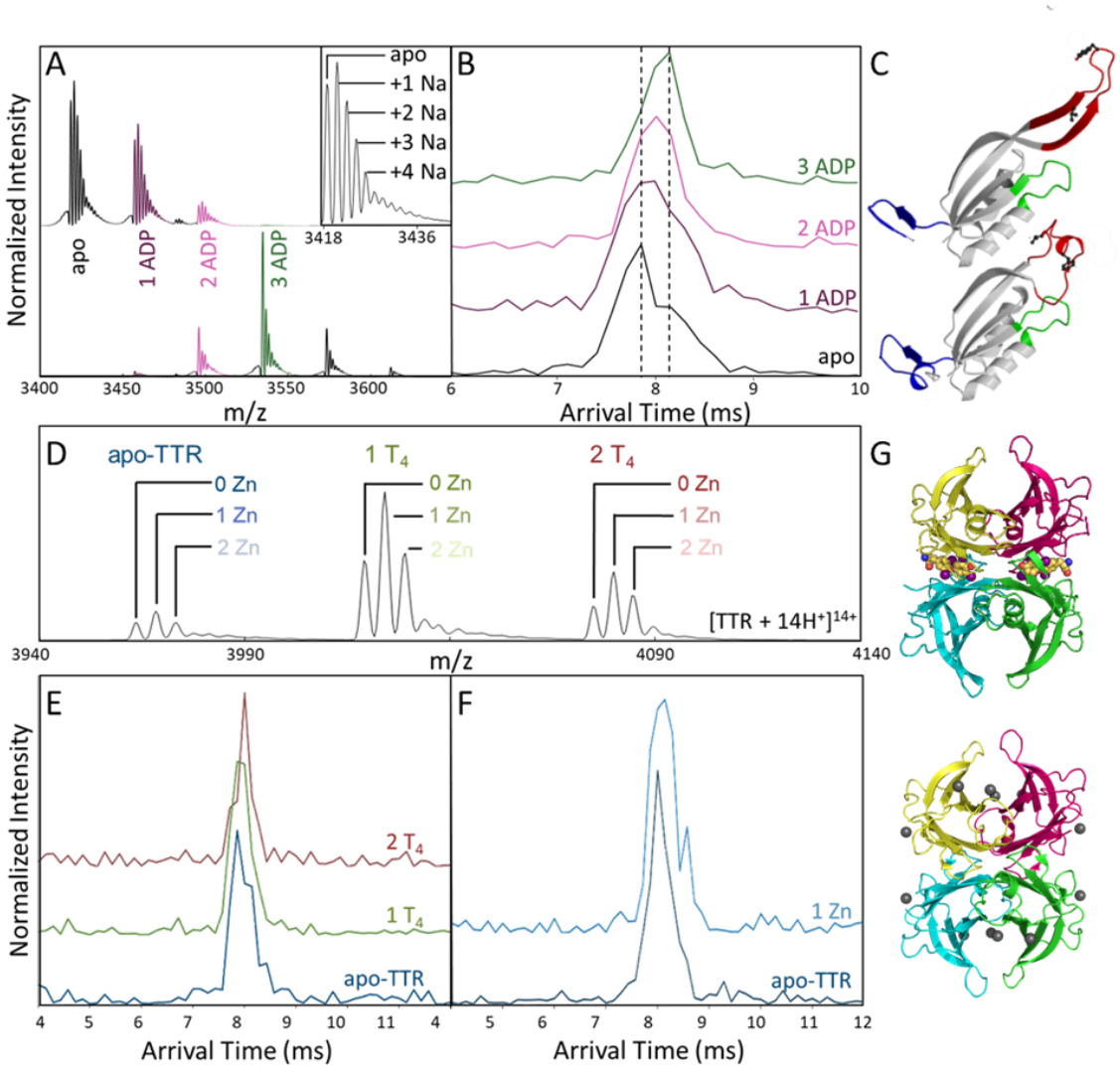

Figure 4. (A) Mass spectrum showing the region of the $[M + 12H^+]^{12+}$ trimeric GlnK complex and the product ions formed upon binding of ADP. (Inset) Magnified mass spectrum of the "apo" peak showing up to ten Na^+ adducts on GlnK. (B) The extracted ATDs of GlnK-ADP complexes excluding any sodiated ions. (C) XRD structures of GlnK (Top: PDB 1QY7,[45] Bottom: PDB 1HWU)[46] showing the two conformers observed by IMS denoting an open (top) and closed (bottom) "T-loop" upon the binding of ADP. (D) Partial mass spectrum showing the region of the $[M + 14H^+]^{14+}$ TTR complex and the product ions formed upon binding two T_4 and Zn(II). A resolving power ($RP_{m/z}$; FWHM) of 840 is required to separate the apo and Zn-containing ions. (E) The extracted ATDs of TTR containing one and two T4's. (F) The extracted ATDs of TTR bound to Zn(II). (G) XRD structures of TTR bound to (Top: PDB 2ROX)[47] T_4 and TTR bound to Zn(II) (Bottom: PDB 3GRG)[48].

The data for transthyretin (TTR) in complex with thyroxine (T_4) and Zn(II) further illustrates the importance of high-resolution IM-MS instrumentation (Figure 4D-G). The high-resolution IM-Orbitrap MS was able to baseline resolve TTR-T_4 interactions for the first time and also provides structural insight into this molecular interaction. That is, a reduction in peak width of the protein when bound to T_4, showing greater structural homogeneity is revealed by the IMS data. Surprisingly, the improved $R_{m/z}$ revealed a phenomenon that has not been reported by IM-MS measurements. Zn(II) bound to the protein was hidden by poor $R_{m/z}$, and therefore had been completely ignored in previous TTR studies using IM-MS.[49] The TTR-Zn(II) complex, however, shows a notable increase in IMS peak width, a phenomenon that is opposite of the structural effects seen be TTR-T_4 complexes. These high-resolution IM-Orbitrap MS measurements illustrate the power of data with higher precision and accuracy than ever before. Most importantly, high resolution data as acquired on our native IM-orbitrap platform will undoubtedly have important biological implications by resolving the unresolvable on low-resolution IM-MS instruments.

High-resolution IM-Orbitrap MS platforms can lend insight into systems that have thus far been difficult or impossible to explore. The newly afforded resolution is set to tease out structural changes associated with post-translational modifications, ligand binding, metal binding, and even drug binding, leading to greater insight into protein structure-function relationship. The advancements in resolution are now challenging the biological questions that can be addressed, including those that remain intractable using other biophysical techniques.

Conclusions

The development of a native-IM-Orbitrap MS has been made possible by the coalescence of many different methods developed over the last few decades coming together into a single platform. This dissertation outlines the development and application of this instrument beginning with developing a novel interface to Orbitrap mass analyzer, developing the IM DT and implementing multiplexing, to using the newly developed platform for applications that were previously masked by poor resolution. Continued improvements in both instrumentation and biological sample preparation will only continue to drive the technology forward.

CHAPTER II

DEVELOPMENT AND EVALUATION OF A REVERSE-ENTRY ION SOURCE ORBITRAP MASS SPECTROMETER[1]

Introduction

Native Ion Mobility-Mass Spectrometry (IM-MS) has rapidly cemented a crucial role in the biophysical characterization of proteins over the last three decades;[19, 50-54] however, the impact of this technique has been hindered by the lack of mobility (R_{IM}) and mass resolutions ($R_{m/z}$). Coupling IM to MS facilitates the studies of protein conformational preferences while also improving MS spectral quality and analytical merits.[31, 40] In the last 10 years, a surge of innovation in MS technology has been spurred in large part by the development of orbitrap mass analyzers, a robust and affordable benchtop MS.[55, 56] Orbitrap mass analyzers rely on electric field-based trapping to measure the transients of trapped ions for mass determination. Coupling an achieved $R_{m/z}$ = 240,000 with a mass range spanning 40,000 *m/z*, these instruments offer excellent performance for the analysis of small molecules up to large proteins and protein complexes.[57] Continuous improvements in ion injection and trapping efficiencies leverages the capabilities of these instruments to achieve performance similar to other trapping-based mass analyzers such as Fourier Transform Ion Cyclotron Resonance (FTICR) instruments at a greatly reduced cost.[58]

---

[1]Reprinted by permission from Springer Nature: *Journal of the American Society for Mass Spectrometry.* "Development and Evaluation of a Reverse-Entry Ion Source Orbitrap Mass Spectrometer" by Poltash, M.P.; McCabe, J.W.; Patrick, J.W.; Laganowsky, A.; Russell, D.H., *Journal of the American Society for Mass Spectrometry*, 2019, *30(1),* 192-198.

Although Orbitrap instruments have dramatically improved performance with regards to $R_{m/z}$ over other benchtop MS, the option for a factory-designed high-resolution IM cell coupled to an Orbitrap mass analyzer does not currently exist. Several groups have modified Orbitrap platforms, however, the modifications generally eliminate the ability to utilize the instrument in its intended configuration.[59-61] Unlike other modifications to Orbitraps reported to date, the completion of the instrument described here preserves the commercial ion source during development. Ultimately, higher R_{IM} and $R_{m/z}$ will provide the necessary detail to study larger, more complex protein assemblies and their interactions. The development of novel instrumentation to achieve these advances remains at the forefront of our developmental efforts.

Herein, we focus on the development and performance characteristics of a novel interface through which IMS or other tandem MS strategies can be coupled to the orbitrap mass analyzers without the need to significantly modify the commercial instrument. The performance of this reverse-entry ion source (REIS) was characterized through the analysis of ubiquitin, the trimeric transmembrane ammonia transport channel (AmtB) complex as well as the products of lipid binding to AmtB. Mass spectra obtained on the novel REIS were compared to spectra obtained using the commercial ion optics as well as a Waters Synapt G1 IM-MS instrument. The data and instrumental developments described herein set the stage for future work wherein IMS can be coupled to an orbitrap mass analyzer. This coupling will enable more targeted structural studies to be performed using an unprecedented combination of ion mobility and mass spectral resolution which has yet to be realized by both commercial and “homebuilt” instrumentation.

Experimental

Sample Preparation

Ubiquitin (bovine erythrocytes, >90% purity) was purchased from Sigma Aldrich (St. Louis, MO). A 5.0 μM stock solution in deionized water (18 MΩ) with 0.1% formic acid was prepared and used without further purification. Ammonia transport channel (AmtB) was expressed and purified as described previously.[10] AmtB was diluted in 200 mM ammonium acetate and 0.5% C8E4. Lipid samples of 1-palmitoyl-2-oleoyl-sn-glycero-3-phosphate (POPA), 1-palmitoyl-2-oleoyl-sn-glycero-3-phospho-L-serine (POPS), 1-palmitoyl-2-oleoyl-sn-glycero-3-phosphoethanolamine (POPE), and 1',3'-bis [1,2-dimyristoyl-sn-glycero-3-phospho]-sn-glycerol (TMCDL) were purchased from Avanti Polar Lipids Inc. (Alabama, USA). Lipids stocks were prepared in 200 mM ammonium acetate and 0.5% C8E4 and used without further purification.

Instrument Details

The homebuilt ion source used for these experiments utilized a radiofrequency (RF) ion funnel consisting of 33 electrodes electrically coupled through a series of capacitors and resistors.[62] Ions enter the funnel through a heated capillary set between 80-95 ºC. A differential pumping region separates a RF-only octupole ion guide built in-house. A dual channel Ardara RF Generator was used to apply RF potentials to both the ion funnel and octupole. This homebuilt source was coupled to the higher-energy C-trap dissociation (HCD) cell of a Thermo Exactive Plus with Extended Mass Range where the HCD endcap was removed and replaced with the octupole. Collision energy (CE) in the

HCD cell was set between 10-156 V, maximum injection time was set to 200 ms, trapping gas pressure was set between 1-4 au, Orbitrap resolution of 70,000 or 140,000 was selected, and each spectrum was collected using 10 microscans and 100 averaging. Samples were introduced to the MS using gold coated capillaries prepared in-house using borosilicate glass capillaries.

Temperature control for the lipid binding studies was achieved using a similar heated source device similar to what has been described recently.[10] Briefly, a temperature-controlled air circulator was used to heat an enclosed chamber around the ion source. Samples were placed inside a glass capillary, allowed to equilibrate at a given temperature, and subsequently analyzed. All experiments were carried out at 29 ºC.

Deconvolution Processing

AmtB lipid binding deconvolution and peak picking were performed using Unidec software with the following settings: *m/z* range of 6500 to 11500, 2.0 smoothing binned every 0.25, charge range of 12 to 19, mass sampling every 2.0 Da, peak FWHM of 0.8, peak detection range of 2.0 Da, and a peak detection threshold of 0.05.[63] The resultant zero-charge mass spectra were then assigned using Python scripts written in-house. Charge state distribution values were calculated using Unidec software.

Results and Discussion

Reverse Entry Ion Source

Native MS requires a great deal of care in sample preparation, ion creation, and manipulation, specifically for biophysical studies.[7, 19, 64-67] In this work, a modified "reverse entry" ion source (REIS) was designed to create a "cold" ion source interfaced to

the higher-energy collisional dissociation (HCD) cell of the orbitrap. This design was chosen to retain the full functionality of the orbitrap and its commercial source while simultaneously being able to design and evaluate ion optics using the REIS.

Here, the novel REIS was constructed by coupling an ion source via an RF-only octupole ion guide to the HCD cell of the instrument as depicted in Figure 5. Ions were introduced into a heated capillary using nanoflow ESI (n-ESI) where they are subsequently focused using an RF ion funnel.[62] Ions exiting the funnel pass through a skimmer region before being focused through a ring electrode and finally enter an RF-only octupole ion guide.[68] The ions entering via REIS are indiscriminately guided and trapped in the HCD cell. The HCD cell retains its functionality: ions can be stored and transmitted to the C-Trap as well as heated or fragmented before mass analysis. Although this configuration retains most of the functionality of the orbitrap, the interface eliminated the ability to use automatic gain control (AGC) to limit space charge effects in the orbitrap. AGC issues can be addressed, however, with manual control of the "maximum injection time" which allows for the tuning of the number of ions loaded into the orbitrap for mass analysis.

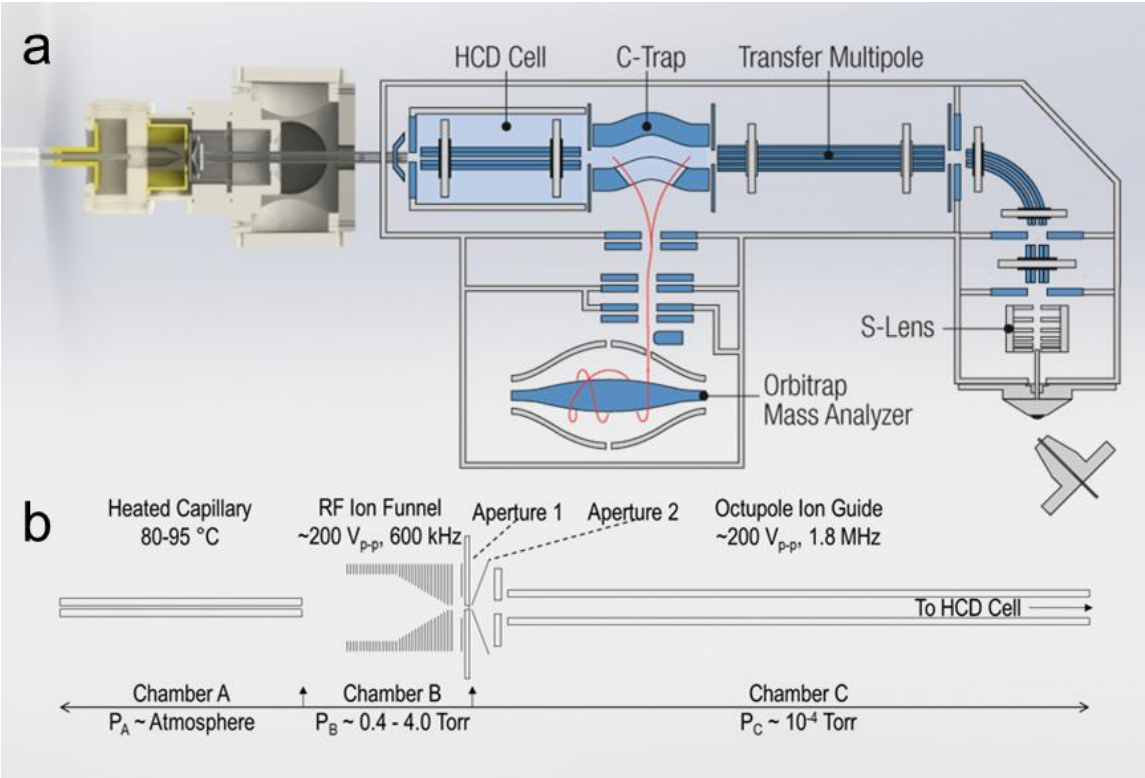

Figure 5. (A) Solidworks rendering of the reverse entry ion source and configuration of the instrument. (B) Starting from left to right, ions enter the instrument through an 11.4 cm, 800 µm i.d. heated capillary and are radially focused by a 5.08 cm in length RF ion funnel. The RF ion funnel consists of 33 electrodes electrically coupled through a series of capacitors and resistors, wherein the first 15 electrodes have inner diameters of 2.54 cm and the last 18 electrodes linearly taper to 2 mm. Ions are then guided through an RF-only octupole ion guide (rod diameter of 1.59 mm and 4.76 mm inscribed diameter) prior to being loaded into the HCD Cell of the Exactive Plus EMR. Reprinted by permission from Springer Nature: Journal of the American Society for Mass Spectrometry. "Development and Evaluation of a Reverse-Entry Ion Source Orbitrap Mass Spectrometer" by Poltash, M.P.; McCabe, J.W.; Patrick, J.W.; Laganowsky, A.; Russell, D.H., Journal of the American Society for Mass Spectrometry, 2019, 30(1), 192-198.

Retention of Mass Performance

Retaining both the native-like structure of ions and the high mass resolution afforded by orbitrap MS were the most important factors in the design of the REIS. Mass

spectral resolution ($R_{m/z}$) can be defined by the ratio of mass to charge (m/z) to its peak width at half maximum (FWHM) as describe in Equation 2 below. $R_{m/z}$ is not only instrument dependent but also analyte specific.

$$R_{m/z} = \frac{m/z}{m/z_{FWHM}} \qquad (2)$$

To evaluate the performance of the modified source, identical samples of ubiquitin were analyzed using both the commercial ion source of the orbitrap and the REIS. As shown in Figure 6, ubiquitin was isotopically resolved for each observed charge state using both ion sources giving nearly identical maximum resolutions of 30.2k and 30.9k for the commercial and REIS, respectively.

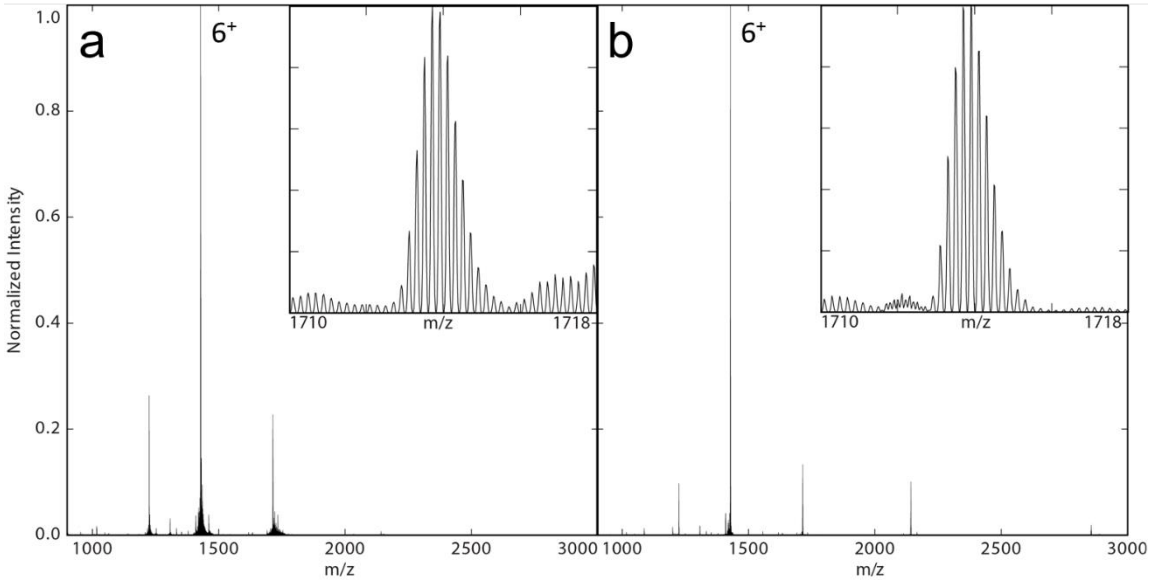

Figure 6. Mass spectra of ubiquitin acquired on the (A) commercial ion source and (B) REIS. Shown in the insets are the 5^+ charge state giving isotopic resolution from both ion sources. Note the lower charge states observed using the REIS giving rise to the 3^+. Reprinted by permission from Springer Nature: Journal of the American Society for Mass Spectrometry. "Development and Evaluation of a Reverse-Entry Ion Source Orbitrap Mass Spectrometer" by Poltash, M.P.; McCabe, J.W.; Patrick, J.W.; Laganowsky, A.; Russell, D.H., Journal of the American Society for Mass Spectrometry, 2019, 30(1), 192-198.

Additionally, a more challenging membrane protein, AmtB (126 kDa), was analyzed on both the commercial (Figure 7A and D) and REIS (Figure 7C and F) ion sources. A maximum resolution of ~10.5k and 9.9 k was achieved for the commercial source and REIS, respectively, on an identical sample of AmtB. We attribute the small difference in resolution to the retention of small molecules non-covalently adducted to the complex using the REIS leading to increased heterogeneity in the observed ion. The commercial source and REIS on the Orbitrap yielded an $R_{m/z}$ that was over 12-fold higher

than the $R_{m/z}$ = 800 achieved by the Waters Synapt G1 (Figure 7E). These results demonstrate that the addition of the REIS did not adversely affect mass performance of the orbitrap EMR instrument. This finding is a crucial step towards the addition of IMS to the orbitrap platform.

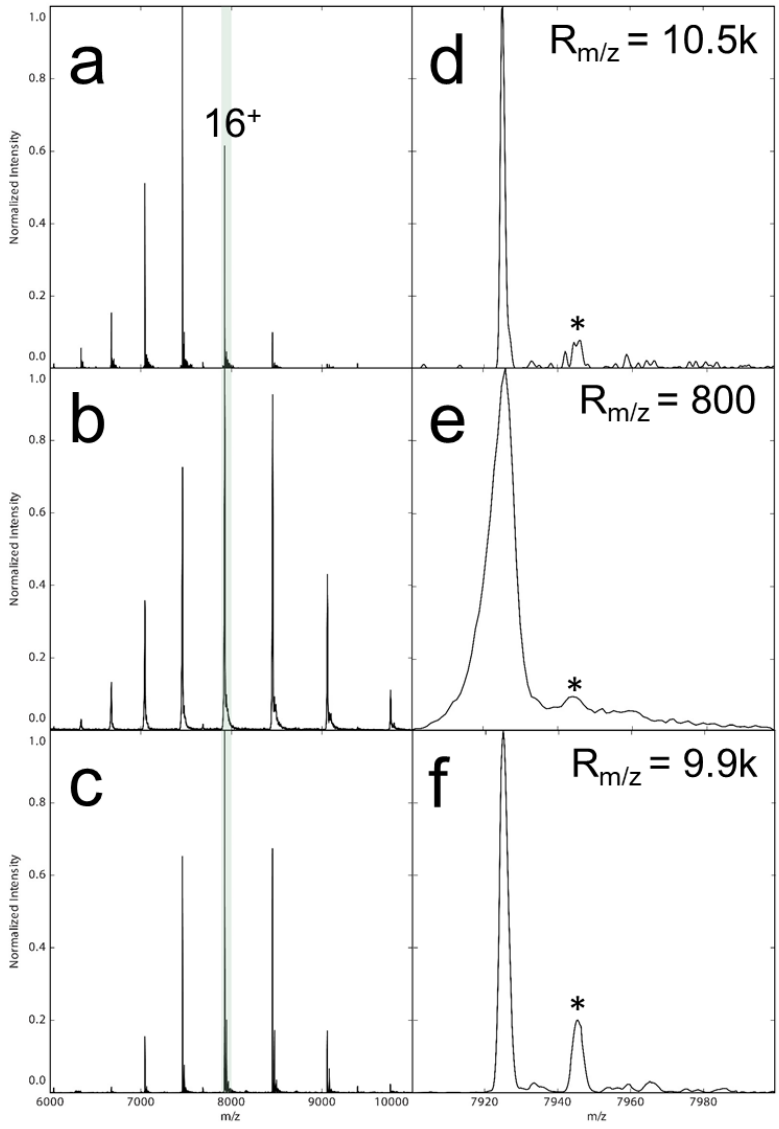

Figure 7. Mass spectra collected from the unmodified orbitrap (A, D), Waters Synapt G1 (B, E), and the REIS (C, F). The full mass spectra are shown on the left, and the 16^+ charge state is expanded on the right. The asterisks denote the adducted C8E4 detergent molecule bound to the AmtB in all three cases which was impossible to strip from the protein complex without dissociation of the complex itself. Reprinted by permission from Springer Nature: Journal of the American Society for Mass Spectrometry. "Development and Evaluation of a Reverse-Entry Ion Source Orbitrap Mass Spectrometer" by Poltash, M.P.; McCabe, J.W.; Patrick, J.W.; Laganowsky, A.; Russell, D.H., Journal of the American Society for Mass Spectrometry, 2019, 30(1), 192-198.

Retention of Native-like Charge States

Native MS refers to the analysis of solution phase protein structure in the gas phase by using biologically relevant solution conditions and careful MS tuning parameters. It is becoming increasingly important for the study of non-covalent interactions and structures of proteins.[17, 69, 70] Typically, native-like structures are confirmed using IMS by matching experimentally measured collisional cross sections (CCS) to those determined from crystal structures.[53] Native structures have also been characterized in MS by their retention of low charge states as the average charge state is related to the solvent accessible surface area.[71, 72] Folded tertiary structures do not typically display all their basic residues to the surface of the droplet in the ESI process and therefore cannot be protonated.[73-75] Notably, native MS can be performed by using biological pH buffers and salts amenable to MS experiments.[67, 71, 76, 77] Furthermore, recent studies have suggested the ability to retain native structures using MS for the analyses of membrane proteins through the addition of detergents and buffers.[17, 78, 79] Detergent molecules surround membrane proteins in the form of micelles, acting as a substitute for a lipid membrane, to maintain their solubility.[30] During early stages of analysis in the gas phase, these detergent molecules can be removed in collision cells; however, careful tuning is necessary to prevent unfolding or activation of the protein upon removal of these detergents.

Although this instrument is not currently equipped with IMS, the charge state distributions of ubiquitin and AmtB were compared to previously published standards for native MS to evaluate whether native-like ions were preserved with REIS. The Clemmer group reported the retention of native compact conformers for the same dominant charge

states observed in our experiment.[80, 81] In the current configuration and solution conditions, the 3^+ charge state was observed and is lower than reported by our group and others, suggesting the REIS is a "cold" source.[19, 82, 83]

Further evidence of native MS can be seen in Figure 7. Note that AmtB retains a Gaussian charge state distribution centered at 16^+ using the REIS, which is similar to that obtained on the Synapt G1, where IMS data have previously shown the retention of a single, compact conformer for the low charge states centered at 16^+.[10] Average charge states of AmtB were found to be 15.93 and 15.88 for the G1 and REIS, respectively. While charge state distributions are not a direct reflection of protein structure, lower charge states are indicative of native-like structures.[84] To further evaluate and tune the REIS, IMS would provide an optimal platform to validate and tune for native-like conditions on the orbitrap EMR instrument.

Importance and Illustration of Mass Resolution

Continual development in instrumentation over the past four decades has pushed mass resolution and resolving powers to heights that were unimaginable when MS was initially developed. The full potential of the REIS-orbitrap instrument could be realized for investigating heterogeneous lipid binding events to membrane proteins, such as for AmtB with $R_{m/z}$ = 10,000. It has recently been shown by Patrick et al. that the binding of two different types of phospholipids to AmtB can be resolved using the Synapt G1.[11] One of the major instrumental limitations cited in this work was a lack of mass resolution that limited the ability to distinguish between lipids of different type with similar molecular

weights, which was overcome by using a non-natural lipid.

AmtB was mixed with three different natural phospholipids to demonstrate the utility of the REIS-orbitrap platform and its ability to overcome the issues described above. Figure 8A shows a mass spectrum of AmtB in the presence of a lipid mixture containing POPA (697 Da), POPS (784 Da), and TMCDL (1285 Da) collected on the REIS-orbitrap and the Waters Synapt G1 instruments (Figure 8B). With a $R_{m/z}$ of ~500 using the Synapt G1, the determination of lipid binding events for the three different lipids was not resolved owing to the overlap of several peaks representing lipid bound species with similar masses. In contrast, up to 26 individual lipid binding events were, for the most part, baseline-resolved when the same analysis was performed on the REIS-orbitrap. In Figure 8, each colored band represents a different combination of lipids bound; the number of POPA, POPS, and TMCDL bound are shown above the respective peak. Binding of lipids with identical headgroups that differ in lipid tail composition to a small membrane protein using an orbitrap instrument has previously been shown by Gault et al.[85] However, the presented mass spectrum represents the first example of fully resolved heterogeneous lipid binding events of three unique lipids. Here, we were able to baseline resolve and observe up to five individual lipids bound in total to AmtB that are composed of mixtures of all three lipids as highlighted in Figure 8. Clearly, at elevated *m/z*, lower resolution instruments do not allow for the same level of detailed analyses as higher resolution instruments. These limitations preclude such instruments from performing such complex experiments on large complexes.

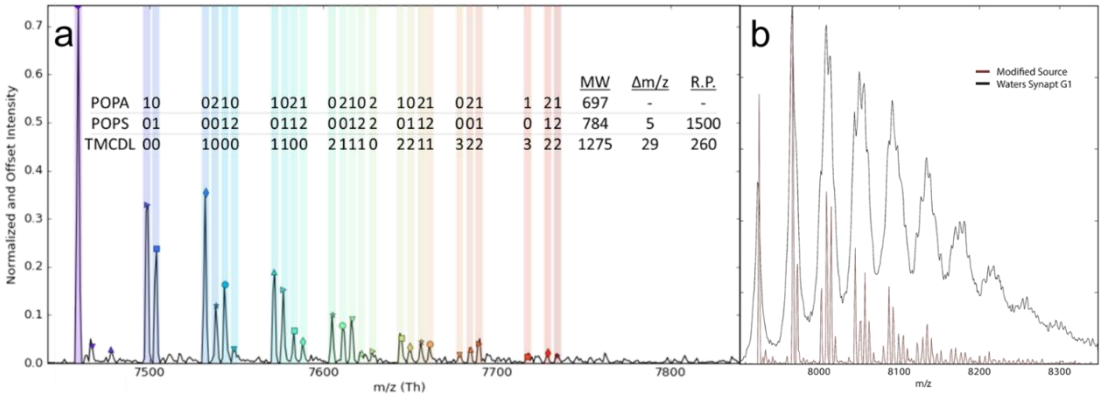

Figure 8. (A) REIS-orbitrap fully resolves AmtB bound to different combinations of POPA, POPS, and TMCDL. A total of twenty-six distinct lipid bound species were observed with up to five total lipids bound to AmtB. (B) Notably, none of these individual lipids species were resolved on the Waters Synapt G1 instrument. Reprinted by permission from Springer Nature: Journal of the American Society for Mass Spectrometry. "Development and Evaluation of a Reverse-Entry Ion Source Orbitrap Mass Spectrometer" by Poltash, M.P.; McCabe, J.W.; Patrick, J.W.; Laganowsky, A.; Russell, D.H., Journal of the American Society for Mass Spectrometry, 2019, 30(1), 192-198.

To further demonstrate the possibilities of REIS-orbitrap instrument resolution, an AmtB sample was prepared in the presence of four natural phospholipids: POPA (697 Da), POPE (718 Da), POPS (784 Da), and TMCDL (1285 Da). Again, lipid binding events were observed, and 45 AmtB-lipid species were assigned (Figure 9). However, it is clear the limitations of this instrument's resolution are becoming realized with this complex mixture of lipids. Though the majority of species were fully resolved, several peaks were seen as shoulders of adjacent peaks. Continual progress in instrument development, protein purification, and lipid modifications will drive us towards these currently "unanswerable" discoveries in the future.

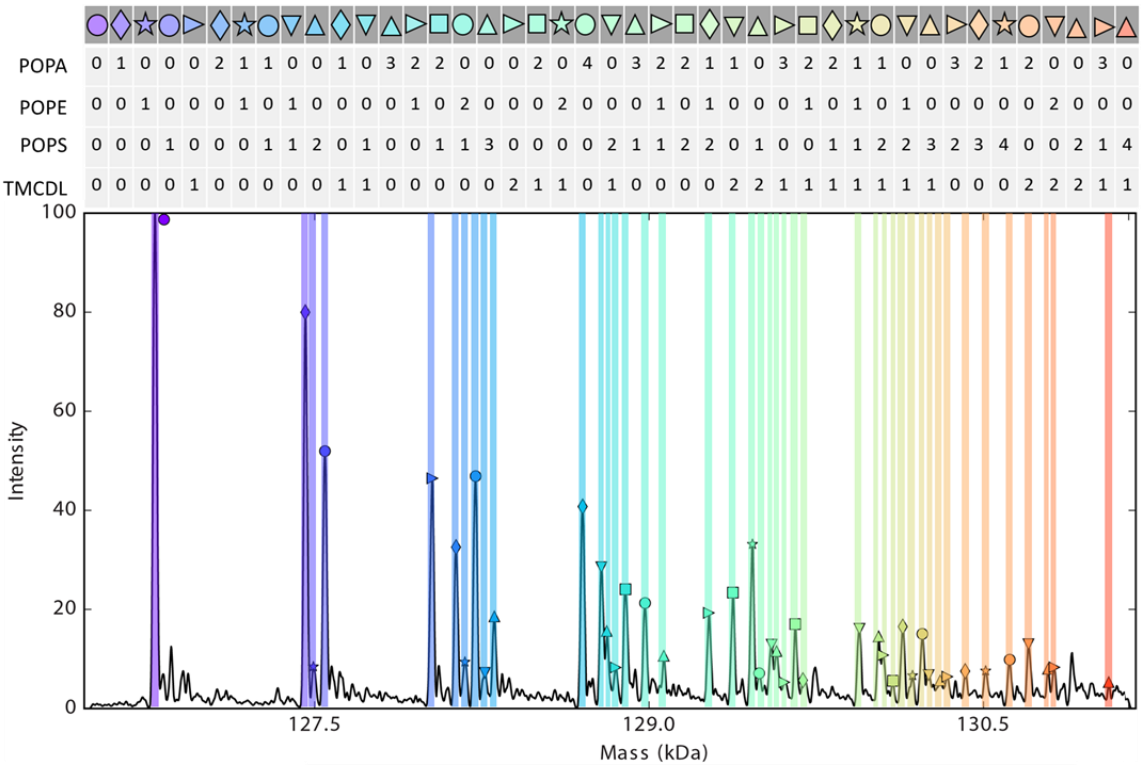

Figure 9. REIS-Orbitrap can resolve complex mixtures of AmtB bound to four different lipid species: POPA, POPE, POPS, and TMCDL. Forty-five lipid species bound to AmtB were observed. Reprinted by permission from Springer Nature: Journal of the American Society for Mass Spectrometry. “Development and Evaluation of a Reverse-Entry Ion Source Orbitrap Mass Spectrometer” by Poltash, M.P.; McCabe, J.W.; Patrick, J.W.; Laganowsky, A.; Russell, D.H., Journal of the American Society for Mass Spectrometry, 2019, 30(1), 192-198.

Conclusions

Here, proof-of-concept experiments were performed to illustrate the ability to modify the orbitrap platforms with REIS. Mass spectra for ubiquitin and AmtB illustrate the retention of functionality of the commercial orbitrap instrument. Furthermore, the REIS was shown to be capable of the same mass spectral performance in terms of mass resolution as the unmodified instrument. Comparisons of the modified source to a Waters

Synapt G1 demonstrate that the modified instrument is capable of recording native measurements. This development opens the door to future instrument modifications wherein additional gas phase coupled techniques such as IMS can be adapted to the existing Exactive platform architecture.

CHAPTER III

FOURIER TRANSFORM-ION MOBILITY-ORBITRAP MASS SPECTROMETER: A NEXT-GENERATION INSTRUMENT FOR NATIVE MASS SPECTROMETRY[1]

Introduction

Mapping the structural heterogeneity (folded and misfolded states) of proteins and protein complexes[13, 64, 65] and how post-translational modifications (PTMs)[86] and interactions with ligands, i.e., metal ions,[87, 88] small molecules,[17, 66, 89] osmolytes (chemical chaperones),[90] influence protein stability as well as the structure-function relationships represents a major challenge to the field of structural biology. Such challenges, previously described as "characterizing the conformationome,"[13] are increasingly studied using native electrospray ionization (ESI)-ion mobility (IM)-mass spectrometry (MS). The term "native-ESI" denotes that the analyte is sprayed from a nondenaturing solvent and conditions (i.e. solvent composition, pH, temperature, etc.) that yield low charge state ions that retain solution-phase conformational preferences and non-covalent interactions.[7, 8, 67] IM-MS, which provides information on the size of the gas phase ion, has rapidly gained popularity for structural (2º, 3º, and 4º) characterization of gas phase ions.[50-52] Combining IM with native MS, which independently measures both size and *m/z* of the ions, imposes additional constraints; ions formed by "native-ESI" must not be perturbed during the

[1] Reprinted with permission from Poltash, M.L.; McCabe, J.W.; Shirzadeh, M.; Laganowsky, A.; Russell, D.H. "Fourier Transform-Ion Mobility-Orbitrap Mass Spectrometer: A Next-Generation Instrument for Native Mass Spectrometry" *Analytical Chemistry*, 2018, *90(17)*, 10472-14078. Copyright 2018 American Chemical Society.

transition from solution to the gas phase as well as during subsequent analysis of the gas-phase ions.[19, 91] Although native-ESI-IM-MS does not provide the same level of structural detail as does spectroscopic techniques such as circular dichroism (CD), Förster resonance energy transfer (FRET), X-ray crystallography, and NMR, which measure the populationally-averaged signals, IM-MS is the only biophysical structural characterization technique capable of determining how protein structure(s) responds to specific changes in the local environment at the populational level.[80, 81, 92] Moreover, temperature-dependent MS binding studies is the only method to elucidate thermochemistry of individual binding events, particularly for systems that bind multiple ligands.[10, 11] However, the resolution of current IM-MS instrumentation is often inadequate for a number of biophysical studies of protein-ligand interactions due to poor resolving power. New instrumentation is needed to address how ligand binding may alter conformational preferences of the target protein, and whether these binding events alter binding of additional ligands. Addressing these types of questions is essential for a better understanding of allostery and cooperativity, fundamental properties of macromolecules. Great strides have been made in the development of IM-MS instrumentation for structural characterization of biomolecules, but the instruments were largely developed for proteomics research. Moreover, these instruments are not optimized for studies of large proteins and their complexes. Realizing the full potential of native-ESI-IM-MS for studies of large proteins and their complexes necessitates major advances in instrumentation, most notably enhanced mobility (R_{IM}) and mass ($R_{m/z}$) resolution, while retaining capabilities for preserving non-covalent interactions and accurate determinations of ion-neutral collision cross sections (CCS).

Coupling DT-IM to high performance MS, such as hybrid IM-q-ToF instruments, is relatively straightforward because IM separation is slow relative to the acquisition of the ToF mass spectrum. However, when using ion trapping MS (e.g. Orbitraps) an inherent duty cycle mismatch exists as both the DT IM separation and the mass scans occur on approximately the same time scale. Consequently, the MS cannot efficiently capture mobility information across the full arrival time distribution (ATD), such limitations have severely hampered the development of IM-Orbitrap instruments.[59, 60]

There exists little doubt that biomolecule IM-MS was greatly accelerated by the introduction of traveling-wave (TW) IM-q-ToF instruments,[93] and remarkable progress has been realized. in spite of the limitations of TWIMS-MS, viz. low-resolution ion mobility ($t_d/\Delta t_d$) measurements, requirement for calibration methods for determining rotationally-averaged ion-neutral collision cross sections (CCS), and limited mass resolving power (RP = M / ΔM, where ΔM = (M2–M1), the difference in mass of two ions having different masses) of the ToF instrument. Here, we describe a novel native-ESI-FT-DT-IM-Orbitrap MS (Figure 10) specifically designed for structural studies of large proteins, protein complexes, and their interactions with small molecules and other proteins. Although other IM-Orbitraps have been developed,[59, 60] these instruments were not designed for preserving non-covalent interactions and are unable to be used for native MS due to their configuration and design. Conversely, this new instrument, which we denote as “next-generation”, incorporates all the essential components developed over the past decade that define “native MS”. Specifically, (i) ion formation conditions are optimized for retention of solution phase structure(s), viz. static-spray ESI emitters

ranging in size from micron to sub-micron that are compatible with the use of "native-like" solvents for forming low charge states that have low internal energy;[7, 8, 94] (ii) periodic focusing (PF) drift tube (DT) IM that operates under low electric field strengths, which minimizes collisional heating of the ions, allows for first-principles determinations of the ion's rotationally-averaged CCS, and provides ion radial focusing for increased ion transmission;[32, 37] (iii) IM data acquisition is performed using a Fourier-transform (FT) IM-MS method first described by Hill and more recently by Clowers;[43, 44] and (iv) mobility separated ions are then mass analyzed using the high RP Orbitrap MS.[24, 55, 56]

We have previously shown the importance of improved RP in native MS using an Orbitrap over IM-ToF MS to characterize heterogeneous lipid binding events to the trimeric ammonia transport channel (AmtB), an integral membrane protein.[24] More specifically, IM-ToF MS simply does not possess sufficient RP to separate the individual lipids bound, whereas the Orbitrap MS successfully separated 46 different combinations of lipids bound to AmtB. Notably, $R_{m/z}$ of native mass spectra are markedly lower than small molecules (viz. metabolites, carbohydrates, lipids, and peptides) due to the size and heterogeneity of large proteins and their complexes; therefore, direct $R_{m/z}$ comparisons between native MS and small molecule MS should not be made.

The major impetus for development of new IM-MS technologies focused on structural biology is the need to study protein complexes and their interactions with small molecules (e.g. drugs), metal ions, peptides/proteins, and nucleic acids. As a first step, the instrument performance was characterized using a number of well-studied model monomeric soluble proteins, i.e. cytochrome C, ubiquitin, and lysozyme. We then

demonstrate the novel capabilities of native-ESI-FT-DT-IM-Orbitrap MS instrument by investigating protein complexes (streptavidin, GlnK, and transthyretin [TTR]) and their interactions with small molecule(s) (streptavidin•biotin, GlnK•ADP and TTR•Zn(II) and TTR•thyroxine [T_4]).

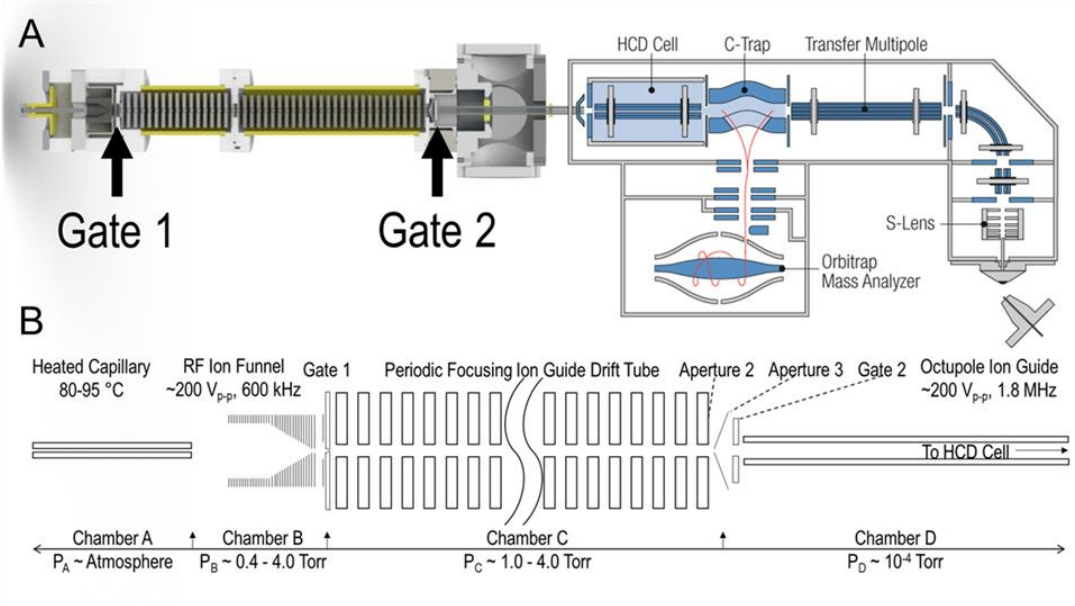

Figure 10. (A) Solidworks rendering of the homebuilt native-ESI-FT-DT-IM coupled to the HCD cell of an Orbitrap MS. (B) A detailed schematic representation of the homebuilt platform. From left to right depicts a heated capillary for ion introduction via nESI (not pictured) and an RF ion funnel to focus ions into the gating region. Ions are injected via gate 1 into a 58 cm PF DT and selectively transmitted through gate 2 into an RF only octupole ion guide. Mobility modulated ions are then loaded and trapped in the HCD cell of the Orbitrap where they are subsequently transferred to the C-Trap then injected into the Orbitrap for mass analysis. Reprinted with permission from Poltash, M.L.; McCabe, J.W.; Shirzadeh, M.; Laganowsky, A.; Russell, D.H. "Fourier Transform-Ion Mobility-Orbitrap Mass Spectrometer: A Next-Generation Instrument for Native Mass Spectrometry" Analytical Chemistry, 2018, 90(17), 10472-14078. Copyright 2018 American Chemical Society.

Experimental

Instrumentation

For these experiments, the nano-ESI source previously described was mounted onto a PF DT.[24] The nano-ESI uses pulled borosilicate glass capillaries, prepared in-house, that are either gold coated or contain a platinum wire (300 µm) inserted into the capillary. ESI potentials of 1.50-2.00 kV were used for all studies. Ions formed by nano-ESI enter a heated metal capillary, where the final stages of ion dehydration occur, and then focused using a radiofrequency (RF) ion funnel (200-250 V_{p-p}, 600 kHz, Ardara Technologies, Ardara, PA) maintained at a gas pressure between 2.0 and 2.5 Torr. Ions exiting the RF ion funnel are focused through gate 1 to introduce a packet of ions into the DT. A 58 cm PF DT, maintained at a constant helium flow, is used for IM separation. PF DTs rely on ion optic geometries (8 mm I.D., 6.35 mm width, 6.35 mm spacing) to produce a distant-dependent effective potential mimicking RF focusing as ions traverse each electrode of the DT.[33-35] A voltage gradient of 10 V/cm at ~2.0 Torr was used for all experiments, which corresponds to being expressed as 5 V/(cm·Torr) or Townsends (T_d). Mobility separated ions exit the DT by modulating gate 2 and are subsequently introduced to an RF-only octupole ion guide (200-250 V_{p-p}, 2.5 MHz), which is used to focus the ions into the HCD cell of an Exactive Plus with Extended Mass Range Orbitrap MS (Thermo Fisher Scientific, San Jose, CA). This interface region and Orbitrap operating parameters have been described in detail previously.[24] Briefly, the Orbitrap mass spectrometer was tuned using typical operating parameters: collision energy (CE) in the HCD cell was set to 10 V to minimize post mobility fragmentation, maximum injection time was set to 200 ms,

trapping gas pressure was set between 4-7 au, and Orbitrap resolution of 17,500-35,000 was selected as it yielded higher quality mass spectra. IMS and Orbitrap electronics were synchronized externally using an Arduino Leonardo to trigger FT-IMS pulsing and contact closure, respectively.

Operation of a Dual Gate Fourier Transform IMS

Many conventional IM-MS instruments use single gate instrument configurations to introduce discrete ion packets into a drift cell followed by detection using comparatively fast mass analyzers to acquire nested IM-MS spectra. This so-called "pulse-and-wait" sampling mode has a duty cycle of less than 1%, i.e., greater than 99% of the total ion population is not sampled. Using a dual gate platform, ion entry into the DT is controlled by gate 1. Gate 2 is positioned at the rear of the DT to select a specific ion arrival time that is then transmitted for mass analysis.[40, 41, 95, 96] The time delay between pulsing gates 1 and 2 defines the drift time of the detected ions; the experiment is repeated with different time delays to acquire an entire ATD. An added benefit to the dual-gate platform is the potential to eliminate the need for multifield calibrations to determine the time ions spend outside of the DT by placing gates directly before and after the DT. While this approach is effective, only 0.01% of ions are analyzed reducing instrument sensitivity and significantly slowing data acquisition, and results are entirely dependent upon highly stable ionization sources.

To overcome the low duty cycle of a basic dual gate pulsing platform, a variety of multiplexed acquisition modes have been developed for IM-MS,[97-99] and very recently

Clowers and co-workers have re-introduced Fourier-transform (FT)-IMS originally introduced by Hill.[43, 44] Here, we implemented FT-IMS which was first described to improve the duty cycle of time dispersive IMS platforms by modulating the dual gates of the DT. This provides 25% ion transmission with improved spectral quality and dramatically improved acquisition times. Operating in FT-IM, the DT is used as a frequency-dependent filter (or $1/t_d$ filter) by synchronously modulating gates 1 and 2 with square waves that are linearly swept from low (5 Hz) to high (7 kHz) frequencies over multiple minutes. The frequency encoding of ion mobility information is possible because ions are transmitted only when their drift time (t_d) is correlated with the frequency ($v = 1 / t_d$) of the gating; therefore, by sampling across a range of frequencies, a signal (S) will be obtained with a frequency dependence of:

$$S(v)_{max} = 0.5\, I_0 \;\; when: \;\; t_d = 0, \frac{1}{v}, \frac{2}{v}, \frac{3}{v}, \ldots \qquad (3)$$

$$S(v)_{min} = 0 \;\; when: \;\; t_d = \frac{1}{2v}, \frac{3}{2v}, \frac{5}{2v}, \ldots \qquad (4)$$

Where I_0 is the ion intensity without any pulsing. The resultant oscillating signal, for an isolated ion, can be Fourier transformed to determine the frequency of transmission. This frequency is directly related to ATD ($t_d = v^{-1}$) and can therefore be correlated by dividing the frequency axis by the sweep rate, resulting in the ATD of an ion. The FT-IMS workflow is summarized in Figure 11.

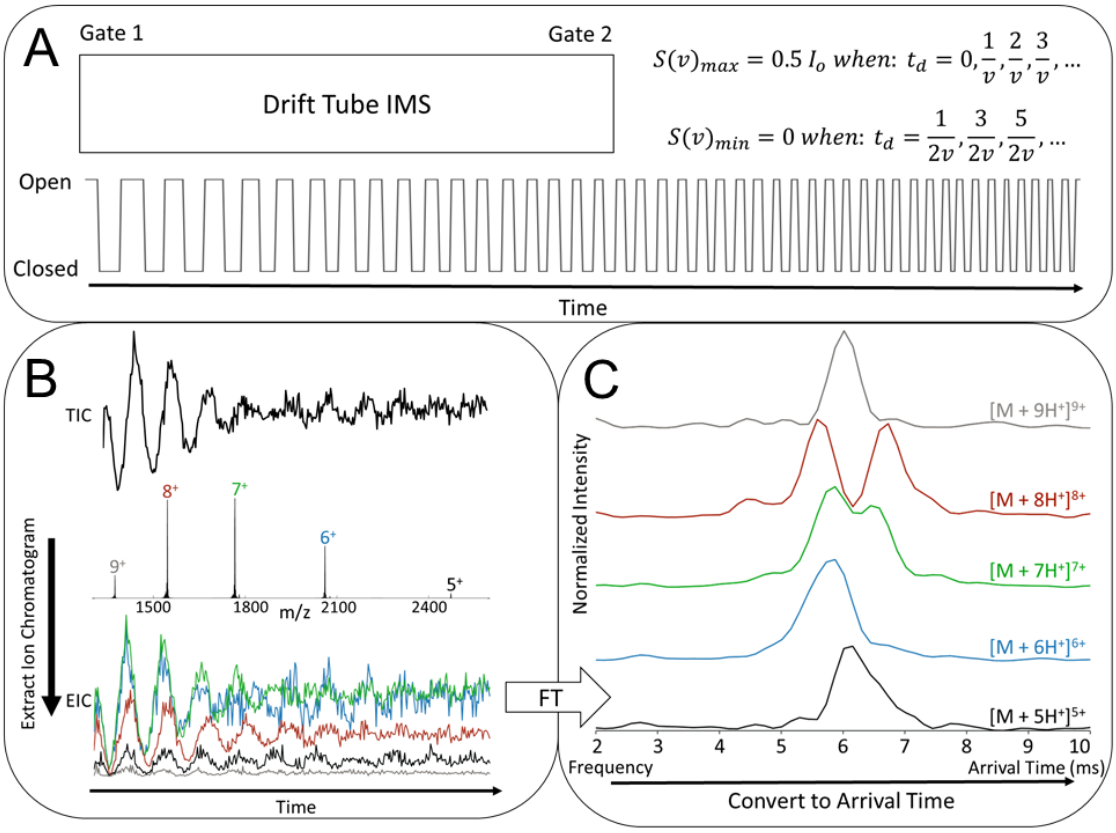

Figure 11. (A) The dual gates at the entrance and exit of the DT are synchronously pulsed with a square waveform with a linear chirp frequency from 5 to 7000 Hz. Applying this waveform turns the DT into a frequency-dependent filter with transmission characteristics aligning with the stated equations. (B) Mass spectral data is acquired with an associated total ion chromatogram (TIC) from which an extracted ion chromatogram (EIC) can be determined by isolating a single *m/z* abundance over time. A TIC, MS, and EIC are shown for the model protein cytochrome C. (C) EIC's can be FT to determine the frequency of transmission which is correlated to arrival time by a direct relationship. Exemplary ATD's were extracted from the cytochrome C data in panel B. Reprinted with permission from Poltash, M.L.; McCabe, J.W.; Shirzadeh, M.; Laganowsky, A.; Russell, D.H. "Fourier Transform-Ion Mobility-Orbitrap Mass Spectrometer: A Next-Generation Instrument for Native Mass Spectrometry" Analytical Chemistry, 2018, 90(17), 10472-14078. Copyright 2018 American Chemical Society.

For this study, FT-IMS was implemented using custom linear sweep waveforms (5 to 7000 Hz over 8 min) generated via a Python script and uploaded to a National Instruments PXI-5421 waveform generator used to trigger gating events. DEI PVX-4140 pulse generators were used to apply square waves to gates 1 and 2.

Benchmarking the Instrument

To benchmark the new instrument, we first analyzed cytochrome C (Figure 11B and C), ubiquitin (Figure 12 and Figure **13**), and lysozyme (Figure **14**). Figure 11 (B and C) shows the MS and extracted ATDs of the five observed charge states of cytochrome C analyzed in water with 1% acetic acid, and align well with ATDs reported by a number of studies.[100-103] The lower charge states of cytochrome C, $[M + 5H^+]^{5+}$ and $[M + 6H^+]^{6+}$, exhibit compact, native-like conformers. A charge-dependent unfolding is then observed where $[M + 7H^+]^{7+}$ populates the partially-unfolded intermediate conformer, $[M + 8H^+]^{8+}$ populates both the intermediate and fully-unfolded extended conformer, and $[M + 9H^+]^{9+}$ populates only the extended conformer. Moreover, ATDs for both ubiquitin and lysozyme are also in agreement with previous studies (Figure 13 and Figure 14).[19, 100, 103, 104]

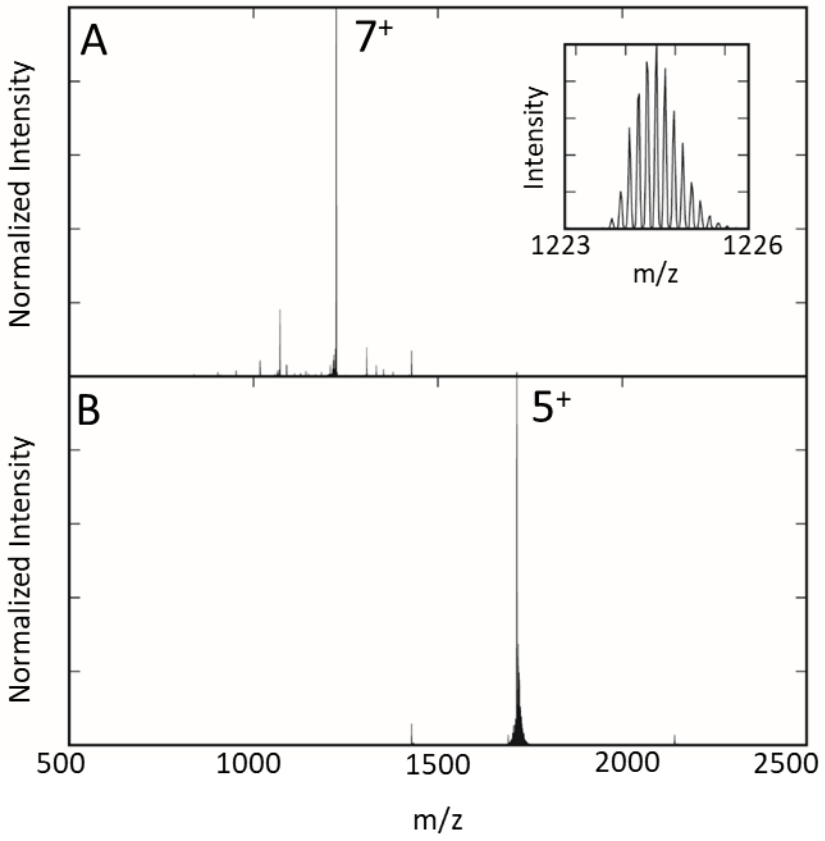

Figure 12. Mass spectra of ubiquitin in (A) water with 1% acetic acid and (B) water with 100 mM ammonium acetate. Ubiquitin charge states in water with 1% acetic acid are centered at $[M + 7H^+]^{7+}$, but in water with 100 mM ammonium acetate the charge state is centered about $[M + 5H^+]^{5+}$. The Orbitrap mass analyzer is able to achieve a max $R_{m/z}$ greater than 35000 for ubiquitin allowing for isotopic resolution as shown in the inset of panel A. Reprinted with permission from Poltash, M.L.; McCabe, J.W.; Shirzadeh, M.; Laganowsky, A.; Russell, D.H. "Fourier Transform-Ion Mobility-Orbitrap Mass Spectrometer: A Next-Generation Instrument for Native Mass Spectrometry" Analytical Chemistry, 2018, 90(17), 10472-14078. Copyright 2018 American Chemical Society.

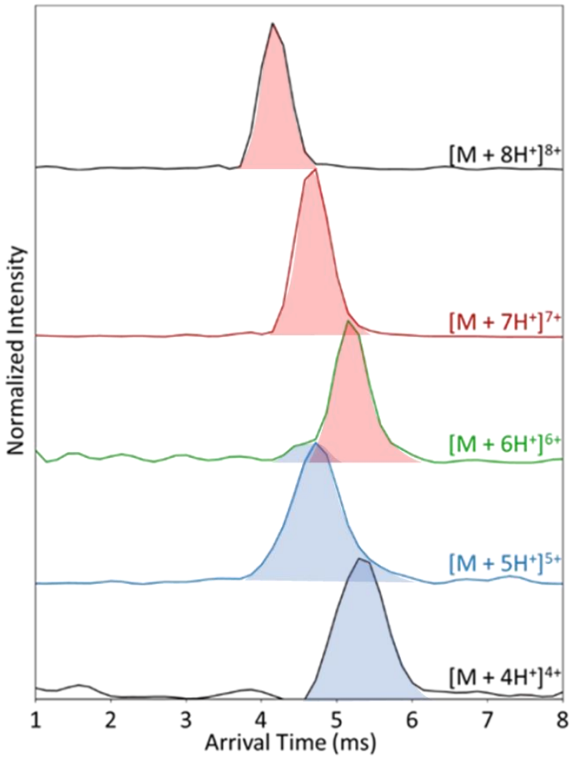

Figure 13. Extracted drift profiles of the $[M + 4H^+]^{4+}$ through $[M + 8H^+]^{8+}$ ions of ubiquitin. The ATD for $[M + 4H^+]^{4+}$ and $[M + 5H^+]^{5+}$ were extracted from the mass spectrum collected in water with 100mM ammonium acetate whereas the ATD for $[M + 6H^+]^{6+}$ through $[M + 8H^+]^{8+}$ ions were extracted from the mass spectrum collected in water with 1% acetic acid. Low charge states of $[M + 4H^+]^{4+}$ and $[M + 5H^+]^{5+}$ exhibit compact, native-like conformers (blue). Additional charges lead to a charge state dependent unfolding where the $[M + 6H^+]^{6+}$ ion populates the compact conformer and the slightly unfolded intermediate conformer (red), and the $[M + 7H^+]^{7+}$ and $[M + 8H^+]^{8+}$ populate only the intermediate conformers. These data match those reported by a number of studies.[19, 101, 104] Reprinted with permission from Poltash, M.L.; McCabe, J.W.; Shirzadeh, M.; Laganowsky, A.; Russell, D.H. "Fourier Transform-Ion Mobility-Orbitrap Mass Spectrometer: A Next-Generation Instrument for Native Mass Spectrometry" Analytical Chemistry, 2018, 90(17), 10472-14078. Copyright 2018 American Chemical Society.

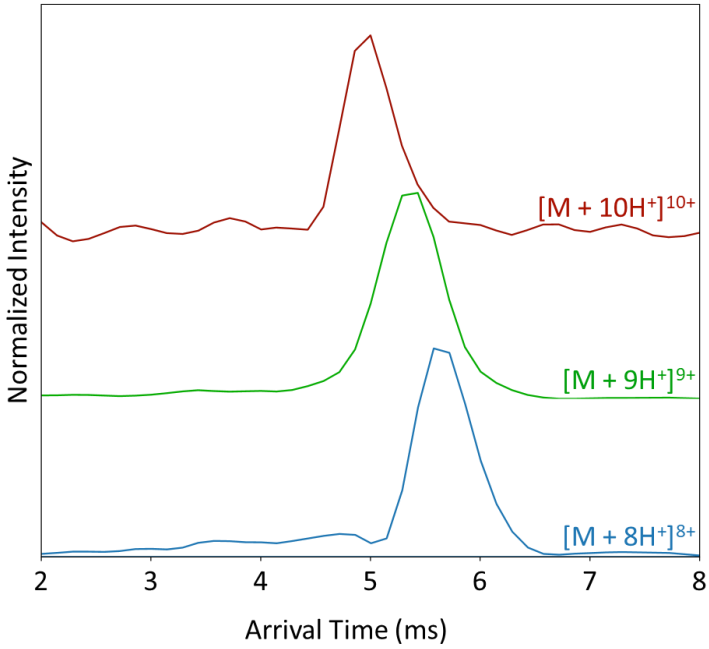

Figure 14. Extracted drift profiles of lysozyme in water and 1% acetic acid for $[M + 8H^+]^{8+}$ through $[M + 10H^+]^{10+}$ ions. Compact conformers are observed for all three charge states, and no charge state-dependent unfolding was observed. This is interpreted as evidence that the ions are formed with low internal energies.[100, 103] Reprinted with permission from Poltash, M.L.; McCabe, J.W.; Shirzadeh, M.; Laganowsky, A.; Russell, D.H. "Fourier Transform-Ion Mobility-Orbitrap Mass Spectrometer: A Next-Generation Instrument for Native Mass Spectrometry" Analytical Chemistry, 2018, 90(17), 10472-14078. Copyright 2018 American Chemical Society.

Data Processing

Mass spectral data were acquired using the Exactive software to generate RAW format data. RAW data was converted using a Python script making use of Multiplierz.51 Extracted ion chromatograms were obtained from RAW MS data using custom Python scripts written in-house, and the extracted data were processed and subjected to Fourier transformation using custom Python scripts.

Chemicals and Materials

GlnK and TTR were expressed and purified in-house as described previously.[10, 105] Streptavidin, cytochrome C, bovine ubiquitin, and lysozyme were purchased from Sigma Aldrich and used without further purification. All complexes were buffer exchanged using a centrifugal buffer exchange device (Micro Bio-Spin 6, Bio-Rad) into 200 mM ammonium acetate before analysis. ADP (ammonium salt), biotin, and T4 were purchased from Sigma Aldrich. Biotin and T_4 were first diluted in DMSO before diluting to 15 µM in 200 mM ammonium acetate. ADP was dissolved and diluted to 15 µM in 200 mM ammonium acetate.

Results and Discussion

Periodic Focusing Drift Tube

A major challenge of uniform field-IM for the analysis of protein complexes is poor transmission of these ions due to radial diffusion as they traverse the DT. To overcome this issue, the IM-Orbitrap MS takes advantage of a PF DT which exhibits high ion transmission by minimizing radial diffusion. The PF DT device also removes the necessity for an ion funnel at the end of the DT as employed in other IM devices.[32, 33] PF-DT IM improves radial focusing through the unique geometry of electrodes utilizing thicker electrodes and a smaller I.D. to generate effective RF (~kHz frequency) potentials between each electrode to periodically focus ions radially, thereby improving ion transmission.[34, 35] Although previous descriptions of PF-IM were limited to studies of peptides and small proteins, more recent SIMION 8.1 trajectory simulations clearly show

that the increased numbers of charges and masses of larger proteins provide even higher radial focusing.[36]

Protein Complexes: Streptavidin, GlnK, and Transthyretin

Improvements over traditional IM-ToF instruments, where RP is most often a limitation, are illustrated by analyzing the 3º and 4º structures of protein complexes and their interactions with ligands. Here, we explored streptavidin•biotin, GlnK•ADP, TTR•T_4 and, TTR•Zn(II) complexes. Monitoring such ligand binding events are difficult or nearly impossible to resolve using ToF mass analyzers.[24, 49, 85, 89] These observations lend insight into the effects of small molecule and ligand binding on the protein structure-function relationships at unprecedented detail.

Streptavidin, a homo-tetrameric 53 kDa protein complex, was analyzed using the native-ESI-FT-DT-IM-Orbitrap MS. Each streptavidin monomer can individually bind one biotin molecule wherein each of the four binding sites of the tetramer are thermodynamically equivalent.[106] The streptavidin-biotin interaction, one of the most stable in nature (K_a of ~2.5 x 10^{13} M^{-1}),[107] has been well-characterized using a variety of techniques.[108] The streptavidin-biotin interaction has been observed in previous IM-MS studies, however, these studies utilized non-natural fluorescein tagged derivatives (biotin-4-fluorescein) to increase mass separation between the unbound and ligated streptavidin complexes to overcome limited RP.[89] Here, we analyzed the streptavidin-biotin complex using natural biotin. Mass spectra of the apo-streptavidin and holo-streptavidin complexes are shown in Figure 15A where a shift in *m/z* denotes the addition of four biotin molecules

to the complex. The additional peaks (*) observed represent streptavidin with additional methionine residues on the N-terminus, a result of the protein expression process. While these modified proteins were observed mass spectrally, extracted ATDs did not include these modifications. Figure 15B shows the extracted ATDs of apo-streptavidin and holo-streptavidin. Apo-streptavidin exhibits a slightly lower drift time compared with holo-streptavidin, an expected shift with the addition of four small molecules. Interestingly, the ATD for holo-streptavidin is narrower than that of the apo-streptavidin. This compaction is associated with an increased structural stability and homogeneity, an observation aligned with previous findings.[108, 109] To our knowledge, this represents the first example of IM-MS resolving the streptavidin and natural biotin interaction.

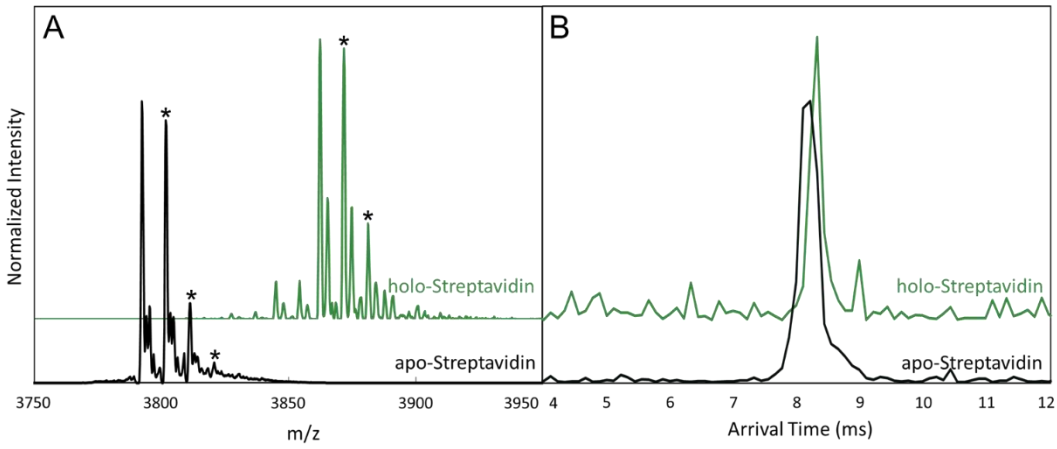

Figure 15. (A) The mass spectrum and (B) extracted ATD of $[M + 14\ H^+]^{14+}$ apo-streptavidin and the holo-streptavidin complexes. A small shift in drift time was observed upon binding four biotin molecules as well as a compaction of peak width. *Denotes additional N-terminal methionine residues on streptavidin and were not included in the extracted ATDs. Reprinted with permission from Poltash, M.L.; McCabe, J.W.; Shirzadeh, M.; Laganowsky, A.; Russell, D.H. "Fourier Transform-Ion Mobility-Orbitrap Mass Spectrometer: A Next-Generation Instrument for Native Mass Spectrometry" Analytical Chemistry, 2018, 90(17), 10472-14078. Copyright 2018 American Chemical Society.

The PII transduction protein GlnK (MW 44 kDa) is a homo-trimeric protein complex that negatively regulates the ammonium ion transport of AmtB by plugging the channel of AmtB,[110] and this process plays a key role in nitrogen regulation of cells.[111] Crystallography data suggest two conformations of GlnK exist where the T-loop of a monomer can form an α-helix (CCS_{TJM} = 2746 Å^2) or extended β-hairpin (CCS_{TJM} = 3427 Å^2);[112] the two conformers are potentially important in regulating its interactions with AmtB.[113] Additionally, each monomer of GlnK is able to bind a single ADP; however, the effects of individual ADP-binding on protein structure and function is not fully understood.[114] GlnK was analyzed via the native-ESI-FT-DT-IM-Orbitrap MS to explore its structure in complex with ADP as seen in Figure 16. Mass spectral data for GlnK after expression and purification showed the presence of the apo-GlnK complex and up to two ADPs bound (Figure 16A). A three-fold addition of ADP shifts the equilibrium to the holo-GlnK complex (three ADP molecules bound), and additional, non-specific ADP binding is observed with four and five ADP bound (Figure 16B).

Extracted ATD of apo-GlnK (Figure 16C) confirms the presence of two distinct protein conformers with the appearance of two peaks potentially representing the T-loop adopting an α-helix or β-hairpin. The more compact, α-helical T-loop conformer "closed-state", appears as the dominant peak and the right shoulder shows the presence of the larger β-hairpin T-loop "open-state". The stepwise addition of ADP to GlnK promotes the open-state, where GlnK•ADP_1 shows a slightly more abundant open-state, GlnK•ADP_2 populates both the open- and closed-states with a slightly higher abundance of open-state, and holo-GlnK shows the open-state with little closed-state present. Sakai et al. previously

suggested holo-GlnK exhibits the disordered T-loop; however, it remains unclear if one or two ADP molecules bound to GlnK is sufficient to promote a regulatory interaction with AmtB.[113]

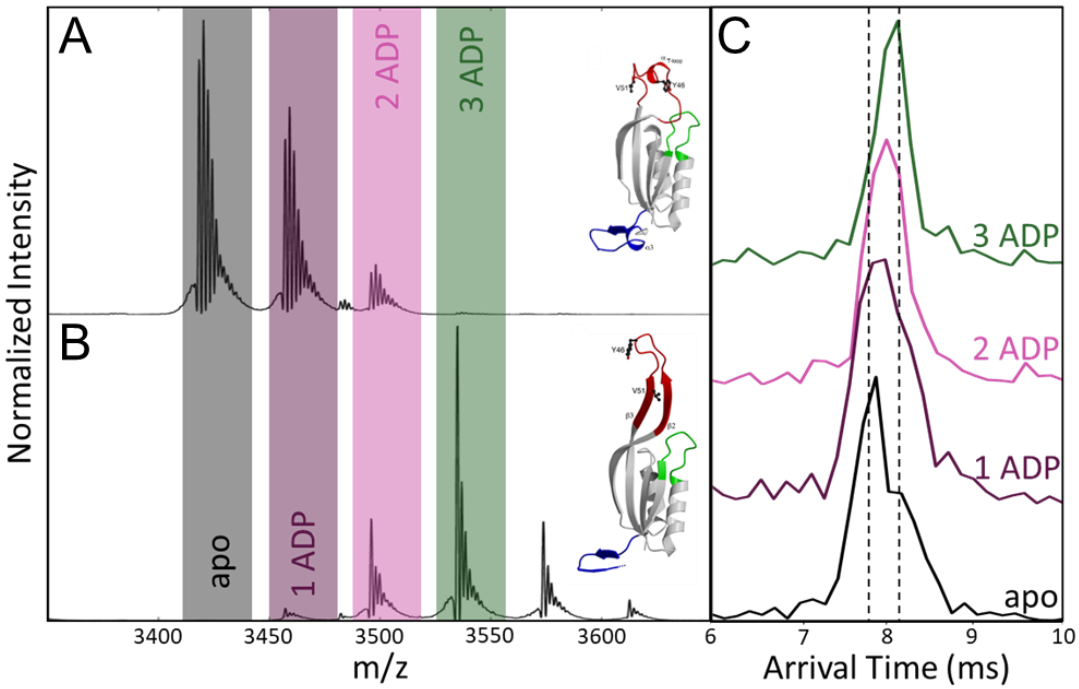

Figure 16. Mass spectra of GlnK (A) and GlnK with a three-fold addition of ADP (B). The observed adducts on the GlnK were sodium adducts and were not included in the ATD extractions. (C) The extracted ATDs of the $[M + 11\ H^+]^{11+}$ GlnK•ADP complexes. PDB ID: (top) 1HWU and (bottom) 1QY7.[113] Reprinted with permission from Poltash, M.L.; McCabe, J.W.; Shirzadeh, M.; Laganowsky, A.; Russell, D.H. "Fourier Transform-Ion Mobility-Orbitrap Mass Spectrometer: A Next-Generation Instrument for Native Mass Spectrometry" Analytical Chemistry, 2018, 90(17), 10472-14078. Copyright 2018 American Chemical Society.

TTR is a 56 kDa, homo-tetrameric protein complex involved in degenerative diseases such as amyloidosis where partially unfolded monomers from tetramer dissociation can result in amyloid fibril formation.[115] TTR participates in the transport of the natural hormone T_4 and the association of TTR and T_4 is effective in inhibiting amyloid fibril formation.[116] Here, TTR was studied in the presence of its transport partner T_4 to explore the effect of binding on protein structure. Figure 17A shows the mass spectrum obtained of TTR in the presence of T_4 and up to 2 T_4 molecules bound to TTR. In addition to T_4 binding, each protein-ligand complex surprisingly exhibits additional binding to Zn(II) discussed in greater detail below. ATDs in Figure 17B exhibit slightly longer drift times of TTR with successive T_4 bound. The peak width of the holo-TTR•T_4 structure was reduced with respect to apo-TTR indicative of greater homogeneity in protein structure as well as greater protein stability.

In addition to its transport activity, TTR is reported to be a metallopeptidase when complexed with Zn(II).[117] While Zn(II) binding is important for proteolytic activity, Palmieri et al. reported Zn(II) binding noticeably increased the rate of TTR aggregation.[48] The high-RP mass analysis fully resolves TTR•Zn(II) complexes, and the overall sensitivity of the instrument is sufficient for IM-MS analysis as shown in Figure 17C. The addition of Zn(II) extends the drift time of TTR which is consistent with the formation of an extended conformation with partial unfolding of the complex. Owing to the limited RP of IM-ToF, previous IM-MS studies for the TTR•T_4 complex may have contained signals relating to TTR•Zn(II) complexes masked by poor resolving power. It should be noted

that the abundances of Zn(II) and T_4 are independent of one another indicating that there is no cooperative or competitive binding between the two.

Observations of protein-ligand complexes such as the streptavidin•biotin, GlnK•ADP, TTR•Zn(II), and TTR•T_4 highlight the importance of high-resolution IM-MS measurements for biophysical studies. Lower RP often mask the intricate details that underlie protein-ligand interactions as it simply cannot adequately resolve such species. Moreover, protein heterogeneity can lead to inaccurate structural measurements of protein complexes rendering protein-ligand species unresolvable. The presented data show the possibility that these ligand-bound species have distinct structures and play a role in the functionality of the protein.

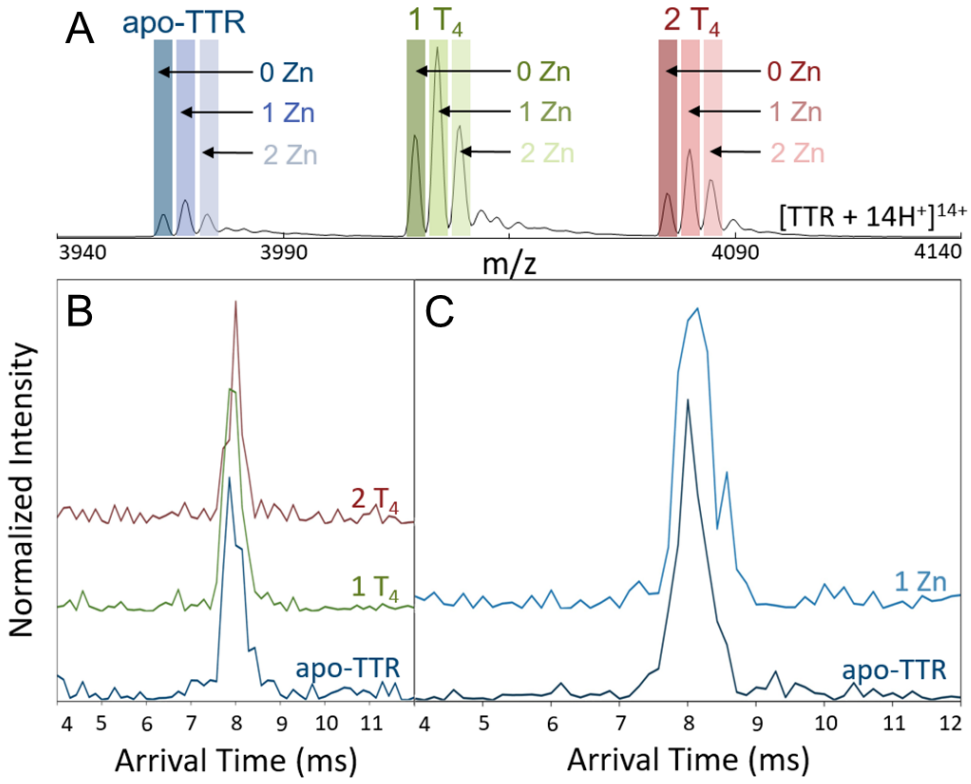

Figure 17. (A) A representative mass spectrum of the $[M + 14\ H^+]^{14+}$ TTR complex with binding of up to two T4 and Zn(II). A mass resolving power of 840 is required to separate the apo-Zn(II) containing ions with the orbitrap. (B) The extracted ATDs of TTR binding to one and two T4's. (C) The extracted ATDs of TTR bound to Zn(II). Reprinted with permission from Poltash, M.L.; McCabe, J.W.; Shirzadeh, M.; Laganowsky, A.; Russell, D.H. "Fourier Transform-Ion Mobility-Orbitrap Mass Spectrometer: A Next-Generation Instrument for Native Mass Spectrometry" Analytical Chemistry, 2018, 90(17), 10472-14078. Copyright 2018 American Chemical Society.

Conclusions

For the first time, IMS was coupled to the HCD cell of an Orbitrap MS for high-resolving power IM-MS measurements, and these results clearly illustrate increased performance of ion mobility-mass spectrometry necessary for the next generation of biophysical studies of intact protein complexes. In its current configuration, a R_{IM} of ~40 was achieved for intact protein complexes and, to best of our knowledge, represents the highest resolution IM measurements made on such systems. The union of PF-DT and FT-IMS provides not only improved ion transmission that aids data acquisition, but also allows for higher throughput sample processing over that obtained using duty cycle mismatched instruments. For example, using the native-ESI-FT-DT-IM-Orbitrap MS instrument the full IM and MS spectrum can be acquired in eight minutes or less. The range of protein complexes analyzed illustrates the importance of understanding the role that metal ions and small molecules play in protein conformational preferences, which would otherwise not be observed. The results reported herein make more detailed studies on other protein complexes possible, including exploring the effects of PTMs, protein-ligand interactions, and protein misfolding using high-resolution IM-MS.

CHAPTER IV

NEW INSIGHTS INTO THE METAL-INDUCED OXIDATIVE DEGRADATION PATHWAYS OF TRANSTHYRETIN[1]

Introduction

Transthyretin (TTR) is a homotetrameric protein complex responsible for the transport of thyroxine (T_4) and retinol through plasma and cerebrospinal fluid.[118, 119] TTR is also reported to be a metallopeptidase when complexed with Zn(II) with three distinct Zn(II) binding sites identified; however, excess Zn(II) binding is associated with decreased retinol transport functionality and increased rates of TTR fibril formation.[119] Aggregation of TTR is involved in degenerative diseases, *viz*. amyloidosis, and it is believed that partially unfolded monomers from tetramer dissociation are implicated in amyloid fibril formation.[120] TTR fibril formation underlies both hereditary and nonhereditary amyloidosis, the former is caused due to protein mutation i.e. familial amyloid polyneuropathy (FAP) and familial amyloid cardiomyopathy (FAC).[121] Wild-type TTR (WT-TTR) is associated with nonhereditary amyloidosis i.e. senile systemic amyloidosis (SSA) resulting in heart failure of 20% of elderly people (>70 years).[122] Furthermore, the role of TTR oxidation on protein stability and fibril formation is still debated. Maleknia et al. reports TTR oxidation occurs at Met-13 which may promote intramolecular tertiary contacts thus stabilizing the protein.[123] In contrast, Gales et al. observed that TTR fibrils contain significant oxidation of both Cys-10 and Met-13;

[1] This chapter was co-authored with Mehdi Shirzadeh.

however, were unable to identify whether oxidation occurred before or after fibril formation.[124] In neither case were the underlying causes or structural perturbation studied.

Native mass spectrometry (MS) has led to increasingly complex studies of proteins and protein complexes by revealing individual species which are often masked by ensemble- averaged measurements using classic structural techniques.[9] Coupling of ion mobility (IM) to native MS further enhances the applications of the technique by providing a second dimension of analysis, a structural collision cross section (CCS) measurement, describing the analyte size and shape nested with mass to charge (*m/z*). Native IM-MS analyses has enabled more detailed structural studies of protein complexes providing more precise and accurate measurements by revealing small perturbations in protein composition while also providing the time-resolved structural evolution of these proteins.[8, 67] We recently developed a novel high resolution (both in mass and mobility domains) IM-Orbitrap MS platform capable of maintaining native-like structures and non-covalent interactions.[38] IM-MS has been used previously to study TTR degradation;[49, 125] however, the detailed chemical interactions between the protein and its environment were masked by poor mass resolution. Here, we describe studies carried out using a specially designed high-resolution IM-Orbitrap MS instrument and a Waters Synapt G2 equipped with a custom surface induced dissociation (SID) cell to better understand the mechanism of metal-induced oxidation of TTR subunits, the first structural IM-MS study of its kind.

Experimental

Ion Mobility and Mass Spectrometry Instrumental Methods

The homebuilt IM-Orbitrap instrument has been described in detail previously. Briefly, ions are generated via static nano-ESI using glass capillaries pulled in-house. Voltages between 2.0 and 3.0 kV are applied to the solution using a platinum wire inserted into the solution. Generated ions are introduced to the instrument through a heated capillary and can be accelerated by a ring electrode before being focused by an RF ion funnel. Ions exiting the ion funnel are modulated using gate 1, thus approximately 50% of the ions enter the 1.45 m PF DT maintained at a helium pressure of ~1.5 Torr for mobility separation. A second gate (gate 2) is positioned at the exit of the DT, thus approximately 50% of the ions are transmitted to an RF-only octuople ion guide. These ions are then collected and trapped in the higher energy collisional dissociation (HCD) cell of the Orbitrap. Ions trapped in the HCD cell are relaxed and transferred to the C-trap which injects ions into the Orbitrap for mass analysis. Orbitrap settings of 100 ms maximum inject times and resolution of 17 500 were used for all experiments. A schematic of the instrument and the details of operation of the instrument with its implementation as a Fourier transform-IM-MS instrument has been described elsewhere.[38]

Surface induced dissociation (SID) experiments were performed on a modified Waters Synapt G2. Samples were also introduced by static nano-ESI with a capillary voltage between ~1.2 and 1.5 kV using the same emitters as described above. Other parameters include: source pressure (5-6 mBar), sampling voltage (20 V), trap flow (2

L/min) and He flow (120 ml/min).

Size-Exclusion Chromatography

Superdex HiLoad 16/600 75 pg column (ÄKTA Explorer, GE Healthcare) was used for size exclusion chromatography. The column was equilibrated and eluted with HEPES (50mM), NaCl (50mM), EDTA (10mM) and DTT (1mM), pH=7.4 at 4 °C.

Data Treatment

Raw MS data was acquired using Exactive software and converted using Python scripts making use of *Multiplierz*. Extracted ion chromatograms were subsequently obtained and processed using custom Python scripts. IMS peak fitting was accomplished using Origin with R^2 thresholds > 0.95.

Transthyretin Preparation

TTR was expressed and purified in-house as described previously.[10] Samples were buffer exchange using centrifugal buffer exchange devices (Micro Bio-Spin 6, Bio-Rad) into 200 mM ammonium acetate before analysis. Copper acetate, zinc acetate, N-ethylmaleimide (NEM), and Chromium(VI) ICP standard were purchased from Sigma Aldrich and diluted in 200 mM ammonium acetate prior to addition.

Sequence of TTR

GSGPT GTGES KCPLM VKVLD AVRGS PAINV AVHVF RKAAD DTWEP FASGK TSESG ELHGL TTEEE FVEGI YKVEI DTKSY WKALG ISPFH EHAEV VFTAN DSGPR RYTIA ALLSP YSYST TAVVT NPKE

Results and Discussion

The time-resolved mass spectra of TTR with endogenous Zn(II) bound is shown in Figure 18. The presence of Zn(II) was confirmed by ICP-MS which also revealed low levels of Cr, Cu, and Ni in descending concentrations (Table 1). Initially, apo-TTR is most abundant with less abundant signals for singly- (64 Da shift) and doubly- (128 Da shift) bound Zn(II) to TTR. After a short time (~32 minutes), a noticeable shift in m/z is observed corresponding to the dominant peak of TTR + 128 Da (2x 64 Da), i.e., 2x Zn(II), the average mass of the Zn isotope cluster. This trend continues towards 64 minutes, upon which the most abundant peak has shifted to TTR + 256 Da (4x 64 Da). On the surface, TTR appears to bind greater numbers of Zn(II) over time; however, the concentration of Zn(II) in solution is too low for this to be a viable explanation.

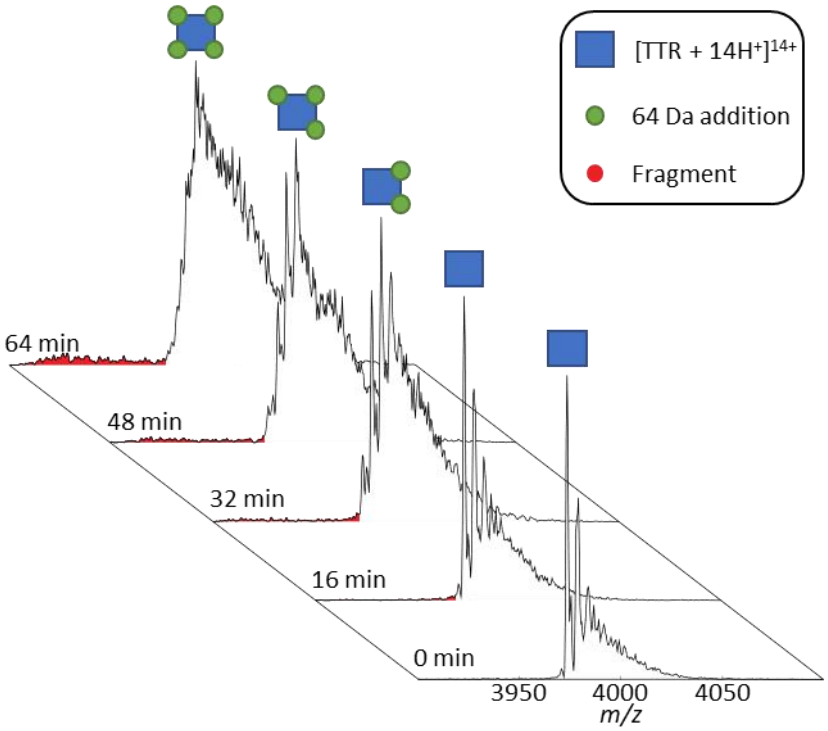

Figure 18. Time evolution of TTR under ambient nano-ESI conditions showing the sequential addition of 64 Da corresponding to either one zinc or four oxidations. At t = 0 min, the peaks to the right of the apo peak correspond to Zn(II) binding; however, at later times, the mass shifts are attributed to Cys-10 oxidation. The red peaks correspond to the backbone fragmentation of TTR between Cys-10 and Pro-11 which occurs simultaneously with TTR oxidation.

Table 1**.** The elemental analysis of the sample by ICP-MS for the buffered TTR sample.

Analyte	**A**	**Conc. (ng/mL)**	**± u (1s)**
V	51	ND	-
Cr	52	251	9
Mn	55	ND	-
Fe	57	ND	-
Co	59	ND	-
Ni	60	64	8
Cu	63	153	4
Zn	66	433	24
Ga	69	ND	-

Interestingly, structural analysis by IM-Orbitrap MS revealed the growth of two additional conformers over time as shown in Figure 19 where arrival time distributions (ATD) of TTR + n*64 Da, where n = 0-4, were collected over time. Degradation was slowed significantly through the analysis of TTR by a dual channel static nano-ESI emitter that separates the two channels by a thin borosilicate wall, called a theta-emitter. Theta-emitters can be used for nano-ESI whereupon the spray potential can be applied to one channel while still ionizing the sample that is present in the other channel. This ionization is possible because droplets form and mix from both channels near the end of the emitter.[126] Thus, theta emitters can isolate one channel from the ESI potential until the analyte is ionized. In the case of TTR, the mass shifts slowed dramatically and allowed

for the capture of intermediate structures by IM-Orbitrap MS. After 20 hours, TTR + n*64Da (where n = 1-4) had shifted from a single conformation denoted by a single Gaussian distribution to three distinct conformations. These new conformations can possibly be ascribed to dynamics of the protein main chain in the edge region His56 to Thr60.[124] Importantly, the formation of these new conformers appeared simultaneously with the Cys-10 and Pro-11 backbone fragmentation in one subunit shown in Figure 1. Formation of such extended conformations occur through a destabilized tetramer resulting in fragmentation in the region of Cys-10/Pro-11. Previous XRD characterization of TTR were unable to capture the N-terminal tail, and often conclude that these portions of the TTR tetramer are unstructured.

To better understand these structural perturbations SID was used to interrogate TTR subunits as shown in Figure 21. The 2D IM-MS plot of TTR collected using the Waters Synapt G2. $[TTR + 14H+]^{14+}$ and $[TTR + 15H+]^{15+}$ both populate the compact, native conformer of the protein which retains both Zn(II) and oxidation.. Analysis of the monomer subunit by SID revealed a surprising phenomenon. Initially, the monomer is dominantly in the apo- form with small amounts bound to Zn(II) and 2-Mercaptoethanol (ME) used for purification.[127] However, as TTR tetramer begins its stepwise shift of 64 Da over time, oxidation of the TTR monomers is observed, not additional Zn(II) binding. The monomer appears to oxidize twice early (32 Da shift) and eventually a third oxidation (48 Da shift) is observed. Similar experiments using CID also showed oxidation (Figure 22), although Zn(II) was dissociated due to gas-phase activation of the monomer. These

data show that the initial 64 Da shifts are due to Zn(II) binding, but the subsequent n*64 Da shifts over time are related to oxidation.

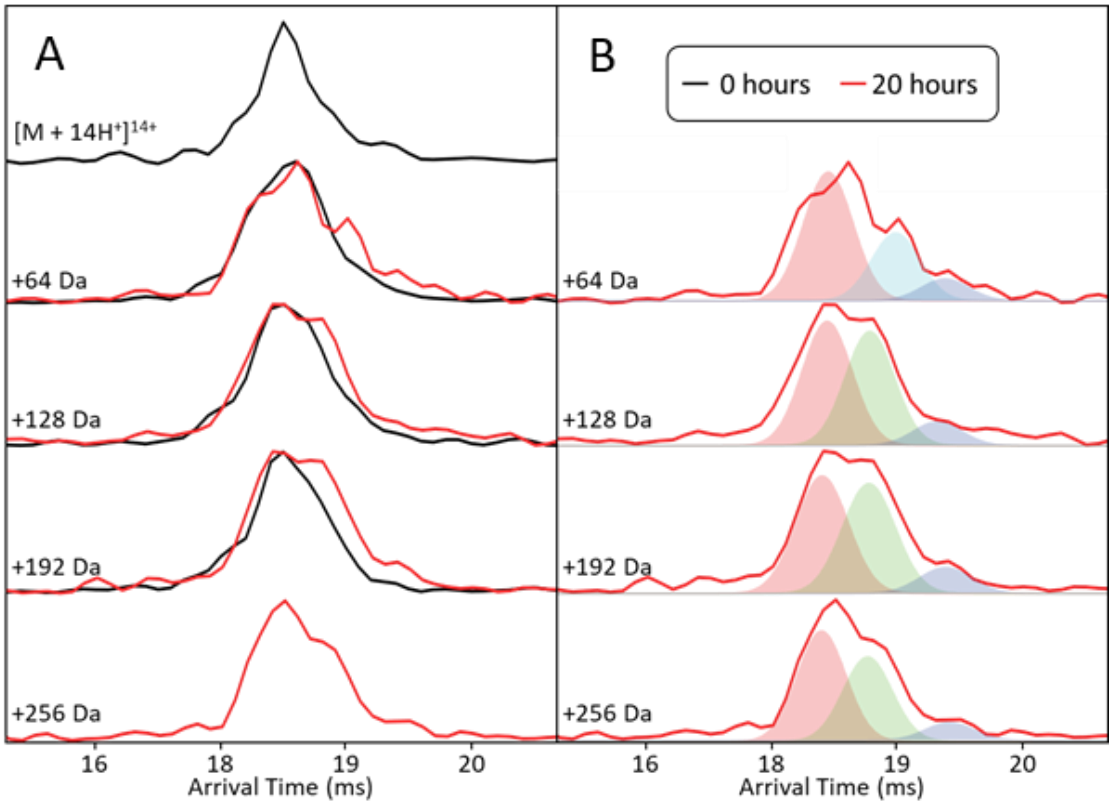

Figure 19. (A) ATDs for the [TTR + $14H^+$ + n*64 Da]$^{14+}$ ions (where n = 0-4) directly after loading (black) and after 20 hours of continuous analysis by a theta emitter (red). ATDs are the average of 8 IM-MS runs. (B) Deconvoluted ATDs of the incubated sample showing two additional conformations populated by TTR after 20 hours.

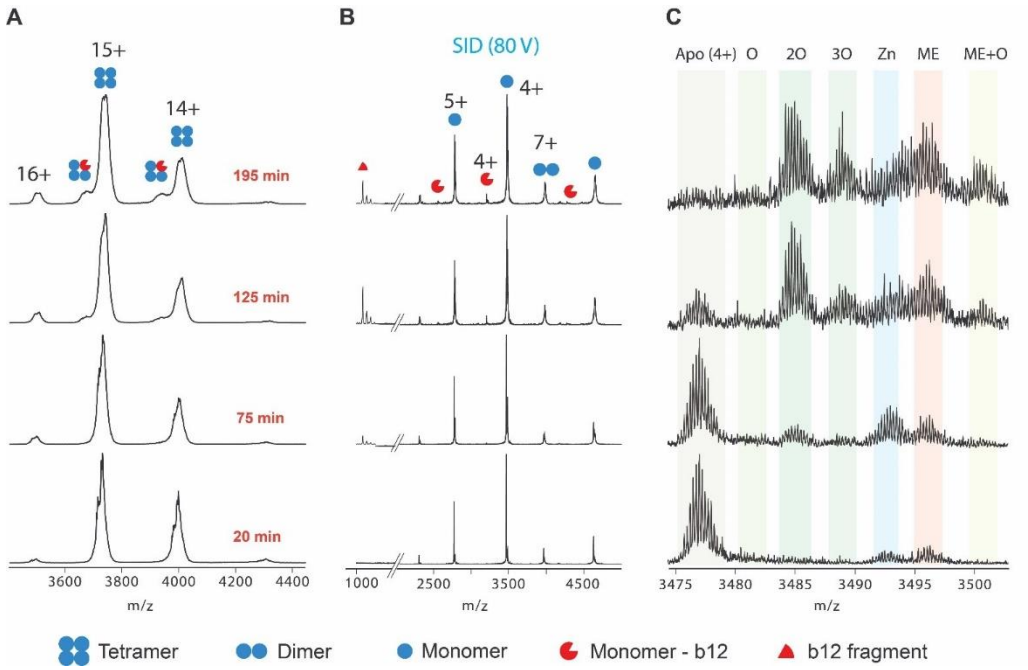

Figure 20. (A) Mass spectra of TTR tetramer as a function of time collected on a Waters Synapt G2 equipped with a custom SID cell. (B) The SID products of the [TTR + $15H^+$]$^{15+}$ tetramer. Monomers, dimers, and b12/y117 fragments are observed. The b12 fragment is doubly oxidized. (C) A magnified look at the [M + $4H^+$]$^{4+}$ monomer of TTR reveals a time dependent oxidation of TTR monomer as well as Zn(II) and 2-mercaptoethanol (ME) binding. [TTR + $15H^+$]$^{15+}$ retains the native conformation (Figure 21) and is used for SID to retain higher ion abundances.

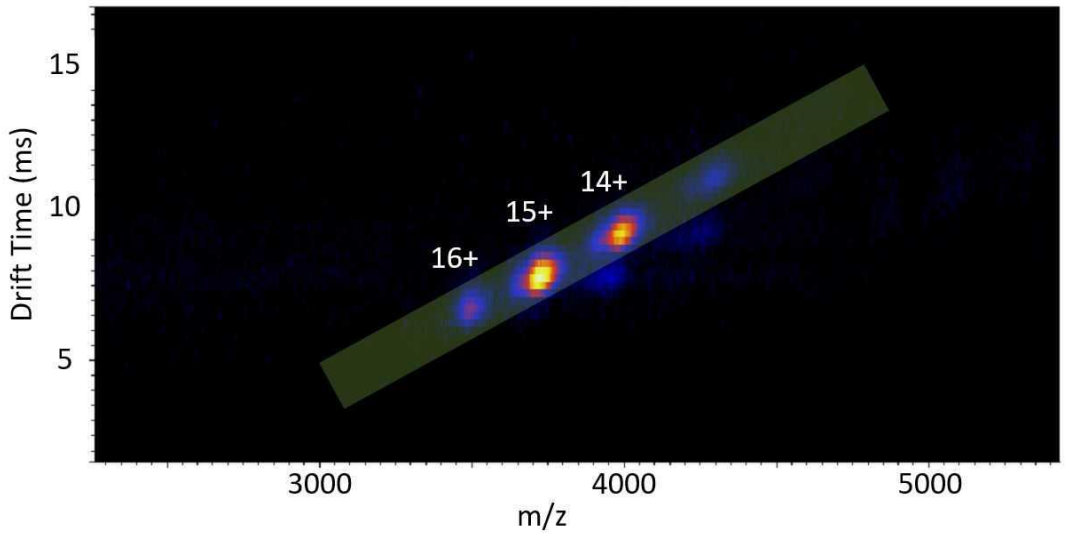

Figure 21. The 2D IM-MS plot of TTR collected using the Waters Synapt G2. [TTR + $14H^+$]$^{14+}$ and [TTR + $15H^+$]$^{15+}$ both populate the compact, native conformer of the protein which retains both Zn(II) and oxidation.

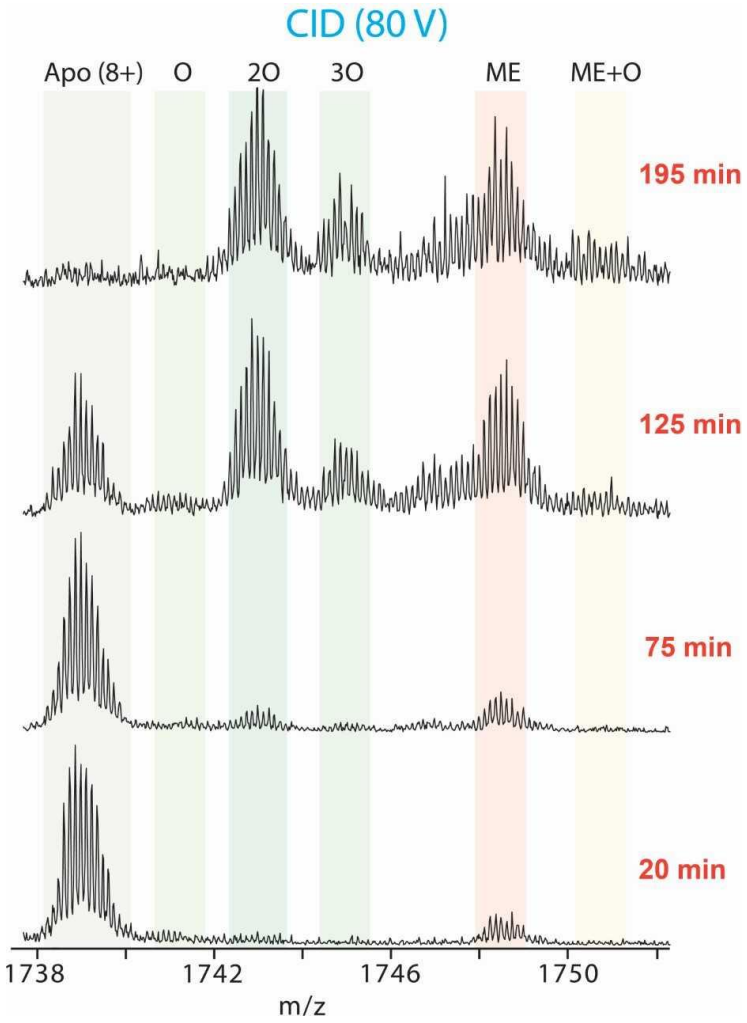

Figure 22. $[TTR + 8H^{+}]^{8+}$ monomer fragment using CID showing the time-dependent oxidation of TTR. CID, however, unfolds the monomer in the gas-phase dissociating the noncovalent Zn(II) interactions observed in SID.

Covalently labelling TTR can be used to further understand the oxidation pathway as two surface accessible oxidation sites exist on each monomer: Cys-10 and Met-13. NEM was used to alkylate the thiol of Cys-10 to prevent both oxidation and Zn(II) binding. MS data reveals that the addition of a 4-fold equivalence of NEM to TTR can successfully label most cysteine residues as denoted by a mass shift in the spectrum (Figure 23). Removing Cys-10 as an oxidation site slows the backbone fragmentation of TTR by approximately 6-fold. These data suggest that Cys-10 is the driving force behind backbone fragmentation that occurs between Cys-10 and Pro-11, which could be destabilized by an oxidation-induced structural change. Notably, the b10 fragment containing Cys-10 is doubly oxidized, corresponding to the oxidative conversion of the thiol to sulfinic acid.[128] This cleavage is similar to the mechano-enzymatic cleavage reported for the S52P TTR mutant18 that has been reported to induce aggregation; the same phenomenon was observed in these experiments where TTR octamers were formed following backbone fragmentation (Figure 24). Interestingly, three oxidations were observed on the intact monomer; however, only two oxidations are observed on the Cys-10 containing b10 fragment. Met-13 remains the only surface accessible oxidation site for the third oxidation.

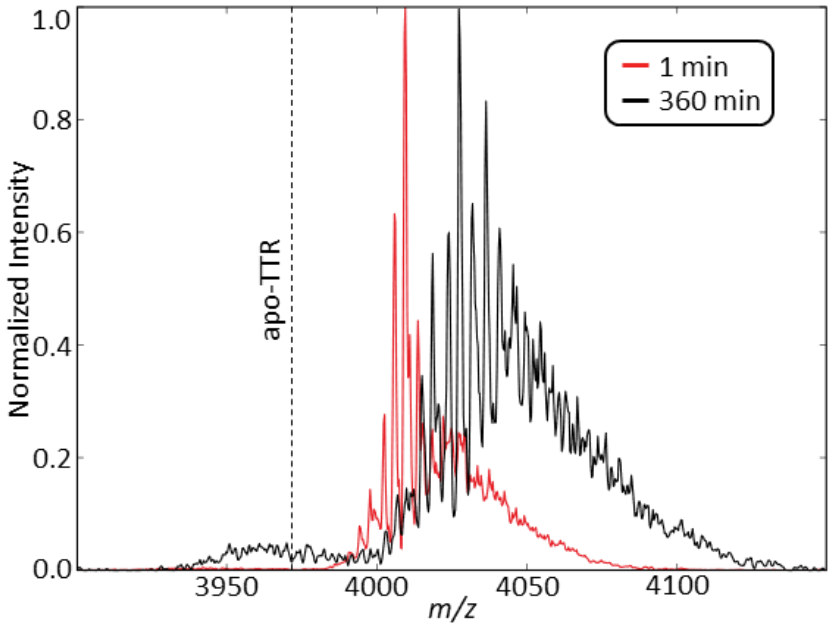

Figure 23. The mass spectra of [TTR + 14 H+ + 4 NEM]14+ at 0 and 360 minutes. Equivalent backbone fragmentation occurs at360 minutes compared to 64 minutes for TTR with Zn(II) and no NEM (Figure 1). The dotted line represents the m/z for apo-TTR.

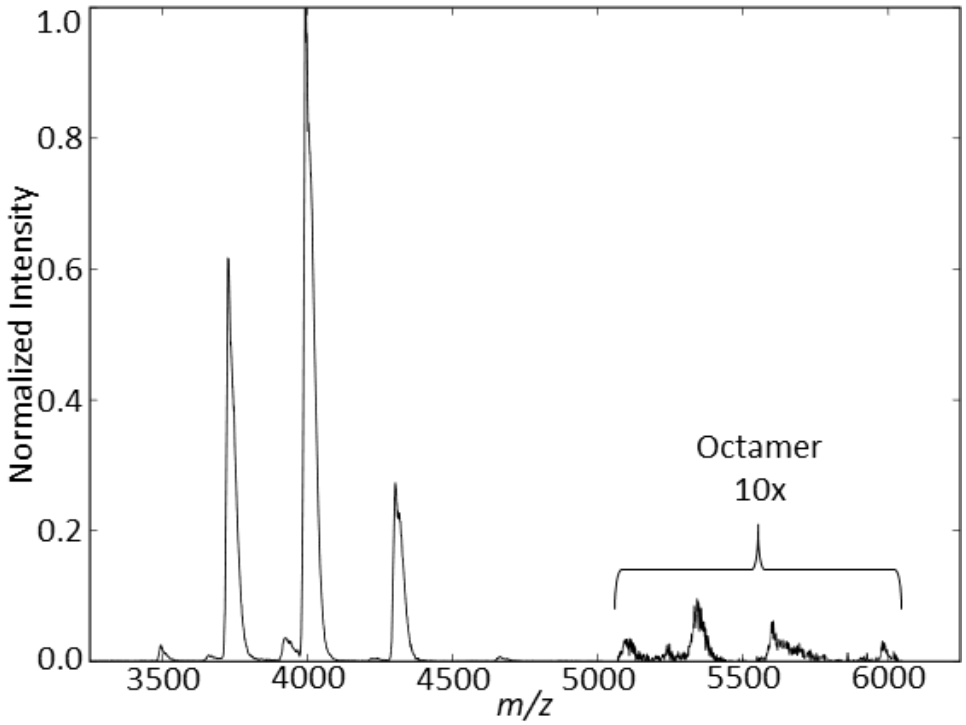

Figure 24. The mass spectrum of TTR after 64 minutes of continuous ESI. Octamer formation occurs simultaneously with Cys-12/Pro-13 backbone fragmentation. Octamer region of the MS is magnified 10x.

Dissociation of Zn(II) is also observed as oxidation proceeds, which is consistent with the crystallographic data that the Cys-10 oxidation site is involved in Zn(II) binding.[48] Coordination of Zn(II) by Cys-10 can inhibit/delay oxidation of the thiol group which was confirmed by adding zinc acetate (5:1 (Zn:TTR)) to apo TTR. This gave rise to a decrease in the oxidation rate by a factor of ~3 (data not shown). Cys-10 oxidation can also increase the accessible surface of Met-13 thereby favoring formation of more extended conformers.

Oxidation reactions during ESI have been observed previously using easily oxidizable metal emitters (i.e. stainless steel, copper, tungsten, etc.);[129, 130] however, the static nano-ESI used in these experiments applies a DC potential through an inert Pt (99.9%) wire, a metal that seldom acts as an oxidizer. Removing the ESI potential from the analyte solution using either a theta emitter (Figure 19) or a gold coated emitter (Figure 25) slows oxidation, and similarly, metal removal by EDTA also slows oxidation (Figure 26). Alternatively, addition of Cr (Figure 27) or Cu (Figure 28) can dramatically accelerate oxidation. Collectively, these data reveal a metal-induced oxidation of Cys-10 that is accelerated in the presence of an applied electrical potential. Bateman et al. proposed that metal catalysed electrolysis of water drives the oxidation of peptides and proteins.[131] Here, Cr and Cu drive Cys-10 oxidation ultimately leading to structural destabilization of TTR tetramer by inducing backbone fragmentation and promoting oligomer formation.

The results presented here contrast with those reported by Maleknia et al.[123] but compliment those reported by Gales et al.[124] Maleknia reported that Met-13 is the most oxidizable native residue and that a non-native N-terminal methionine also oxidizes;

however, there were no evidences of Cys-10 oxidation. Gales reported oxidation of both Cys-10 and Met-13 in mature TTR fibrils, both of which were observed here. Collectively, the results reported by Maleknia, Gales and our study suggest that metal-induced oxidation of TTR may underlie fibril formation by destabilizing TTR structure. The IM-MS and SID data reported here also offer definitive evidence of metal-induced Cys-10 and Met-13 oxidation, including structural rearrangement and backbone fragmentation.

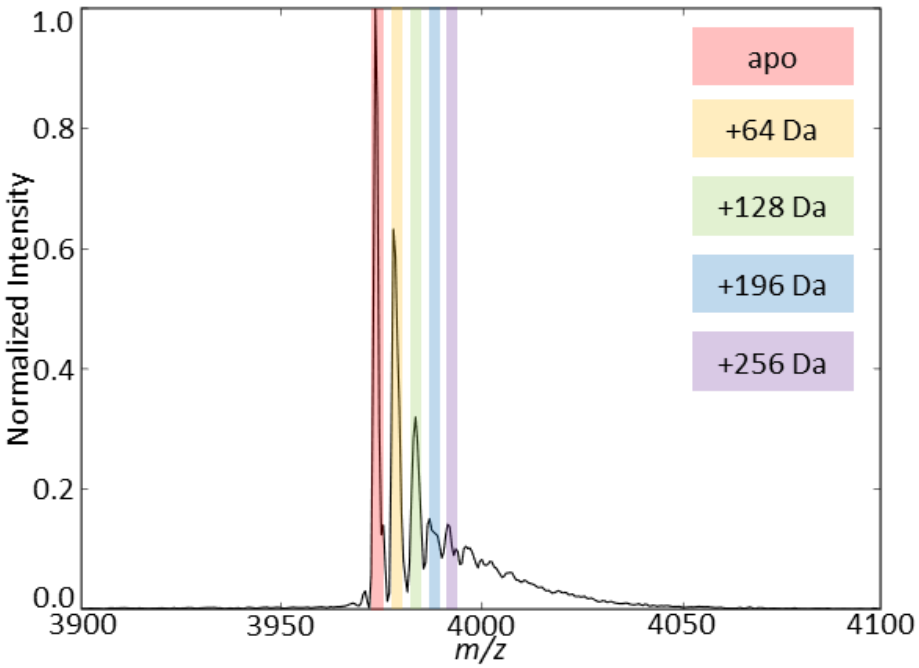

Figure 25. $[TTR + 14H^+]^{14+}$ tetramer after 60 minutes of analysis using a gold-coated nano-ESI emitter. Oxidation occurs much more slowly; however, peak broadening is observed attributed to Na^+ adduction over time.

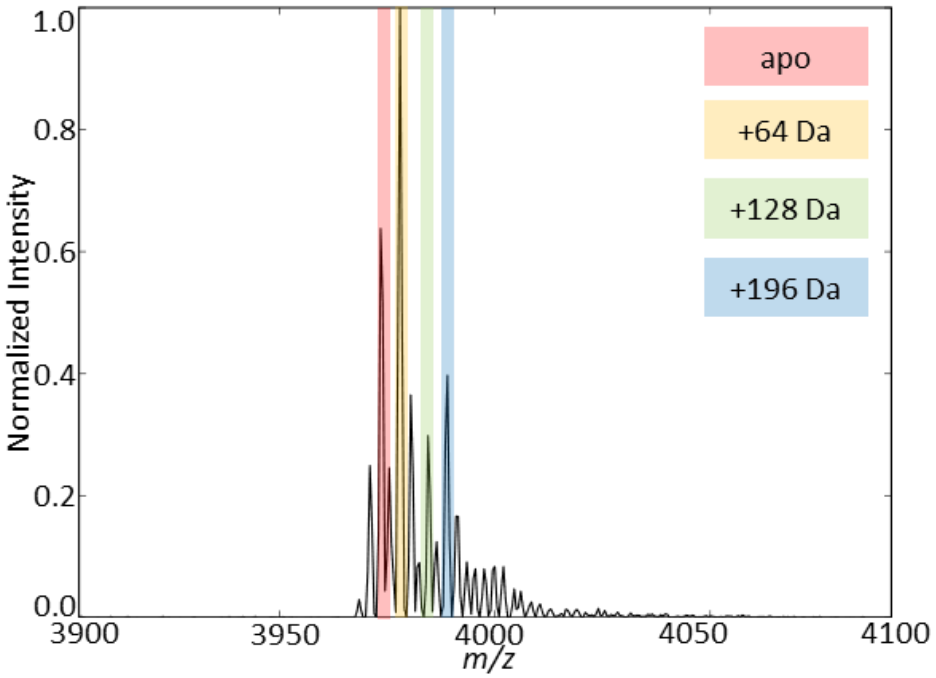

Figure 26. $[TTR + 14H^{+}]^{14+}$ tetramer after 60 minutes of analysis after size exclusion chromatography in the presence of EDTA to strip metals from solution before analysis. Metal removal resulted slowed oxidation and fragmentation approximately 2-fold. Importantly, EDTA chelates metals most readily at pH > 9 at which point TTR denatures, therefore, optimal conditions for chelation were not attainable without perturbing the structure of TTR.

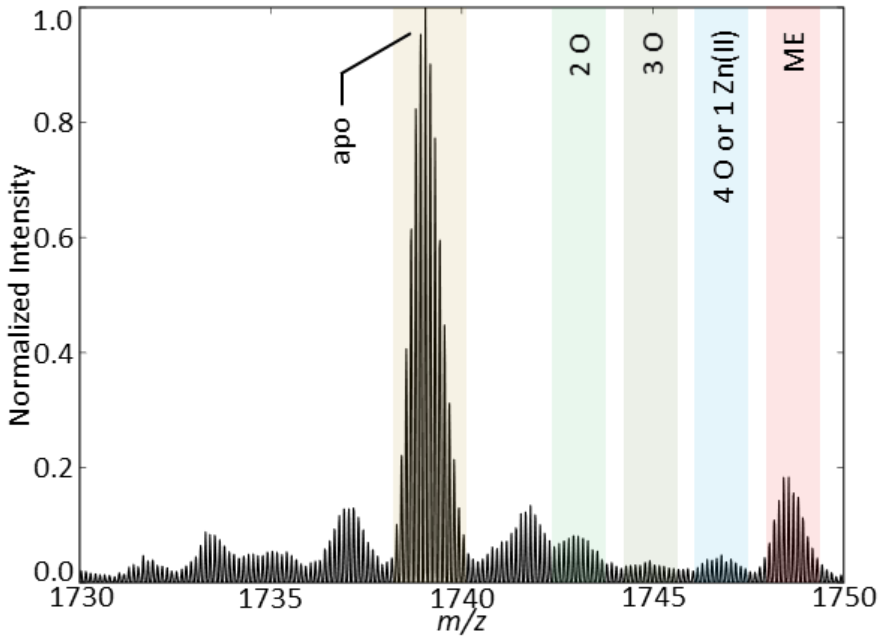

Figure 27. [TTR + 8H+]8+ monomer fragment obtained directly after the addition of equimolar Cr. This addition of Cr in solution immediately induces oxidation without the need for an applied potential.

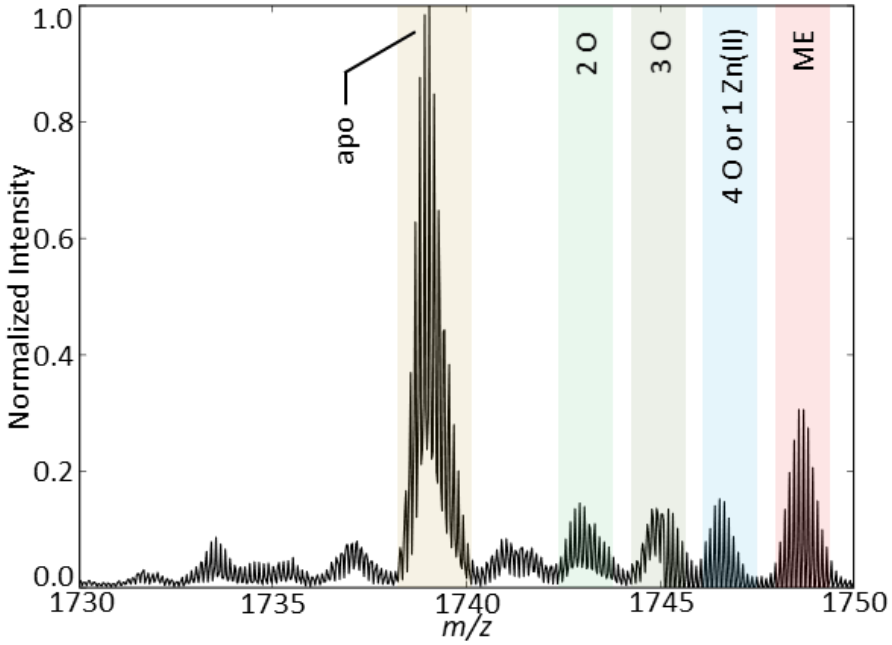

Figure 28. $[TTR + 8H^{+}]^{8+}$ monomer fragment obtained directly after the addition of equimolar $CuCH_3OOH$. Addition of Cu(II) in solution immediately induces oxidation without the need for an applied potential.

The results obtained here contrast those reported previously by Maleknia *et al.*; however, several differences in experimental design, can account for the differences observed.[132] Importantly, the TTR used in the aforementioned work possesses a slightly different sequence (see supplementary information for complete sequence), specifically, an additional N-terminal methionine that may affect the structure of the protein before and after oxidation. Moreover, IM-MS used here offer greater structural fidelity than the techniques used previously and offers definitive evidence of metal binding, oxidation, structural rearrangement, and backbone fragmentation.

Conclusions

Here, we describe metal-induced oxidation of Cys-10 of TTR that causes a structural elongation and subsequent backbone fragmentation between Cys-10 and Pro-11. The truncated protein then leads to eventual oligomer formation. Furthermore, NEM, metal stripping, and isolation from the ESI emitter voltage slow TTR oxidation and subsequent degradation. Future studies using amyloidogenic mutants i.e. V30M and L55P will reveal the correlation between fibril formation and oxidation and how metal-induced oxidation can affect TTR aggregation. Moreover, continued studies of the degradation mechanism for amyloidogenic proteins is critical for understanding the underlying physiological causes and potential therapeutics of related diseases. Small perturbations in the protein environment, specifically the presence of trace metals, can have a significant, deleterious impact on protein structure, function, and stability. The identification of metal-induced oxidation observed here using high-resolution IM-MS instrumentation underscore the importance of rigorous analytical measurements to understand protein behavior.

CHAPTER V

CONCLUSIONS AND FUTURE DIRECTIONS

IM-MS technology continues to evolve incorporating new concepts, methods, and developments. Each iteration of these instruments continues to push forward the understanding of both instrumentation as well as our understanding of applied chemical principles. Here, native-FT-PFDT IM-Orbitrap MS was implemented to overcome the limited availability of native, high-resolution IM-MS instruments for applications in biophysical analyses of large proteins and protein complexes.

A novel reverse entry ion source was developed for this platform to enable the coupling of IMS to Orbitrap MS. While the implementation of IMS to Orbitraps was the goal of this research, the interface could easily be couple to any gas-phase technique that has can be couple to MS. This setup retains the original ion optics and ion source that allows for the continued use of the Orbitrap throughout the instrument development and beyond, in essence, removing the opportunity cost of the instrument development timeline. Importantly, the reverse entry ion source does not hinder the performance of Orbitraps as it retains the same duty cycle and $R_{m/z}$. This was illustrated by the first example of three heterolipids being bound to a membrane protein and resolved using MS. Even more, four individual lipids were also resolved on AmtB with up to five total lipids bound resulting in 45 individually resolved protein-lipid species in a single mass spectrum. These spectra exemplify the importance and utility of improved $R_{m/z}$ and illustrate the need for high-resolution MS in IM-MS platforms while retaining noncovalent interactions and protein structure.

The IM-MS instrument described herein was ultimately a coalescence of new developments that were incorporated into a single platform. For example, pairing careful sample preparation with nano-ESI promotes the ability of this instrument to generate native ions. Careful design of the ion transfer optics continues to preserve the structure of ions throughout the IM separation and mass analysis. PFDT allows for high R_{IM} measurements while simultaneously providing high ion transmission, both of which are critical for the analysis of native proteins. Orbitrap MS enable high $R_{m/z}$ and allows for the detection of small perturbations in protein composition. Lastly, the FT acquisition mode overcomes the duty cycle mismatch between temporal DT separation and Orbitrap mass analysis. The exclusion of just one of these principles can prevent the high-resolution native biophysical studies portrayed in this dissertation. The IM-Orbitrap platform culminated in the first measurements of chemical phenomena observed by IM-MS, and a R_{IM} of ~60 for a native protein complex, about double that of which has been reported by any other IM-MS platform.

Several biological systems were shown here where rich chemical information can be had from a quick IM-MS experiment, just an eight-minute acquisition period. Importantly, the instrument preserves native structures and non-covalent interactions while offering the required resolution to study subtle differences upon protein-ligand bindings. For example, GlnK functional activation was illustrated through the stepwise addition of ADP, where holo-GlnK locks into an open conformation preference allowing the protein to bind to AmtB to negatively regulate nitrogen uptake. Furthermore, biotin was shown to significantly stabilize streptavidin upon binding to the complex. Thyroxine

was shown to stabilize TTR, whereas Zn(II) binding was shown to slightly destabilize the TTR tetramer.

TTR destabilization was further explored to understand the amyloidogenic pathway of the tetrameric protein complex. High-resolution IM-MS data showed the promotion of two additional extended conformation upon the successive oxidation of Cys-12. Surface induced dissociation data further confirmed the observed mass shift of 64 Da was a result of oxidation. NEM was used to chemically modify Cys-12 and reveal that Cys-12 was the oxidation site which ultimately led to a backbone fragmentation between Cys-12 and Pro-13. This fragmentation, upon tetramer dissociation, can lead to a oligomer formation. ICP-MS provided insight into the solution composition and aided in the revelation of chromium and copper coupled with a spray current induced the oxidation and eventual degradation of TTR.

The utility of IM-MS for the analyses of protein complexes is quickly being realized, and the data ascertained from the platform described here can help promote the advances of IM-MS as a biophysical tool.

R_{IM} and $R_{m/z}$, despite the improvements described herein, continue to limit the biophysical applications of IM-MS and necessitate future instrument development. Since the inception of the instrument two new components were installed to further improve upon the functionality and versatility of the IM-Orbitrap MS: (i) a 1.45 m PF DT replaced the 0.58 m PF DT used previously and (ii) a method for collision induced dissociation (CID) was added to the heated capillary vacuum interface.

Moving towards a DT nearly three times the length of the "alpha-version" of the instrument achieved a maximum R_{IM} of ~60 for a native protein complex, nearly double the highest previously reported value. Increased DT lengths lead to improved R_{IM} with a square-root relationship and remains the simplest method for improving R_{IM}. Limitations in Paschen breakdown, however, limit the length of DT by inducing electrical breakdown at high potentials at intermediate pressures (~1-10 Torr). Careful instrument design, especially at the heated capillary, ion funnel, and IMS gating regions can help mitigate Paschen breakdown by altering pressure regimes and ion optic design.

Importantly, the $R_{m/z}$ remains high with Orbitrap MS; however, Orbitrap MS technology has continued to progress and new instrumentation continues to push the boundaries of MS performance metrics. For example, the newest Thermo Scientific Q Exactive UHMR now touts a mass range of up to *m/z* 80,000 and a resolution of 200,000 at *m/z* 400 compared with *m/z* 20,000 and $R_{m/z}$ of 140,000 at *m/z* 400. Moreover, the scan rates have doubled in speed compared to the MS platform described herein. Recently, a $R_{m/z}$ of 1,000,000 was reported using an Orbitrap for the first time. Nevertheless, the IMS technology and interface described herein remain a viable solution for integrating high-resolution Orbitrap MS measurements with DT-IMS.

Native IM-MS has become an incredibly versatile tool and recently has been used to analyze the structure and behavior of membrane proteins. To maintain native solution conditions for insoluble protein complexes, membrane proteins are encapsulated by detergent micelles to maintain solubility for ESI. After ionization, the proteins retain the micelles which must be stripped in the gas-phase by CID prior to IMS or MS analysis.

Precise control of CID energy must be maintained to strip the detergent micelles without stripping important noncovalent interactions or unfolding the protein complex. Here, a combination of an accelerating electrode and elevated heated capillary temperature was added directly proceeding the heated capillary to destabilize the micelles and generate a greater potential drop to accelerate ions and induce CID. The combination allowed for the analysis of the membrane protein complex, the large conductance mechanosensitive ion channel (MscL), an osmotic release valve in the lipid bilayer. Detergents surrounding MscL were successfully removed with the added energy owed to the accelerating voltage and added thermal energy as shown in Figure **29**. MscL successfully binds nine POPI lipids, a lipid which was reported to regulate the opening and closing of the pore.

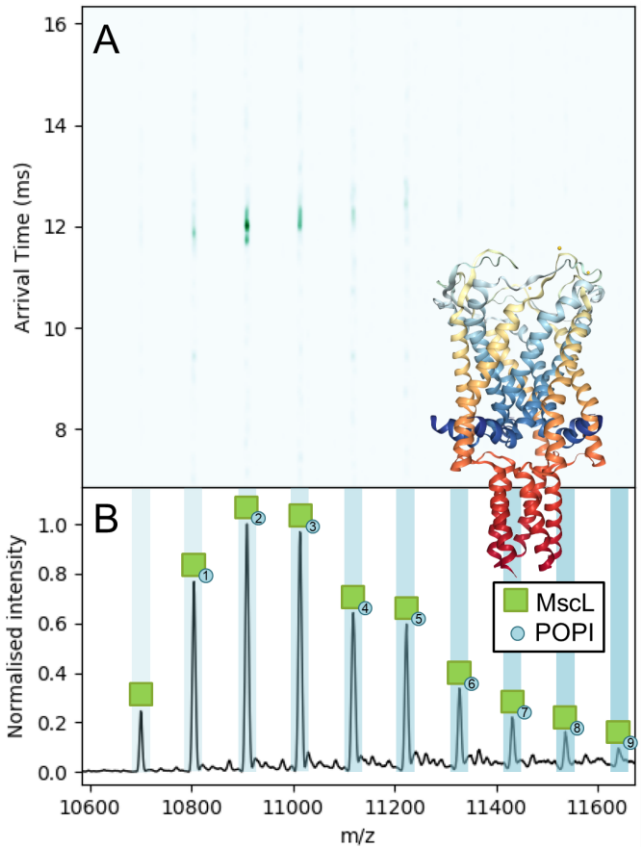

Figure 29. (A) IM-MS spectrum of the MscL membrane protein binding up to 9 POPI lipids. (B) The extracted mass spectrum of MscL with colored bands representing individual POPI binding events.

Here, we have described an instrument that utilizes a number of cutting-edge technologies to improve the measurements made using IM-MS. However, the instrument performance for intact protein complexes is largely set by the quality of the biological samples. For example, small adducts can easily complicate ion mobility and mass spectra owing to overlapping peaks, peak broadening, and overall chemical heterogeneity. This in turn would result in mass spectra that are below the analytical-figures-of-merit of the instrument. While such phenomena are often hard to decipher with poor RP, these issues in sample preparation are now amplified by high RP instruments. Alarmingly, these small perturbations can have impactful, deleterious effects when exploring protein structure or significant biological consequences. Methods for improving sample purity and homogeneity are critical when it comes to utilizing the technology available today. In fact, high $R_{m/z}$ afforded by these platforms can be used to gain insight into unknown chemical species that are present in biological samples. Such information can then lead to improved purification and protein expression workflows. It is clear that IM-MS can significantly improve not only final biophysical analyses, but also improve the means by which proteins are produced. For example, in Figure 4, TTR was observed in the presence of Zn(II) for the first time. With this new information, we can better understand the role that Zn(II) plays in altering protein structure, but we can also develop efficient purification methods for metal removal, such as treating the sample with metal chelators. Improved protein purity lends itself to more accurate and reproducible results with fewer independent variables but substantial raises the bar for protein standards.

Moreover, improved R_{IM} and $R_{m/z}$ can facilitate analysis of new proteins and the observation of new phenomena that have not yet been revealed by IM-MS. For example, Figure 30 illustrates three membrane protein channels, LeuT,[133, 134] GltPH,[135, 136] and Kir2.2.[137] For these structures, two crystallographic conformations are overlaid along with their root mean square deviation (RMSD). Interestingly, the minimum required resolution to observe these structural changes, for example upon channel gating for Kir2.2,[138] is not correlated with RMSD. Disappointingly, commercial IM-MS instruments are currently unable to resolve such differences. These examples highlight the necessity for high-resolution IM measurement capabilities.

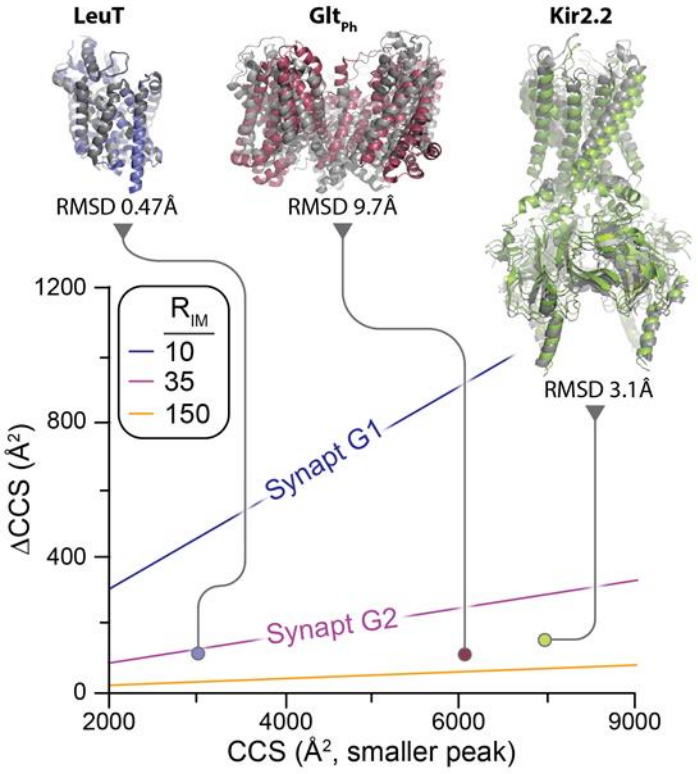

Figure 30. Plot of the minimum ΔCCS from the smaller peak yielding resolved peaks given a defined mobility resolving power. Shown are inward-outward and open-to-out states of LeuT,[133, 134] outward- and inward- facing states of GltPH,[135, 136] and closed and open states of Kir2.2.[137, 138]

Several challenges still limit the capabilities of native IM-MS, and many new methods were not incorporated into the platform described herein. Many tools can further improve the utility of this instrument such as the inclusion of novel dissociation techniques, especially surface-induced dissociation for studies of the topology of protein complexes,[139] ultraviolet photodissociation,[140] and electron transfer dissociation.[141] Moreover, the addition of mass filters and the ability to mobility select ions could provide even greater biophysical analyses.

However, IM-MS is not simply a biophysical tool, it is also a separation technique that is generally amenable to LC-MS, but FT-IMS acquisition prevents the use of this instrument for LC-IM-MS due to a duty cycle mismatch. Therefore, FT-IMS acquisition times must be reduced in order to gain widespread adoption for LC-IM-MS experiments. Coupling LC to high-resolution IM-MS could improve qualitative and quantitative measurements and elucidate countless phenomena that are hidden by the measurements our current instruments are able to make.

REFERENCES

1. Lapthorn, C.; Pullen, F.; Chowdhry, B. Z., Ion mobility spectrometry-mass spectrometry (IMS-MS) of small molecules: Separating and assigning structures to ions. **2013,** *32* (1), 43-71.

2. Paglia, G.; Angel, P.; Williams, J. P.; Richardson, K.; Olivos, H. J.; Thompson, J. W.; Menikarachchi, L.; Lai, S.; Walsh, C.; Moseley, A.; Plumb, R. S.; Grant, D. F.; Palsson, B. O.; Langridge, J.; Geromanos, S.; Astarita, G., Ion Mobility-Derived Collision Cross Section As an Additional Measure for Lipid Fingerprinting and Identification. *Analytical Chemistry* **2015,** *87* (2), 1137-1144.

3. Kyle, J. E.; Zhang, X.; Weitz, K. K.; Monroe, M. E.; Ibrahim, Y. M.; Moore, R. J.; Cha, J.; Sun, X.; Lovelace, E. S.; Wagoner, J.; Polyak, S. J.; Metz, T. O.; Dey, S. K.; Smith, R. D.; Burnum-Johnson, K. E.; Baker, E. S., Uncovering biologically significant lipid isomers with liquid chromatography, ion mobility spectrometry and mass spectrometry. *Analyst* **2016,** *141* (5), 1649-1659.

4. May, J. C.; Morris, C. B.; McLean, J. A., Ion Mobility Collision Cross Section Compendium. *Analytical Chemistry* **2017,** *89* (2), 1032-1044.

5. McLean, J. A.; Ruotolo, B. T.; Gillig, K. J.; Russell, D. H., Ion mobility–mass spectrometry: a new paradigm for proteomics. *International Journal of Mass Spectrometry* **2005,** *240* (3), 301-315.

6. Zhong, Y.; Hyung, S.-J.; Ruotolo, B. T., Ion mobility–mass spectrometry for structural proteomics. *Expert Review of Proteomics* **2012,** *9* (1), 47-58.

7. Heck, A. J. R., Native mass spectrometry: a bridge between interactomics and structural biology. *Nature Methods* **2008,** *5*, 927.

8. Leney, A. C.; Heck, A. J. R., Native Mass Spectrometry: What is in the Name? *Journal of the American Society for Mass Spectrometry* **2017,** *28* (1), 5-13.

9. M Young, L.; Saunders, J.; Mahood, R.; H Revill, C.; J Foster, R.; Tu, L.-H.; P Raleigh, D.; Radford, S.; Ashcroft, A., Screening and classifying small molecule inhibitors of amyloid formation using ion mobility spectrometry-mass spectrometry. *Nature chemistry* **2015,** *7*, 73-81.

10. Cong, X.; Liu, Y.; Liu, W.; Liang, X.; Russell, D. H.; Laganowsky, A., Determining Membrane Protein–Lipid Binding Thermodynamics Using Native Mass Spectrometry. *Journal of the American Chemical Society* **2016,** *138* (13), 4346-4349.

11. Patrick, J. W.; Boone, C. D.; Liu, W.; Conover, G. M.; Liu, Y.; Cong, X.; Laganowsky, A., Allostery revealed within lipid binding events to membrane proteins. *Proceedings of the National Academy of Sciences* **2018**.

12. Daneshfar, R.; Kitova, E. N.; Klassen, J. S., Determination of Protein−Ligand Association Thermochemistry Using Variable-Temperature Nanoelectrospray Mass Spectrometry. *Journal of the American Chemical Society* **2004,** *126* (15), 4786-4787.

13. Clemmer, D. E.; Russell, D. H.; Williams, E. R., Characterizing the Conformationome: Toward a Structural Understanding of the Proteome. *Accounts of Chemical Research* **2017,** *50* (3), 556-560.

14. Ruotolo, B. T.; Benesch, J. L. P.; Sandercock, A. M.; Hyung, S.-J.; Robinson, C. V., Ion mobility-mass spectrometry analysis of large protein complexes. *Nat. Protocols* **2008,** *3* (7), 1139-1152.

15. Allison, T. M.; Landreh, M.; Benesch, J. L. P.; Robinson, C. V., Low Charge and Reduced Mobility of Membrane Protein Complexes Has Implications for Calibration of Collision Cross Section Measurements. *Analytical Chemistry* **2016,** *88* (11), 5879-5884.

16. Bush, M. F.; Hall, Z.; Giles, K.; Hoyes, J.; Robinson, C. V.; Ruotolo, B. T., Collision Cross Sections of Proteins and Their Complexes: A Calibration Framework and Database for Gas-Phase Structural Biology. *Analytical Chemistry* **2010,** *82* (22), 9557-9565.

17. Laganowsky, A.; Reading, E.; Allison, T. M.; Ulmschneider, M. B.; Degiacomi, M. T.; Baldwin, A. J.; Robinson, C. V., Membrane proteins bind lipids selectively to modulate their structure and function. *Nature* **2014,** *510* (7503), 172-175.

18. Giles, K.; Pringle Steven, D.; Worthington Kenneth, R.; Little, D.; Wildgoose Jason, L.; Bateman Robert, H., Applications of a travelling wave-based radio-frequency-only stacked ring ion guide. *Rapid Communications in Mass Spectrometry* **2004,** *18* (20), 2401-2414.

19. Chen, S.-H.; Russell, D. H., How Closely Related Are Conformations of Protein Ions Sampled by IM-MS to Native Solution Structures? *Journal of The American Society for Mass Spectrometry* **2015,** *26* (9), 1433-1443.

20. Loo, J. A.; DeJohn, D. E.; Du, P.; Stevenson, T. I.; Ogorzalek Loo, R. R., Application of mass spectrometry for target identification and characterization. **1999,** *19* (4), 307-319.

21. Mortensen, D. N.; Susa, A. C.; Williams, E. R., Collisional Cross-Sections with T-Wave Ion Mobility Spectrometry without Experimental Calibration. *Journal of The American Society for Mass Spectrometry* **2017,** *28* (7), 1282-1292.

22. Mortensen, D. N.; Williams, E. R., Ultrafast (1 μs) Mixing and Fast Protein Folding in Nanodrops Monitored by Mass Spectrometry. *Journal of the American Chemical Society* **2016,** *138* (10), 3453-3460.

23. Xia, Z.; Williams, E. R., Effect of droplet lifetime on where ions are formed in electrospray ionization. *Analyst* **2019,** *144* (1), 237-248.

24. Poltash, M. L.; McCabe, J. W.; Patrick, J. W.; Laganowsky, A.; Russell, D. H., Development and Evaluation of a Reverse-Entry Ion Source Orbitrap Mass Spectrometer. *Journal of The American Society for Mass Spectrometry* **2018**.

25. Lippens, J. L.; Nshanian, M.; Spahr, C.; Egea, P. F.; Loo, J. A.; Campuzano, I. D. G., Fourier Transform-Ion Cyclotron Resonance Mass Spectrometry as a Platform for Characterizing Multimeric Membrane Protein Complexes. *Journal of The American Society for Mass Spectrometry* **2018,** *29* (1), 183-193.

26. Bluhm, B., K.; Gillig, K. J.; Russell, D. H., Development of a Fourier-transform ion cyclotron resonance mass spectrometer-ion mobility spectrometer. *Review of Scientific Instruments* **2000,** *71* (11), 4078-4086.

27. Bluhm, B. K.; North, S. W.; Russell, D. H., Separation of spin–orbit coupled metastable states of Kr+ and Xe+ by ion mobility. *The Journal of Chemical Physics* **2001,** *114* (4), 1709-1715.

28. Ridgeway, M. E.; Lubeck, M.; Jordens, J.; Mann, M.; Park, M. A., Trapped ion mobility spectrometry: A short review. *International Journal of Mass Spectrometry* **2018,** *425*, 22-35.

29. Dit Fouque, K. J.; Moreno, J.; Hegemann, J. D.; Zirah, S.; Rebuffat, S.; Fernandez-Lima, F., Identification of Lasso Peptide Topologies Using Native Nanoelectrospray Ionization-Trapped Ion Mobility Spectrometry–Mass Spectrometry. *Analytical Chemistry* **2018,** *90* (8), 5139-5146.

30. Barrera, N. P.; Di Bartolo, N.; Booth, P. J.; Robinson, C. V., Micelles Protect Membrane Complexes from Solution to Vacuum. *Science* **2008,** *321* (5886), 243.

31. Revercomb, H. E.; Mason, E. A., Theory of plasma chromatography/gaseous electrophoresis. Review. *Analytical Chemistry* **1975,** *47* (7), 970-983.

32. Gillig, K. J.; Ruotolo, B. T.; Stone, E. G.; Russell, D. H., An electrostatic focusing ion guide for ion mobility-mass spectrometry. *International Journal of Mass Spectrometry* **2004,** *239* (1), 43-49.

33. Blase, R. C.; Silveira, J. A.; Gillig, K. J.; Gamage, C. M.; Russell, D. H., Increased ion transmission in IMS: A high resolution, periodic-focusing DC ion guide ion mobility spectrometer. *International Journal of Mass Spectrometry* **2011,** *301* (1–3), 166-173.

34. Gamage, C. M.; Silveira, J. A.; Blase, R. C.; Russell, D. H., Gas-phase ion dynamics in a periodic-focusing DC ion guide (Part II): Discrete transport modes. *International Journal of Mass Spectrometry* **2011,** *303* (2–3), 154-163.

35. Silveira, J. A.; Gamage, C. M.; Blase, R. C.; Russell, D. H., Gas-phase ion dynamics in a periodic-focusing DC ion guide. *International Journal of Mass Spectrometry* **2010,** *296* (1–3), 36-42.

36. Manura, D.; Dahl, D., SIMION (R) 8.0 User Manual (Scientific Instrument Services, Inc. Ringoes, NJ 08551, <http://simion.com>, January 2008). **2008**.

37. Silveira, J. A.; Jeon, J.; Gamage, C. M.; Pai, P.-J.; Fort, K. L.; Russell, D. H., Damping Factor Links Periodic Focusing and Uniform Field Ion Mobility for Accurate Determination of Collision Cross Sections. *Analytical Chemistry* **2012,** *84* (6), 2818-2824.

38. Poltash, M. L.; McCabe, J. W.; Shirzadeh, M.; Laganowsky, A.; Clowers, B. H.; Russell, D. H., Fourier Transform-Ion Mobility-Orbitrap Mass Spectrometer: A Next-Generation Instrument for Native Mass Spectrometry. *Analytical Chemistry* **2018,** *90* (17), 10472-10478.

39. Karasek, F. W., Plasma chromatography of the polychlorinated biphenyls. *Analytical Chemistry* **1971,** *43* (14), 1982-1986.

40. Karasek, F. W.; Kilpatrick, W. D.; Cohen, M. J., Qualitative studies of trace constituents by plasma chromatography. *Analytical Chemistry* **1971,** *43* (11), 1441-1447.

41. Karasek, F. W.; Tatone, O. S., Plasma chromatography of the monohalogenated benzenes. *Analytical Chemistry* **1972,** *44* (11), 1758-1763.

42. Low, I. A.; Liu, R. H.; Barker, S. A.; Fish, F.; Settine, R. L.; Piotrowski, E. G.; Damert, W. C.; Liu, J. Y., Selected ion monitoring mass spectrometry: Parameters affecting quantitative determination. **1985,** *12* (11), 633-637.

43. Knorr, F. J.; Eatherton, R. L.; Siems, W. F.; Hill, H. H., Fourier Transform Ion Mobility Spectrometry. *Analytical Chemistry* **1985,** *57* (2), 402-406.

44. Morrison, K. A.; Siems, W. F.; Clowers, B. H., Augmenting Ion Trap Mass Spectrometers Using a Frequency Modulated Drift Tube Ion Mobility Spectrometer. *Analytical Chemistry* **2016,** *88* (6), 3121-3129.

45. Xu, Y.; Carr, P. D.; Clancy, P.; Garcia-Dominguez, M.; Forchhammer, K.; Florencio, F.; Tandeau de Marsac, N.; Vasudevan, S. G.; Ollis, D. L., The structures of the PII proteins from the cyanobacteria Synechococcus sp. PCC 7942 and Synechocystis sp. PCC 6803. *Acta Crystallographica Section D* **2003,** *59* (12), 2183-2190.

46. Machado Benelli, E.; Buck, M.; Polikarpov, I.; Maltempi de Souza, E.; Cruz, L. M.; Pedrosa, F. O., Herbaspirillum seropedicae signal transduction protein PII is structurally similar to the enteric GlnK. *European Journal of Biochemistry* **2002,** *269* (13), 3296-3303.

47. Wojtczak, A.; Cody, V.; Luft, J. R.; Pangborn, W., Structures of Human Transthyretin Complexed with Thyroxine at 2.0 A Resolution and 3',5'-Dinitro-N-acetyl-l-thyronine at 2.2 A Resolution. *Acta Crystallographica Section D* **1996,** *52* (4), 758-765.

48. de C. Palmieri, L.; Lima, L. M. T. R.; Freire, J. B. B.; Bleicher, L.; Polikarpov, I.; Almeida, F. C. L.; Foguel, D., Novel Zn(2+)-binding Sites in Human Transthyretin:

IMPLICATIONS FOR AMYLOIDOGENESIS AND RETINOL-BINDING PROTEIN RECOGNITION. *The Journal of Biological Chemistry* **2010,** *285* (41), 31731-31741.

49. Hyung, S.-J.; Robinson, C. V.; Ruotolo, B. T., Gas-Phase Unfolding and Disassembly Reveals Stability Differences in Ligand-Bound Multiprotein Complexes. *Chemistry & Biology* **2009,** *16* (4), 382-390.

50. Lanucara, F.; Holman, S. W.; Gray, C. J.; Eyers, C. E., The power of ion mobility-mass spectrometry for structural characterization and the study of conformational dynamics. *Nat Chem* **2014,** *6* (4), 281-294.

51. von Helden, G.; Wyttenbach, T.; Bowers, M. T., Inclusion of a MALDI ion source in the ion chromatography technique: conformational information on polymer and biomolecular ions. *International Journal of Mass Spectrometry and Ion Processes* **1995,** *146-147*, 349-364.

52. Wittmer, D.; Chen, Y. H.; Luckenbill, B. K.; Hill, H. H., Electrospray Ionization Ion Mobility Spectrometry. *Analytical Chemistry* **1994,** *66* (14), 2348-2355.

53. Jurneczko, E.; Barran, P. E., How useful is ion mobility mass spectrometry for structural biology? The relationship between protein crystal structures and their collision cross sections in the gas phase. *Analyst* **2011,** *136* (1), 20-28.

54. Bleiholder, C.; Dupuis, N. F.; Wyttenbach, T.; Bowers, M. T., Ion mobility–mass spectrometry reveals a conformational conversion from random assembly to β-sheet in amyloid fibril formation. *Nat Chem* **2011,** *3* (2), 172-177.

55. Hu, Q.; Noll, R. J.; Li, H.; Makarov, A.; Hardman, M.; Graham Cooks, R., The Orbitrap: a new mass spectrometer. *Journal of Mass Spectrometry* **2005,** *40* (4), 430-443.

56. Makarov, A. A., Mass spectrometer. Google Patents: 1999.

57. Rose, R. J.; Damoc, E.; Denisov, E.; Makarov, A.; Heck, A. J. R., High-sensitivity Orbitrap mass analysis of intact macromolecular assemblies. *Nature Methods* **2012,** *9*, 1084.

58. Fort, K. L.; van de Waterbeemd, M.; Boll, D.; Reinhardt-Szyba, M.; Belov, M. E.; Sasaki, E.; Zschoche, R.; Hilvert, D.; Makarov, A. A.; Heck, A. J. R., Expanding the structural analysis capabilities on an Orbitrap-based mass spectrometer for large macromolecular complexes. *Analyst* **2018,** *143* (1), 100-105.

59. Ibrahim, Y. M.; Garimella, S. V. B.; Prost, S. A.; Wojcik, R.; Norheim, R. V.; Baker, E. S.; Rusyn, I.; Smith, R. D., Development of an Ion Mobility Spectrometry-Orbitrap Mass Spectrometer Platform. *Analytical Chemistry* **2016,** *88* (24), 12152-12160.

60. Keelor, J. D.; Zambrzycki, S.; Li, A.; Clowers, B. H.; Fernández, F. M., Atmospheric Pressure Drift Tube Ion Mobility–Orbitrap Mass Spectrometry: Initial Performance Characterization. *Analytical Chemistry* **2017,** *89* (21), 11301-11309.

61. Hagan, N.; Goldberg, I.; Graichen, A.; St. Jean, A.; Wu, C.; Lawrence, D.; Demirev, P., Ion Mobility Spectrometry - High Resolution LTQ-Orbitrap Mass Spectrometry for Analysis of Homemade Explosives. *Journal of The American Society for Mass Spectrometry* **2017,** *28* (8), 1531-1539.

62. Shaffer, S. A.; Tang, K.; Anderson, G. A.; Prior, D. C.; Udseth, H. R.; Smith, R. D., A novel ion funnel for focusing ions at elevated pressure using electrospray ionization mass spectrometry. *Rapid Commun. Mass Spectrom.* **1997,** *11*, 1813-1817.

63. Marty, M. T.; Baldwin, A. J.; Marklund, E. G.; Hochberg, G. K. A.; Benesch, J. L. P.; Robinson, C. V., Bayesian Deconvolution of Mass and Ion Mobility Spectra: From Binary Interactions to Polydisperse Ensembles. *Analytical chemistry* **2015,** *87* (8), 4370-4376.

64. Sharon, M., How far can we go with structural mass spectrometry of protein complexes? *Journal of the American Society for Mass Spectrometry* **2010,** *21* (4), 487-500.

65. Sharon, M.; Robinson, C. V., The Role of Mass Spectrometry in Structure Elucidation of Dynamic Protein Complexes. *Annual Review of Biochemistry* **2007,** *76* (1), 167-193.

66. Kitova, E. N.; El-Hawiet, A.; Schnier, P. D.; Klassen, J. S., Reliable Determinations of Protein–Ligand Interactions by Direct ESI-MS Measurements. Are We There Yet? *Journal of The American Society for Mass Spectrometry* **2012,** *23* (3), 431-441.

67. van den Heuvel, R. H. H.; Heck, A. J. R., Native protein mass spectrometry: from intact oligomers to functional machineries. *Current Opinion in Chemical Biology* **2004,** *8* (5), 519-526.

68. Tosi, P.; Fontana, G.; Longano, S.; Bassi, D., Transport of an ion beam through an octopole guide operating in the R.F.-only mode. *International Journal of Mass Spectrometry and Ion Processes* **1989,** *93* (1), 95-105.

69. Loo, J. A., Studying Noncovalent Protein Complexes by Electrospray Ionization Mass Spectrometry. *Mass Spectrometry Reviews* **1997,** *16* (1), 1-23.

70. Robinson, C. V.; Chung, E. W.; Kragelund, B. B.; Knudsen, J.; Aplin, R. T.; Poulsen, F. M.; Dobson, C. M., Probing the Nature of Noncovalent Interactions by Mass Spectrometry. A Study of Protein−CoA Ligand Binding and Assembly. *Journal of the American Chemical Society* **1996,** *118* (36), 8646-8653.

71. Benesch, J. L. P.; Ruotolo, B. T., Mass spectrometry: come of age for structural and dynamical biology. *Current Opinion in Structural Biology* **2011,** *21* (5), 641-649.

72. Hall, Z.; Politis, A.; Bush, M. F.; Smith, L. J.; Robinson, C. V., Charge-State Dependent Compaction and Dissociation of Protein Complexes: Insights from Ion Mobility and Molecular Dynamics. *Journal of the American Chemical Society* **2012,** *134* (7), 3429-3438.

73. Kaltashov, I. A.; Mohimen, A., Estimates of Protein Surface Areas in Solution by Electrospray Ionization Mass Spectrometry. *Analytical Chemistry* **2005,** *77* (16), 5370-5379.

74. Li, J.; Santambrogio, C.; Brocca, S.; Rossetti, G.; Carloni, P.; Grandori, R., Conformational effects in protein electrospray-ionization mass spectrometry. *Mass Spectrometry Reviews* **2016,** *35* (1), 111-122.

75. Testa, L.; Brocca, S.; Grandori, R., Charge-Surface Correlation in Electrospray Ionization of Folded and Unfolded Proteins. *Analytical Chemistry* **2011,** *83* (17), 6459-6463.

76. Uetrecht, C.; Rose, R. J.; van Duijn, E.; Lorenzen, K.; Heck, A. J. R., Ion mobility mass spectrometry of proteins and protein assemblies. *Chemical Society Reviews* **2010,** *39* (5), 1633-1655.

77. Wyttenbach, T.; Pierson, N. A.; Clemmer, D. E.; Bowers, M. T., Ion Mobility Analysis of Molecular Dynamics. *Annual Review of Physical Chemistry* **2014,** *65* (1), 175-196.

78. Mehmood, S.; Allison, T. M.; Robinson, C. V., Mass Spectrometry of Protein Complexes: From Origins to Applications. *Annual Review of Physical Chemistry* **2015,** *66* (1), 453-474.

79. Laganowsky, A.; Reading, E.; Hopper, J. T. S.; Robinson, C. V., Mass Spectrometry of Intact Membrane Protein Complexes. *Nature protocols* **2013,** *8* (4), 639-651.

80. El-baba, T. J.; Woodall, D. W.; Raab, S. A.; Fuller, D. R.; Laganowsky, A.; Russell, D. H.; Clemmer, D. E., Melting Proteins: Evidence for Multiple Stable Structures upon Thermal Denaturation of Native Ubiquitin from IMS-MS Measurements. *Journal of the American Chemical Society* **2017**.

81. Shi, L.; Holliday, A. E.; Shi, H.; Zhu, F.; Ewing, M. A.; Russell, D. H.; Clemmer, D. E., Characterizing Intermediates Along the Transition from Polyproline I to Polyproline II Using Ion Mobility Spectrometry-Mass Spectrometry. *Journal of the American Chemical Society* **2014,** *136* (36), 12702-12711.

82. Kostyukevich, Y.; Kononikhin, A.; Popov, I.; Nikolaev, E., Conformational changes of ubiquitin during electrospray ionization as determined by in-ESI source H/D exchange combined with high-resolution MS and ECD fragmentation. *Journal of The American Society for Mass Spectrometry* **2014,** *49* (10), 989-994.

83. Shi, H.; Atlasevich, N.; Merenbloom, S. I.; Clemmer, D. E., Solution Dependence of the Collisional Activation of Ubiquitin [M+7H](7+) Ions. *Journal of the American Society for Mass Spectrometry* **2014,** *25* (12), 2000-2008.

84. Hall, Z.; Robinson, C. V., Do Charge State Signatures Guarantee Protein Conformations? *Journal of The American Society for Mass Spectrometry* **2012,** *23* (7), 1161-1168.

85. Gault, J.; Donlan, J. A. C.; Liko, I.; Hopper, J. T. S.; Gupta, K.; Housden, N. G.; Struwe, W. B.; Marty, M. T.; Mize, T.; Bechara, C.; Zhu, Y.; Wu, B.; Kleanthous, C.; Belov, M.; Damoc, E.; Makarov, A.; Robinson, C. V., High-resolution mass spectrometry of small molecules bound to membrane proteins. *Nature methods* **2016,** *13* (4), 333-336.

86. Aebersold, R.; Agar, J. N.; Amster, I. J.; Baker, M. S.; Bertozzi, C. R.; Boja, E. S.; Costello, C. E.; Cravatt, B. F.; Fenselau, C.; Garcia, B. A.; Ge, Y.; Gunawardena, J.; Hendrickson, R. C.; Hergenrother, P. J.; Huber, C. G.; Ivanov, A.

R.; Jensen, O. N.; Jewett, M. C.; Kelleher, N. L.; Kiessling, L. L.; Krogan, N. J.; Larsen, M. R.; Loo, J. A.; Ogorzalek Loo, R. R.; Lundberg, E.; MacCoss, M. J.; Mallick, P.; Mootha, V. K.; Mrksich, M.; Muir, T. W.; Patrie, S. M.; Pesavento, J. J.; Pitteri, S. J.; Rodriguez, H.; Saghatelian, A.; Sandoval, W.; Schlüter, H.; Sechi, S.; Slavoff, S. A.; Smith, L. M.; Snyder, M. P.; Thomas, P. M.; Uhlén, M.; Van Eyk, J. E.; Vidal, M.; Walt, D. R.; White, F. M.; Williams, E. R.; Wohlschlager, T.; Wysocki, V. H.; Yates, N. A.; Young, N. L.; Zhang, B., How many human proteoforms are there? *Nature Chemical Biology* **2018,** *14*, 206.

87. Chen, L.; Gao, Y. Q.; Russell, D. H., How Alkali Metal Ion Binding Alters the Conformation Preferences of Gramicidin A: A Molecular Dynamics and Ion Mobility Study. *The Journal of Physical Chemistry A* **2012,** *116* (1), 689-696.

88. Chen, S.-H.; Russell, D. H., Reaction of Human Cd7metallothionein and N-Ethylmaleimide: Kinetic and Structural Insights from Electrospray Ionization Mass Spectrometry. *Biochemistry* **2015,** *54* (39), 6021-6028.

89. Allison, T. M.; Reading, E.; Liko, I.; Baldwin, A. J.; Laganowsky, A.; Robinson, C. V., Quantifying the stabilizing effects of protein–ligand interactions in the gas phase. *Nature Communications* **2015,** *6*, 8551.

90. Brien, E. P.; Ziv, G.; Haran, G.; Brooks, B. R.; Thirumalai, D., Effects of denaturants and osmolytes on proteins are accurately predicted by the molecular transfer model. *Proceedings of the National Academy of Sciences* **2008,** *105* (36), 13403.

91. Breuker, K.; McLafferty, F. W., Stepwise evolution of protein native structure with electrospray into the gas phase, 10−12 to 102 s. *Proceedings of the National Academy of Sciences* **2008,** *105* (47), 18145-18152.

92. Servage, K. A.; Silveira, J. A.; Fort, K. L.; Clemmer, D. E.; Russell, D. H., Water-Mediated Dimerization of Ubiquitin Ions Captured by Cryogenic Ion Mobility-Mass Spectrometry. *The Journal of Physical Chemistry Letters* **2015,** *6* (24), 4947-4951.

93. Giles, K.; Pringle, S. D.; Worthington, K. R.; Little, D.; Wildgoose, J. L.; Bateman, R. H., Applications of a travelling wave-based radio-frequency-only stacked ring ion guide. *Rapid Communications in Mass Spectrometry* **2004,** *18* (20), 2401-2414.

94. Susa, A. C.; Xia, Z.; Williams, E. R., Small Emitter Tips for Native Mass Spectrometry of Proteins and Protein Complexes from Nonvolatile Buffers That Mimic the Intracellular Environment. *Analytical Chemistry* **2017,** *89* (5), 3116-3122.

95. Karasek, F. W.; Denney, D. W.; Dedecker, E. H., Plasma Chromatography of Normal Alkanes and Its Relationship to Chemical Ionization Mass-Spectrometry. *Analytical Chemistry* **1974,** *46* (8), 970-973.

96. Clowers, B. H.; Hill, H. H., Mass Analysis of Mobility-Selected Ion Populations Using Dual Gate, Ion Mobility, Quadrupole Ion Trap Mass Spectrometry. *Analytical Chemistry* **2005,** *77* (18), 5877-5885.

97. Davis, A. L.; Liu, W.; Siems, W. F.; Clowers, B. H., Correlation ion mobility spectrometry. *Analyst* **2017,** *142* (2), 292-301.

98. Tummalacherla, M.; Garimella, S. V. B.; Prost, S. A.; Ibrahim, Y. M., Toward artifact-free data in Hadamard transform-based double multiplexing of ion mobility-Orbitrap mass spectrometry. *Analyst* **2017,** *142* (10), 1735-1745.

99. Szumlas, A. W.; Ray, S. J.; Hieftje, G. M., Hadamard Transform Ion Mobility Spectrometry. *Analytical Chemistry* **2006,** *78* (13), 4474-4481.

100. Pringle, S. D.; Giles, K.; Wildgoose, J. L.; Williams, J. P.; Slade, S. E.; Thalassinos, K.; Bateman, R. H.; Bowers, M. T.; Scrivens, J. H., An investigation of the mobility separation of some peptide and protein ions using a new hybrid quadrupole/travelling wave IMS/oa-ToF instrument. *International Journal of Mass Spectrometry* **2007,** *261* (1), 1-12.

101. May, J. C.; Jurneczko, E.; Stow, S. M.; Kratochvil, I.; Kalkhof, S.; McLean, J. A., Conformational landscapes of ubiquitin, cytochrome c, and myoglobin: Uniform field ion mobility measurements in helium and nitrogen drift gas. *International Journal of Mass Spectrometry* **2018,** *427*, 79-90.

102. Clemmer, D. E.; Hudgins, R. R.; Jarrold, M. F., Naked Protein Conformations: Cytochrome c in the Gas Phase. *Journal of the American Chemical Society* **1995,** *117* (40), 10141-10142.

103. Clemmer, D. E.; Jarrold, M. F., Ion Mobility Measurements and their Applications to Clusters and Biomolecules. *Journal of Mass Spectrometry* **1997,** *32* (6), 577-592.

104. Wyttenbach, T.; Bowers, M. T., Structural Stability from Solution to the Gas Phase: Native Solution Structure of Ubiquitin Survives Analysis in a Solvent-Free Ion Mobility–Mass Spectrometry Environment. *The Journal of Physical Chemistry B* **2011,** *115* (42), 12266-12275.

105. Lashuel, H. A.; Wurth, C.; Woo, L.; Kelly, J. W., The Most Pathogenic Transthyretin Variant, L55P, Forms Amyloid Fibrils under Acidic Conditions and Protofilaments under Physiological Conditions. *Biochemistry* **1999,** *38* (41), 13560-13573.

106. Jones, M. L.; Kurzban, G. P., Noncooperativity of Biotin Binding to Tetrameric Streptavidin. *Biochemistry* **1995,** *34* (37), 11750-11756.

107. Chilkoti, A.; Stayton, P. S., Molecular Origins of the Slow Streptavidin-Biotin Dissociation Kinetics. *Journal of the American Chemical Society* **1995,** *117* (43), 10622-10628.

108. Gonzalez, M.; Bagatolli, L. A.; Echabe, I.; Arrondo, J. L.; Argarana, C. E.; Cantor, C. R.; Fidelio, G. D., Interaction of biotin with streptavidin. Thermostability and conformational changes upon binding. *J Biol Chem* **1997,** *272* (17), 11288-94.

109. Deng, L.; Kitova, E. N.; Klassen, J. S., Dissociation Kinetics of the Streptavidin–Biotin Interaction Measured Using Direct Electrospray Ionization Mass Spectrometry Analysis. *Journal of The American Society for Mass Spectrometry* **2013,** *24* (1), 49-56.

110. Conroy, M. J.; Durand, A.; Lupo, D.; Li, X.-D.; Bullough, P. A.; Winkler, F. K.; Merrick, M., The crystal structure of the AmtB–GlnK complex reveals how GlnK regulates the ammonia channel. *Proceedings of the National Academy of Sciences* **2007,** *104* (4), 1213.

111. Arcondéguy, T.; Jack, R.; Merrick, M., P(II) Signal Transduction Proteins, Pivotal Players in Microbial Nitrogen Control. *Microbiology and Molecular Biology Reviews* **2001,** *65* (1), 80-105.

112. Marklund, Erik G.; Degiacomi, Matteo T.; Robinson, Carol V.; Baldwin, Andrew J.; Benesch, Justin L. P., Collision Cross Sections for Structural Proteomics. *Structure* **2015,** *23* (4), 791-799.

113. Sakai, H.; Wang, H.; Takemoto-Hori, C.; Kaminishi, T.; Yamaguchi, H.; Kamewari, Y.; Terada, T.; Kuramitsu, S.; Shirouzu, M.; Yokoyama, S., Crystal structures of the signal transducing protein GlnK from Thermus thermophilus HB8. *Journal of Structural Biology* **2005,** *149* (1), 99-110.

114. Radchenko, M. V.; Thornton, J.; Merrick, M., Control of AmtB-GlnK Complex Formation by Intracellular Levels of ATP, ADP, and 2-Oxoglutarate. *The Journal of Biological Chemistry* **2010,** *285* (40), 31037-31045.

115. Hammarström, P.; Jiang, X.; Hurshman, A. R.; Powers, E. T.; Kelly, J. W., Sequence-dependent denaturation energetics: A major determinant in amyloid disease diversity. *Proceedings of the National Academy of Sciences* **2002,** *99* (suppl 4), 16427.

116. Hammarström, P.; Wiseman, R. L.; Powers, E. T.; Kelly, J. W., Prevention of Transthyretin Amyloid Disease by Changing Protein Misfolding Energetics. *Science* **2003,** *299* (5607), 713.

117. Liz, Márcia A.; Leite, Sérgio C.; Juliano, L.; Saraiva, Maria J.; Damas, Ana M.; Bur, D.; Sousa, Mónica M., Transthyretin is a metallopeptidase with an inducible active site. *Biochemical Journal* **2012,** *443* (3), 769.

118. Palha Joana, A., Transthyretin as a Thyroid Hormone Carrier: Function Revisited. In *Clinical Chemistry and Laboratory Medicine*, 2002; Vol. 40, p 1292.

119. Monaco, H. L., The transthyretin-retinol-binding protein complex. *Biochimica et Biophysica Acta (BBA) - Protein Structure and Molecular Enzymology* **2000,** *1482* (1), 65-72.

120. Lai, Z.; Colón, W.; Kelly, J. W., The Acid-Mediated Denaturation Pathway of Transthyretin Yields a Conformational Intermediate That Can Self-Assemble into Amyloid. *Biochemistry* **1996,** *35* (20), 6470-6482.

121. Yoshiki, S.; Jeffery, W. K.; Shu-ichi, I., Pathogenesis of and Therapeutic Strategies to Ameliorate the Transthyretin Amyloidoses. *Current Pharmaceutical Design* **2008,** *14* (30), 3219-3230.

122. Westermark, P.; Sletten, K.; Johansson, B.; Cornwell, G. G., Fibril in Senile Systemic Amyloidosis Is Derived from Normal Transthyretin. *Proceedings of the National Academy of Sciences of the United States of America* **1990,** *87* (7), 2843-2845.

123. Maleknia, S. D.; Reixach, N.; Buxbaum, J. N., Oxidation inhibits amyloid fibril formation of transthyretin. *The FEBS Journal* **2006,** *273* (23), 5400-5406.

124. Gales, L. s.; Cardoso, I.; Fayard, B.; Quintanilha, A.; Saraiva, M. J.; Damas, A. M., X-ray Absorption Spectroscopy Reveals a Substantial Increase of Sulfur Oxidation in Transthyretin (TTR) upon Fibrillization. *Journal of Biological Chemistry* **2003,** *278* (13), 11654-11660.

125. Shirzadeh, M.; Boone, C. D.; Laganowsky, A.; Russell, D. H., Topological Analysis of Transthyretin Disassembly Mechanism: Surface-Induced Dissociation Reveals Hidden Reaction Pathways. *Analytical Chemistry* **2019**.

126. Mortensen, D. N.; Williams, E. R., Investigating Protein Folding and Unfolding in Electrospray Nanodrops Upon Rapid Mixing Using Theta-Glass Emitters. *Analytical Chemistry* **2015,** *87* (2), 1281-1287.

127. Kingsbury, J. S.; Klimtchuk, E. S.; Théberge, R.; Costello, C. E.; Connors, L. H., Expression, purification, and in vitro cysteine-10 modification of native sequence recombinant human transthyretin. *Protein Expression and Purification* **2007,** *53* (2), 370-377.

128. Chung Heaseung, S.; Wang, S.-B.; Venkatraman, V.; Murray Christopher, I.; Van Eyk Jennifer, E., Cysteine Oxidative Posttranslational Modifications. *Circulation Research* **2013,** *112* (2), 382-392.

129. Konermann, L.; Silva, E. A.; Sogbein, O. F., Electrochemically Induced pH Changes Resulting in Protein Unfolding in the Ion Source of an Electrospray Mass Spectrometer. *Analytical Chemistry* **2001,** *73* (20), 4836-4844.

130. Chen, M.; Cook, K. D., Oxidation Artifacts in the Electrospray Mass Spectrometry of Aβ Peptide. *Analytical Chemistry* **2007,** *79* (5), 2031-2036.

131. Bateman, K. P., Electrochemical properties of capillary electrophoresis-nanoelectrospray mass spectrometry. *Journal of the American Society for Mass Spectrometry* **1999,** *10* (4), 309-317.

132. Maleknia, S. D.; Reixach, N.; Buxbaum, J. N., Oxidation inhibits amyloid fibril formation of transthyretin. **2006,** *273* (23), 5400-5406.

133. Krishnamurthy, H.; Gouaux, E., X-ray structures of LeuT in substrate-free outward-open and apo inward-open states. *Nature* **2012,** *481*, 469.

134. Singh, S. K.; Piscitelli, C. L.; Yamashita, A.; Gouaux, E., A Competitive Inhibitor Traps LeuT in an Open-to-Out Conformation. *Science* **2008,** *322* (5908), 1655.

135. Yernool, D.; Boudker, O.; Jin, Y.; Gouaux, E., Structure of a glutamate transporter homologue from Pyrococcus horikoshii. *Nature* **2004,** *431*, 811.

136. Reyes, N.; Ginter, C.; Boudker, O., Transport mechanism of a bacterial homologue of glutamate transporters. *Nature* **2009,** *462*, 880.

137. Tao, X.; Avalos, J. L.; Chen, J.; MacKinnon, R., Crystal Structure of the Eukaryotic Strong Inward-Rectifier K⁺ Channel Kir2.2 at 3.1 Å Resolution. *Science* **2009,** *326* (5960), 1668.

138. Hansen, S. B., Lipid agonism: The PIP2 paradigm of ligand-gated ion channels. *Biochimica et Biophysica Acta (BBA) - Molecular and Cell Biology of Lipids* **2015,** *1851* (5), 620-628.

139. Galhena, A. S.; Dagan, S.; Jones, C. M.; Beardsley, R. L.; Wysocki, V. H., Surface-Induced Dissociation of Peptides and Protein Complexes in a Quadrupole/Time-of-Flight Mass Spectrometer. *Analytical Chemistry* **2008,** *80* (5), 1425-1436.

140. Goolsby, B. J.; Brodbelt, J. S., Characterization of β-lactams by photodissociation and collision-activated dissociation in a quadrupole ion trap. *Journal of Mass Spectrometry* **1998,** *33* (8), 705-712.

141. Syka, J. E. P.; Coon, J. J.; Schroeder, M. J.; Shabanowitz, J.; Hunt, D. F., Peptide and protein sequence analysis by electron transfer dissociation mass spectrometry. *Proceedings of the National Academy of Sciences of the United States of America* **2004,** *101* (26), 9528-9533.

APPENDIX

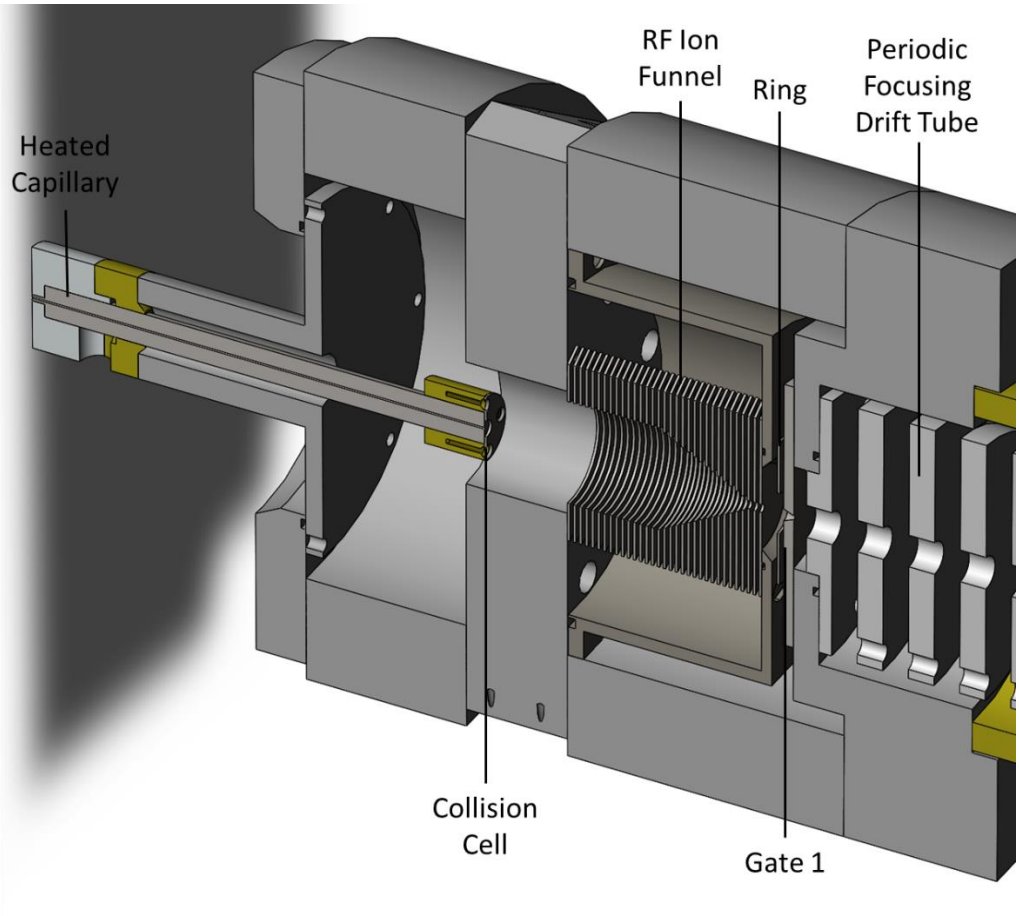

A-1. Magnified Ion Source

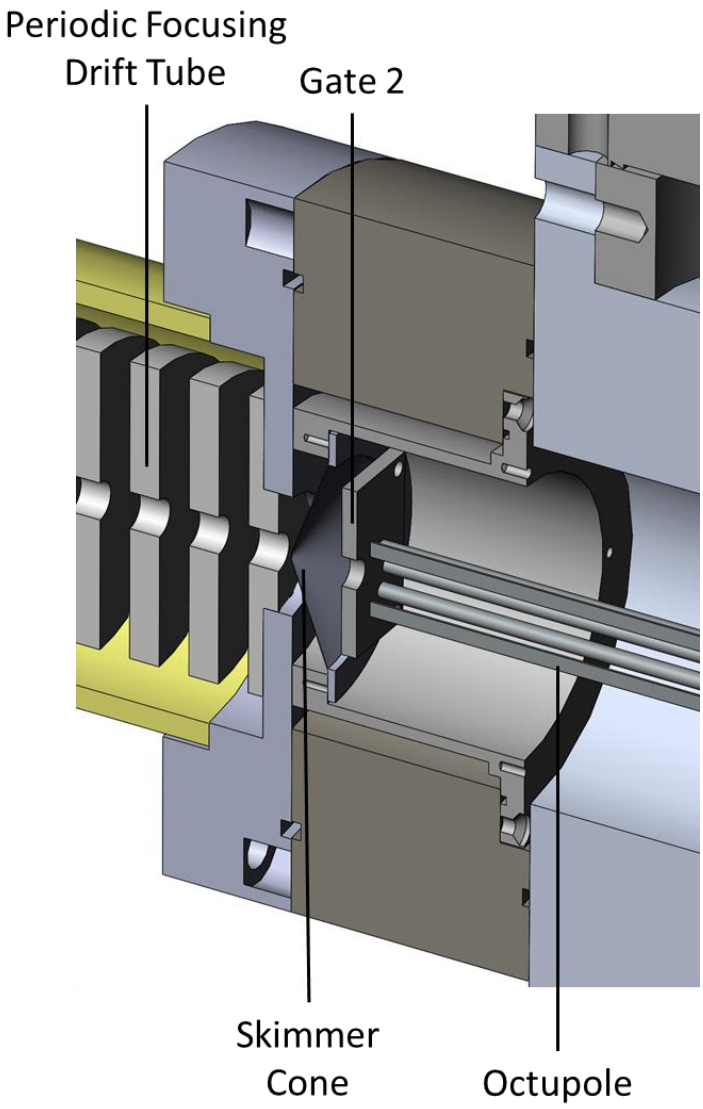

A-2. Magnified Post-Mobility Ion Optics

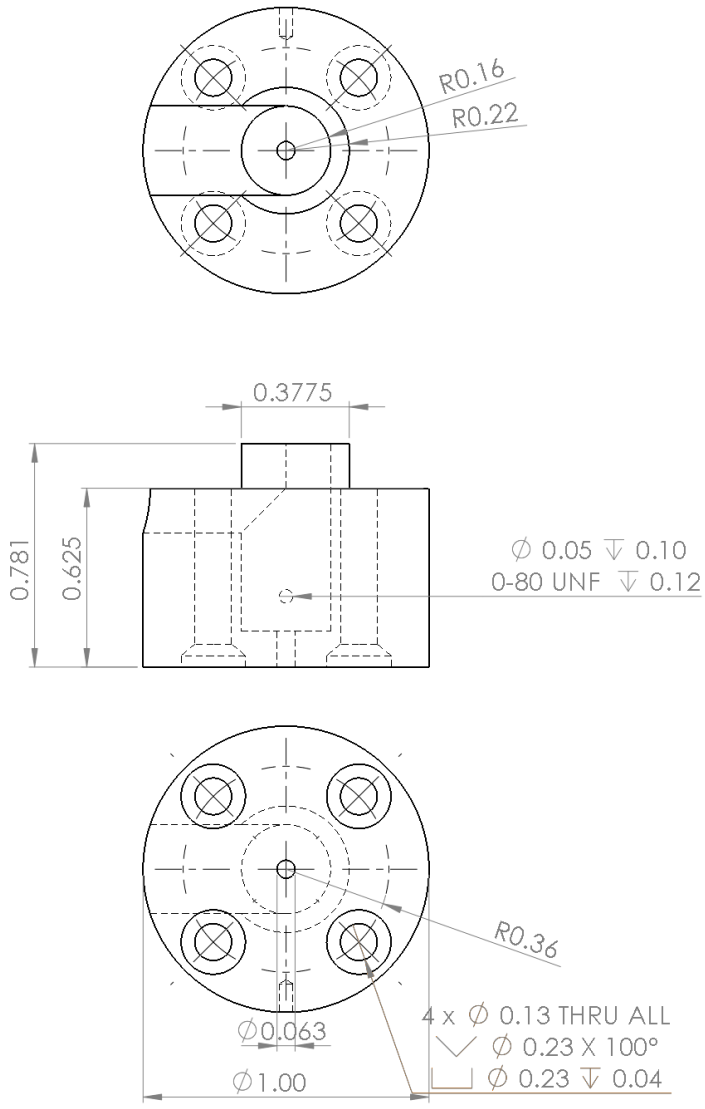

A-3. Aluminum Heated Capillary Cover

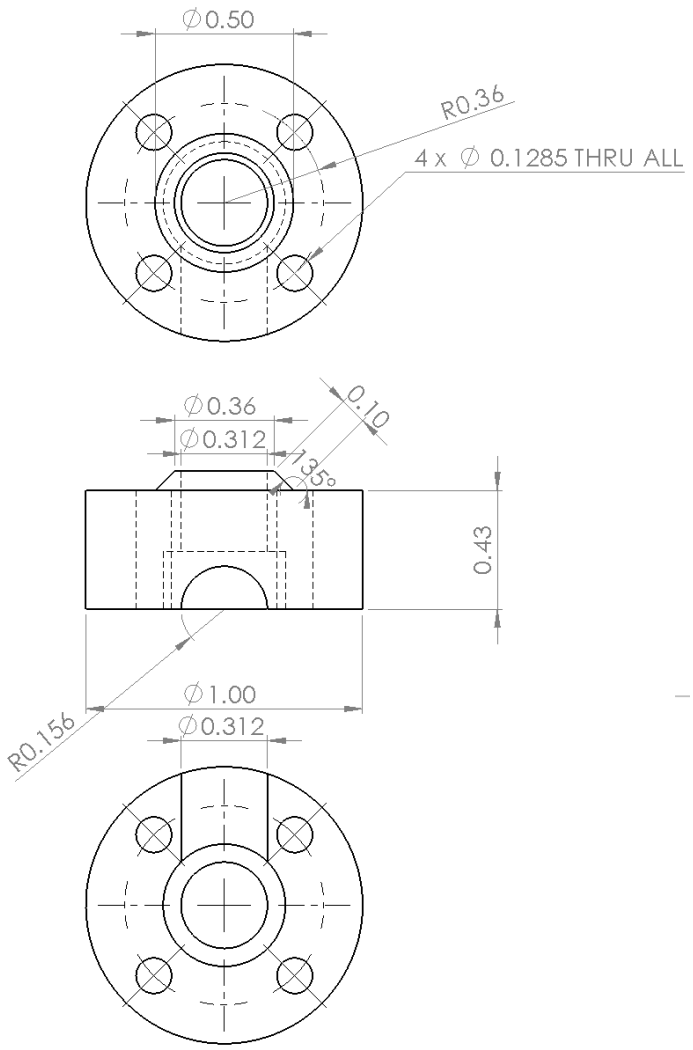

A-4. PEEK Heated Capillary Housing

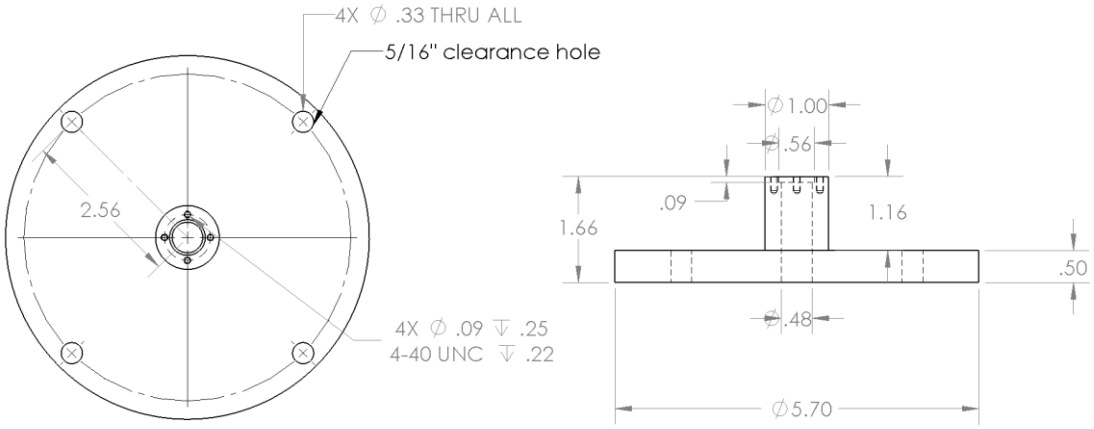

A-5. Heated Capillary Mount Flange

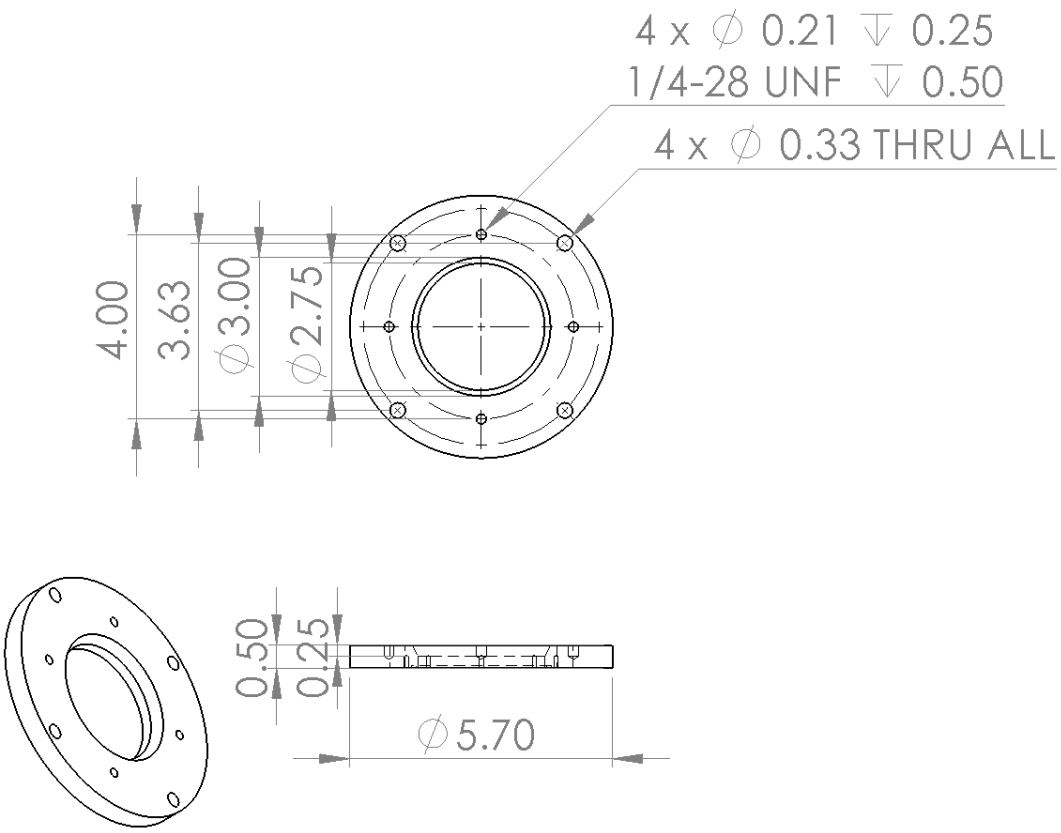

A-6. Source/Heated Capillary Interface Flange

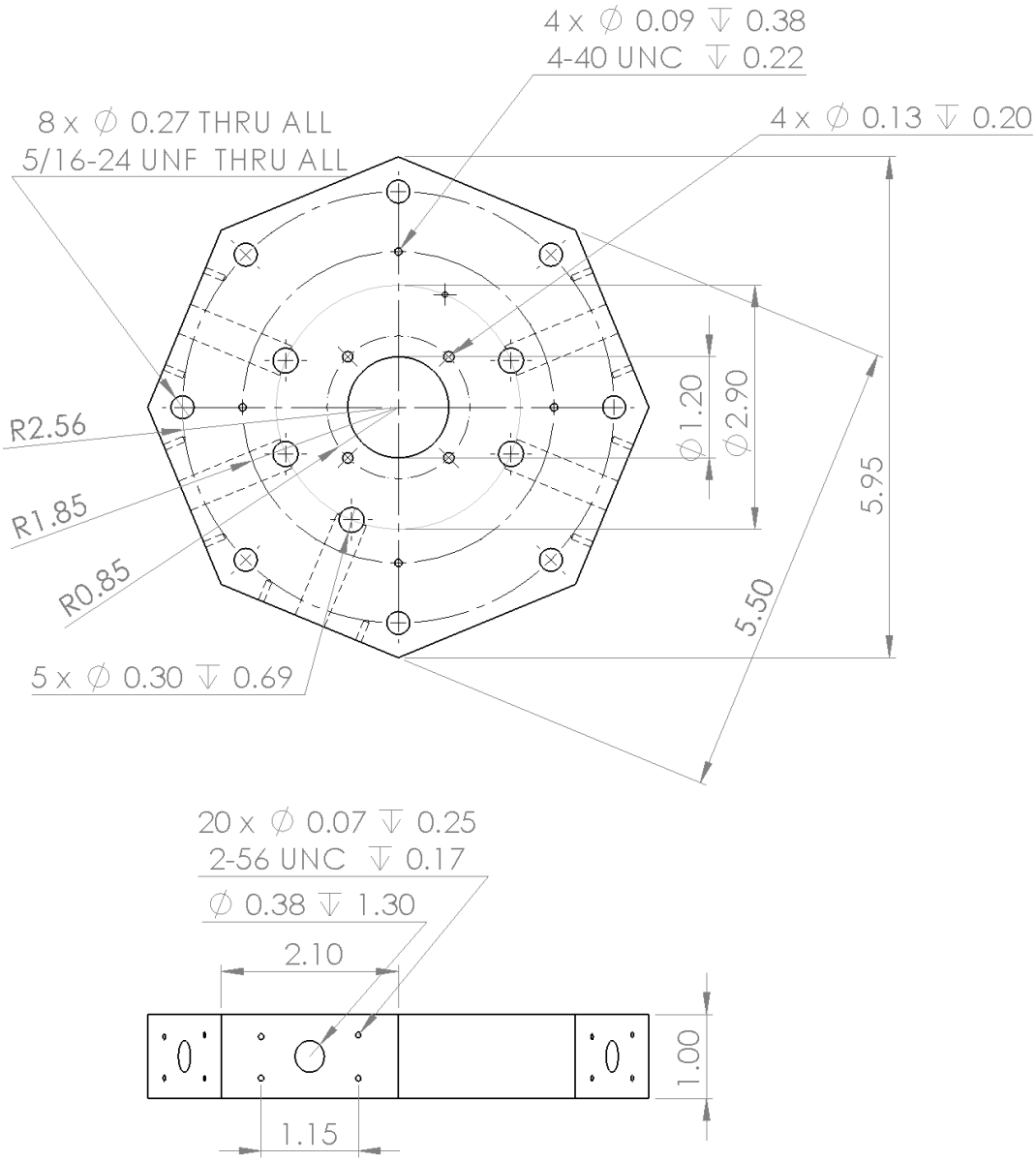

A-7. RF Ion Funnel Support Flange

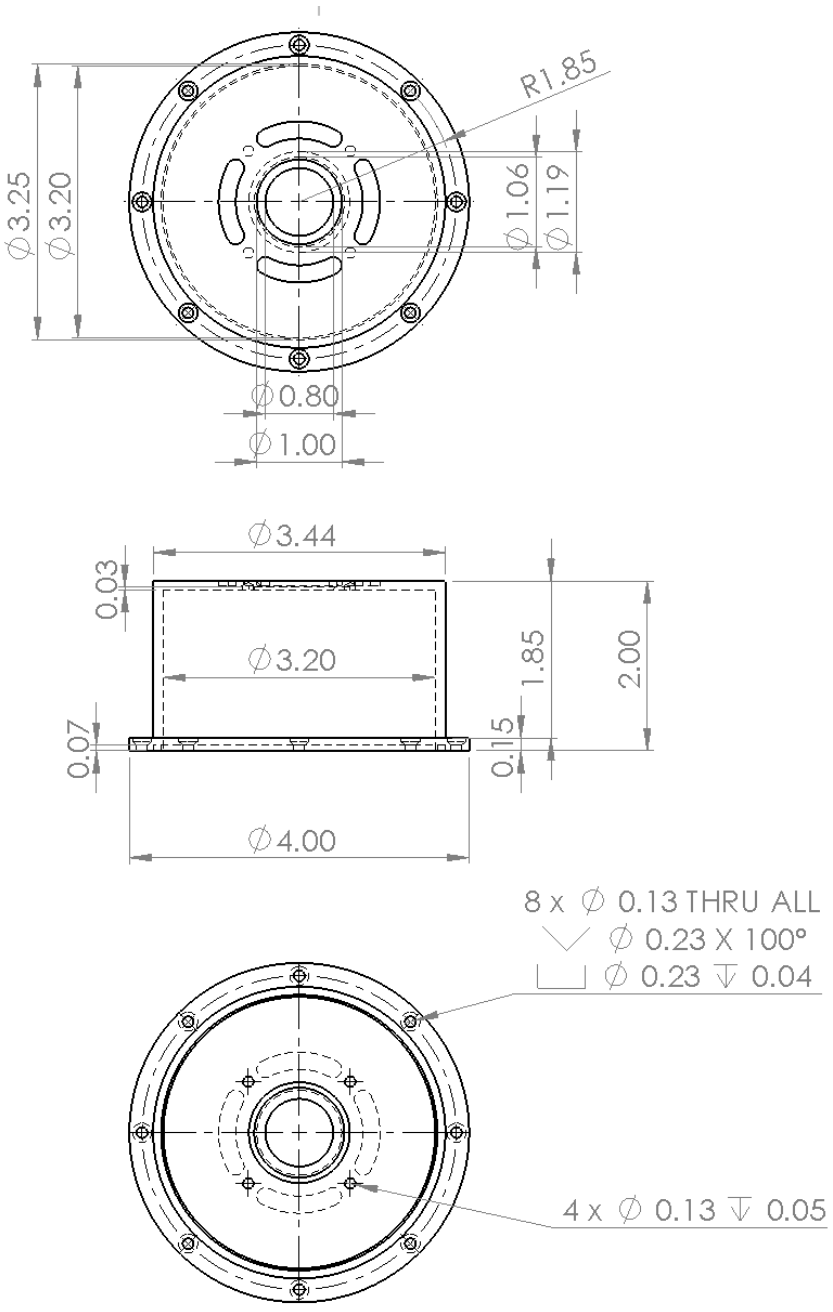

A-8. RF Ion Funnel Housing

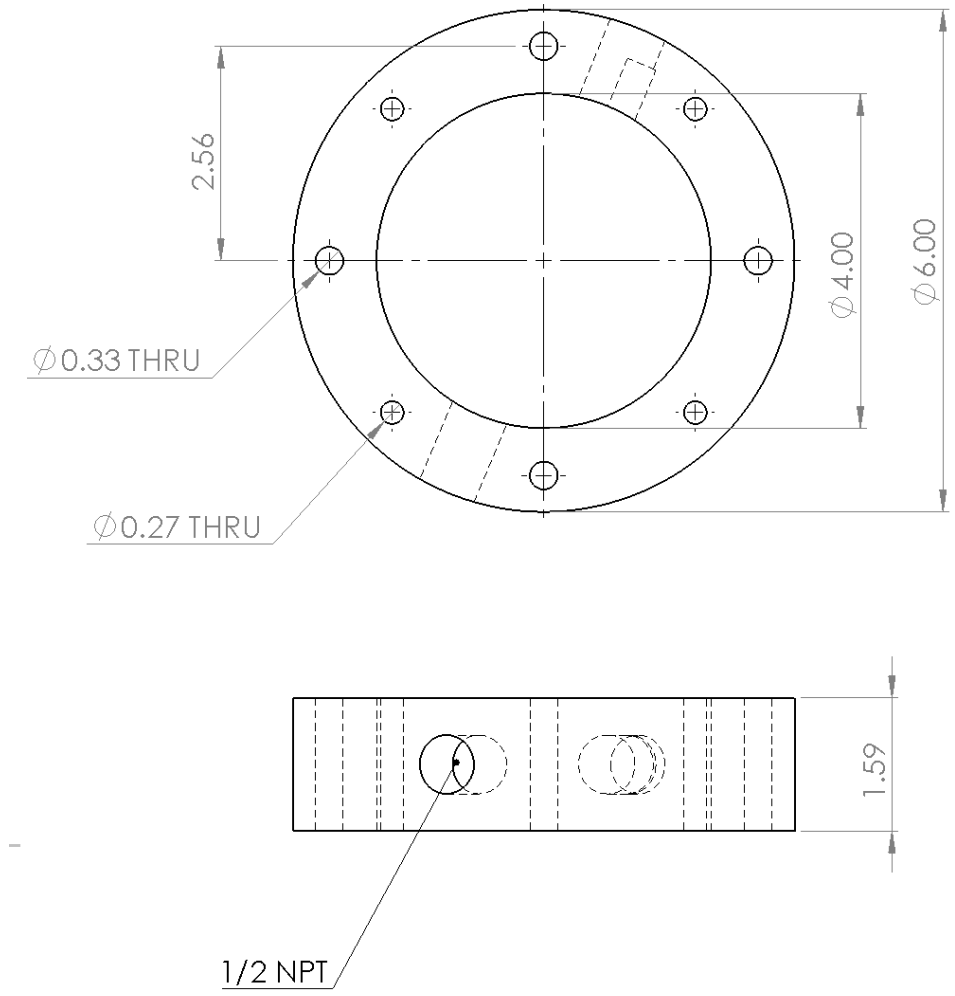

A-9. Post-Funnel Differential Pumping Flange

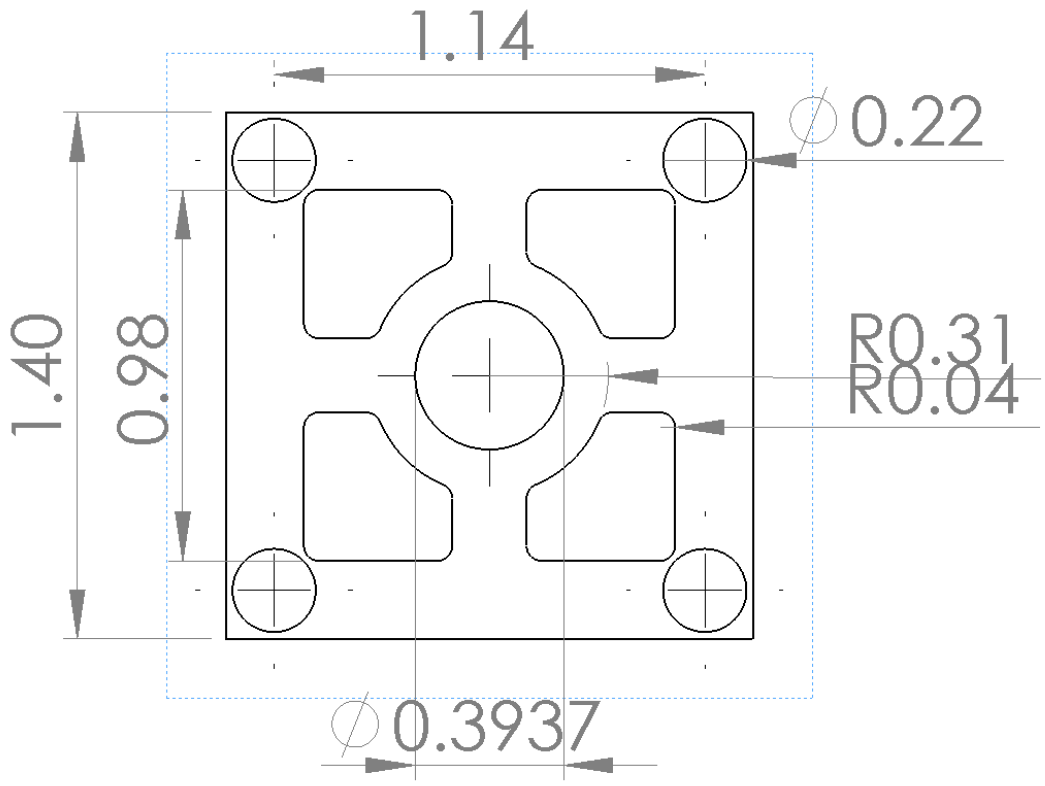

A-10. Ring Electrode

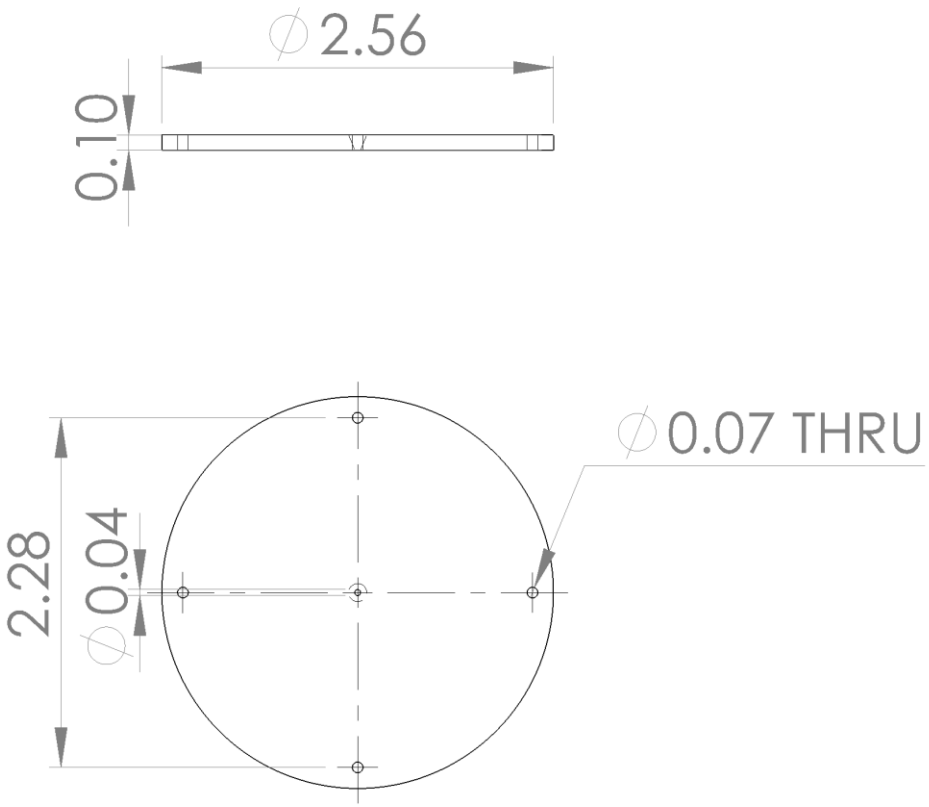

A-11. Gate 1

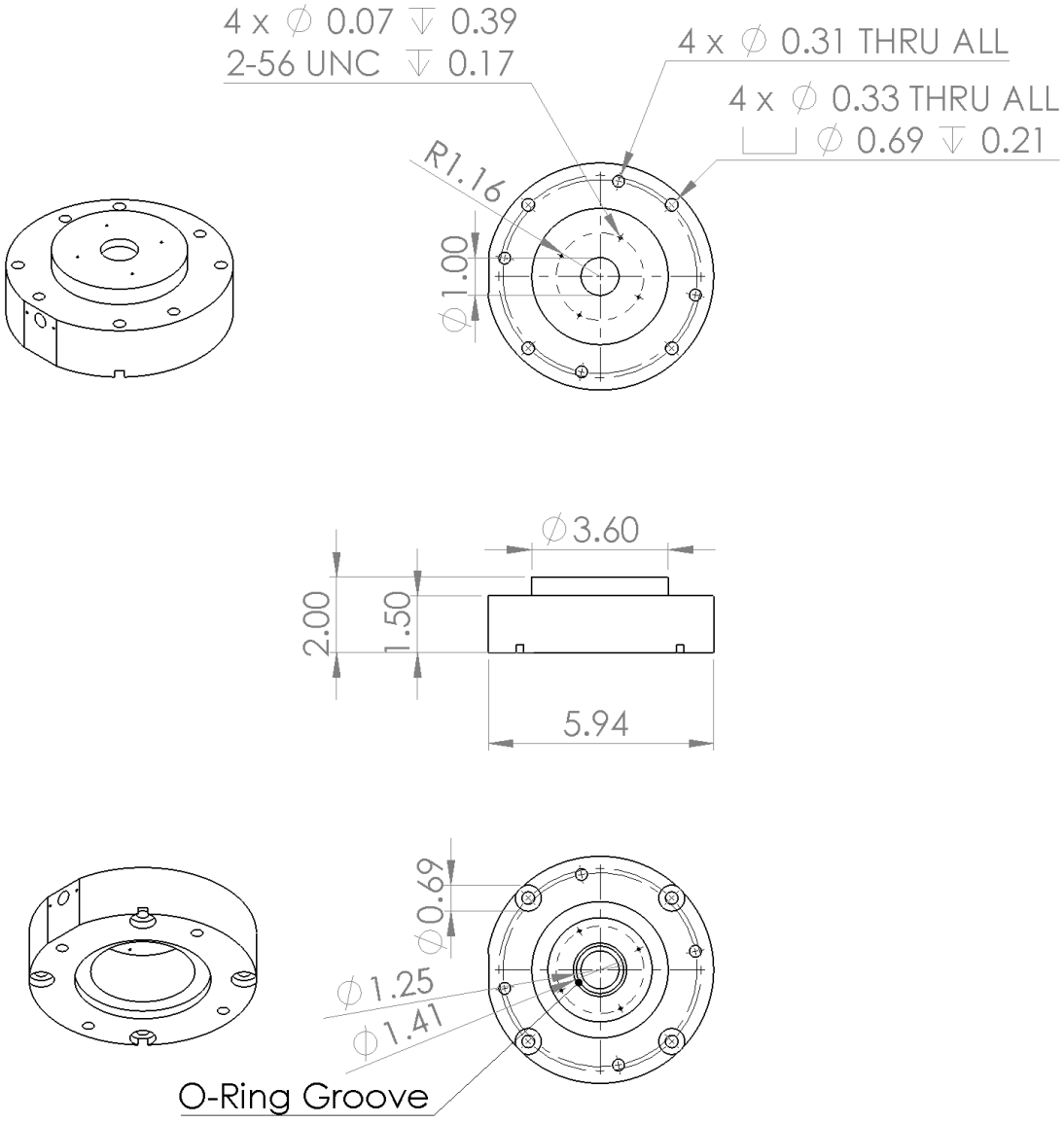

A-12. Front Flange of PF DT

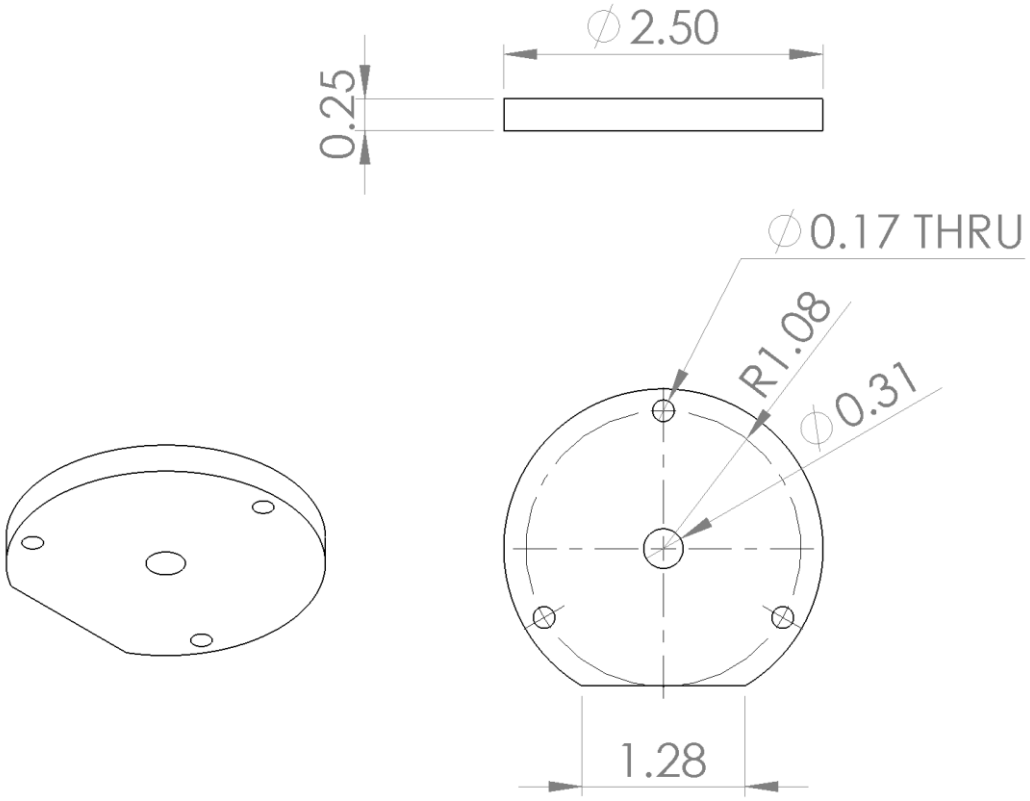

A-13. PF DT Electrode

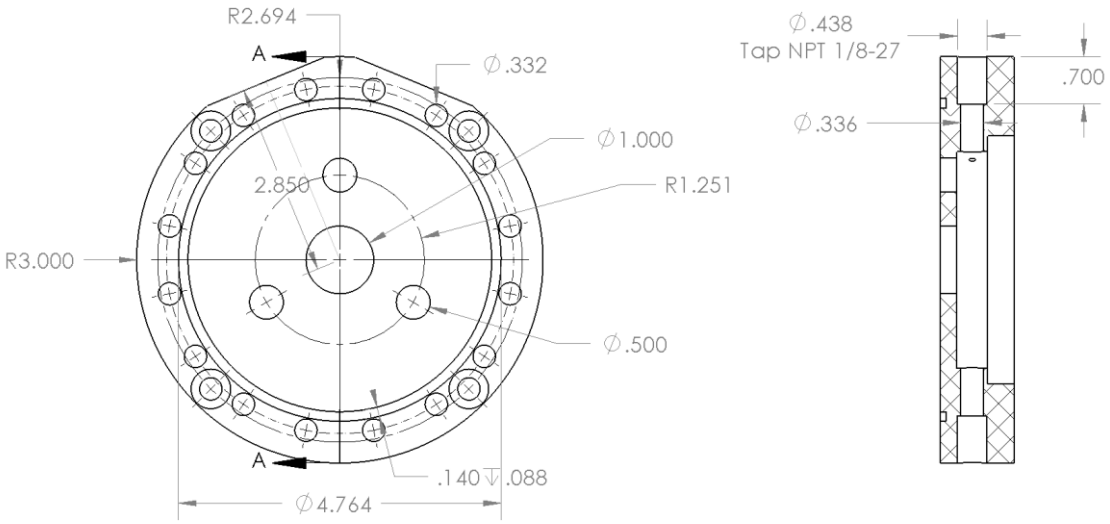

A-14. Rear Flange of PF DT

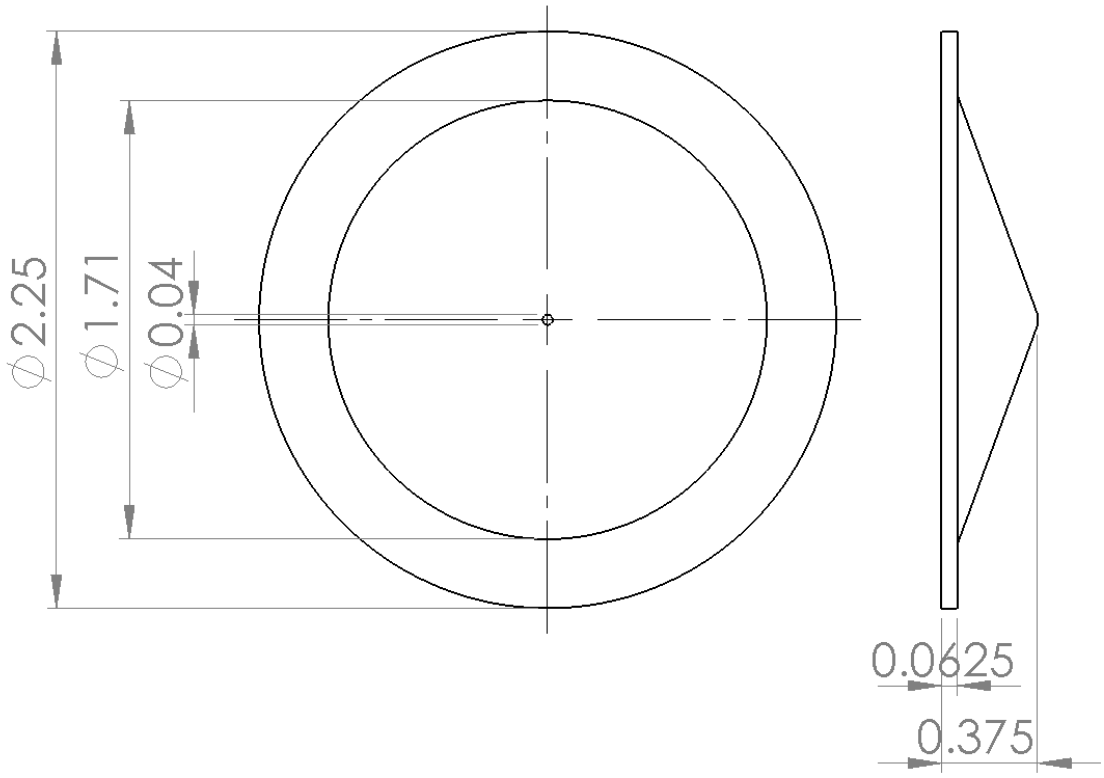

A-15. Post-Mobility Skimmer Cone

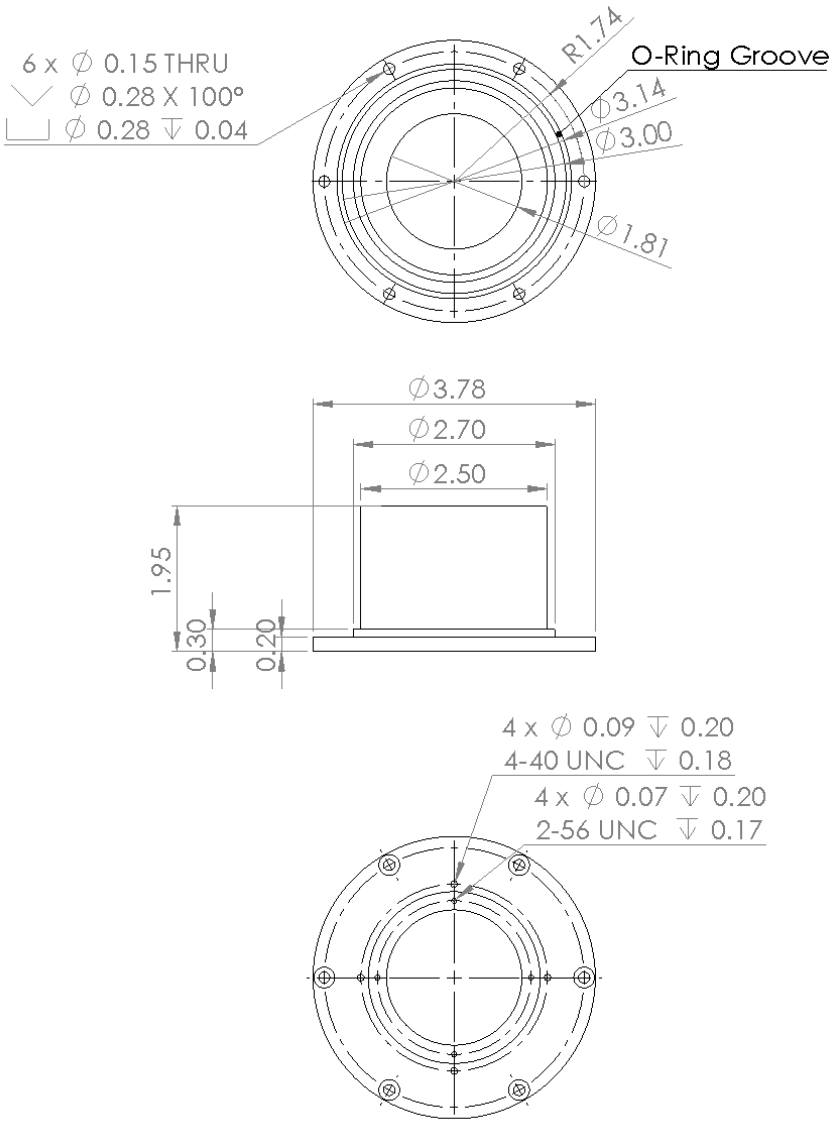

A-16. Post-Mobility Skimmer Cone Housing

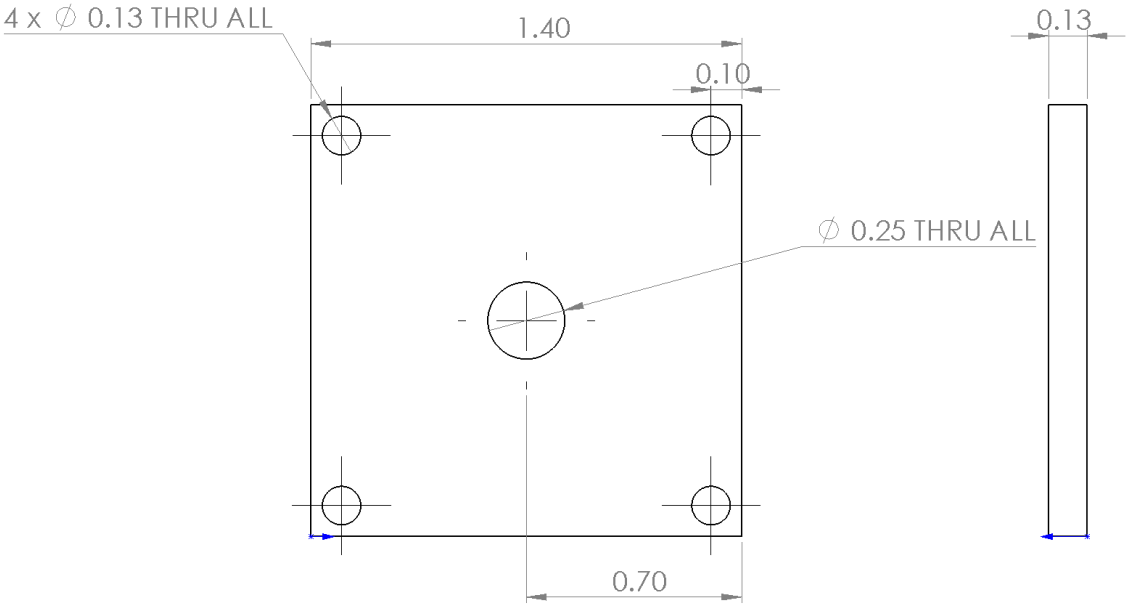

A-17. Gate 2 Electrode

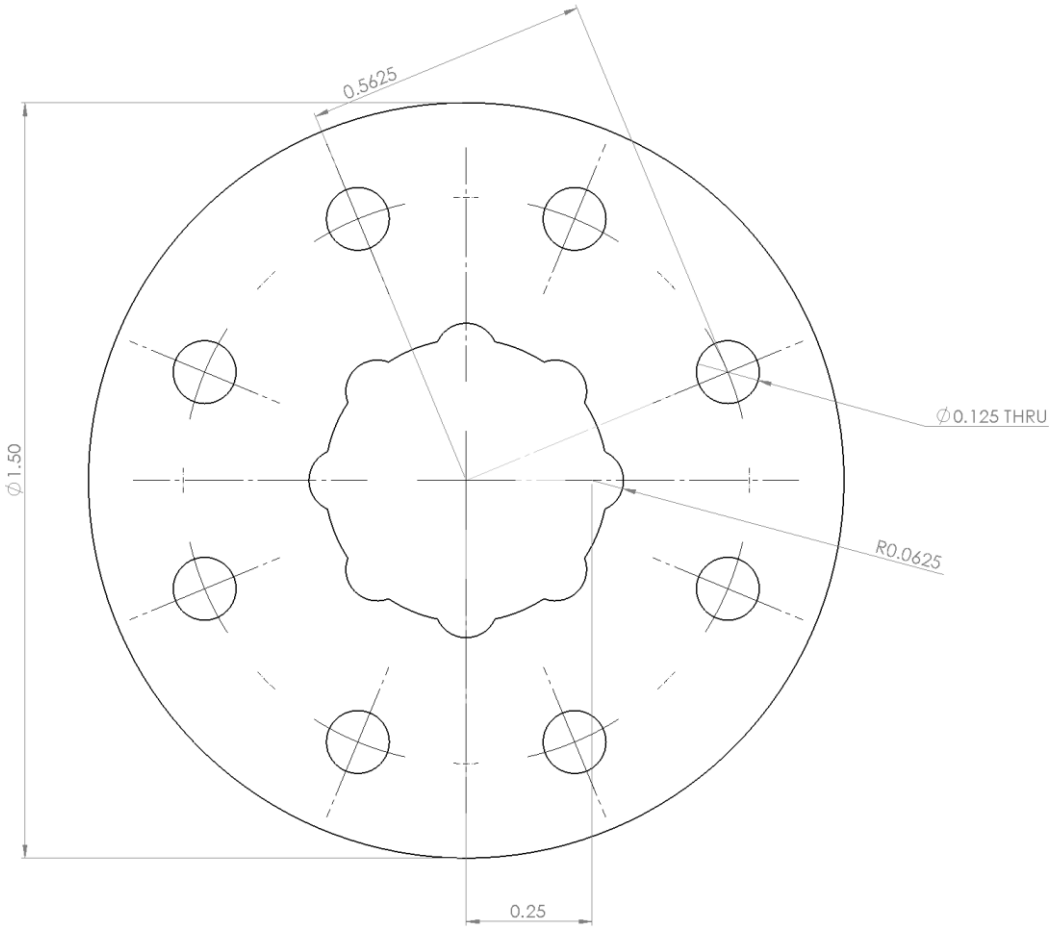

A-18. Octupole Housing 1

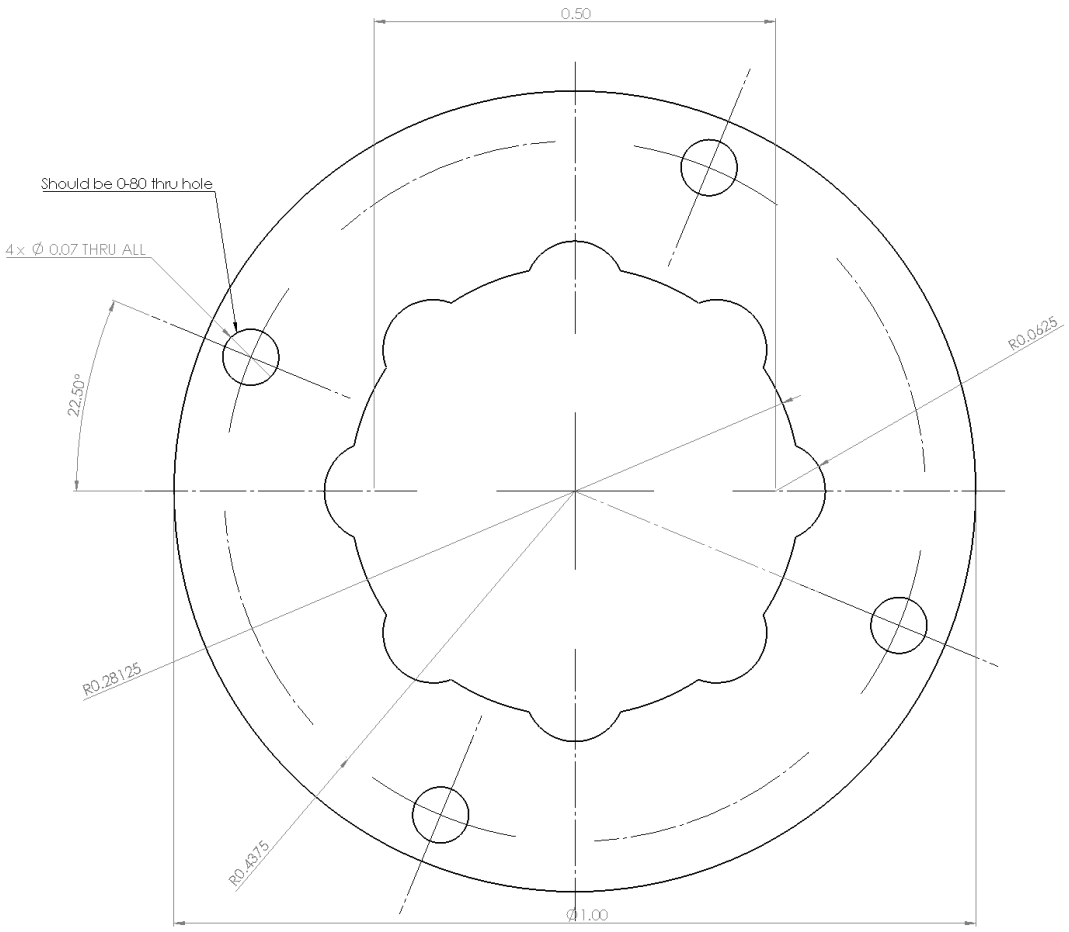

A-19. Octupole Housing 2

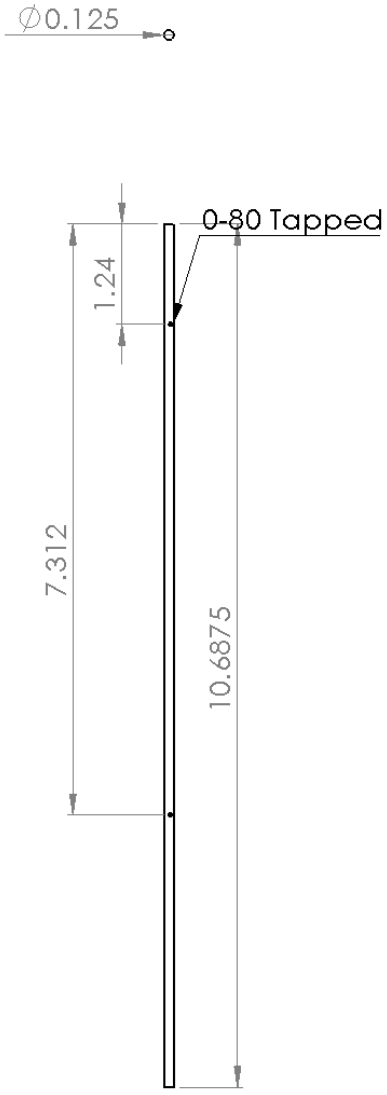

A-20. Octupole Rod